MECHANISTIC AND THERMOCHEMICAL STUDIES OF THE REACTIONS OF TRANSITION METAL IONS AND URANIUM IONS WITH SMALL MOLECULES IN THE GAS PHASE

Thesis by

Peter B. Armentrout

In Partial Fulfillment of the Requirements

for the Degree of

Doctor of Philosophy

California Institute of Technology

Pasadena, California

1980

(Submitted December 14, 1979)

For Mary Ann

Acknowledgments

It is a great pleasure to thank Jack Beauchamp, my advisor, for his contribution to my scientific development both in the past and, I hope, in the future. I have enjoyed our collaboration.

It is always difficult to thank everyone for everything. Friends should know who they are and need no special mention. Many members of both the machine and electronics shops have been helpful. I wish Joyce Lundsteds speedy return. Henriette Wymar deserves special thanks for typing this thesis.

I thank my family for always providing me with support. Mary Ann, of course, played a small part in my life during these last four years. I hope to thank her soon.

Finally, I thank the California Institute of Technology for providing the financial support for my graduate studies.

Abstract

An ion beam apparatus is employed to study the reactions of metal ions with small molecules. The experiments yield reaction cross sections as a function of ion kinetic energy. Simple models are developed in Chapters IV and VI to interpret the energy dependent cross sections for endothermic reactions. Analysis of reaction thresholds using these models yields thermochemical data of interest. Chapter I is a brief introduction to these topics.

Chapter II describes the reactions of U^+ and UO^+ with O_2, CO, CO_2, COS, CS_2 and D_2O. Results are in good accord with literature thermochemistry except for the exothermic reactions of UO^+ with CO_2 and COS to yield UO_2^+ where an energy barrier is observed. In Chapter III, the collision induced dissociation of UO^+ and UO_2^+ impacting on Ar is studied.

Chapters IV, V and VIII report experiments of metal ions, Ba^+ Ni^+ and Co^+, respectively, reacting with hydrogen. Interpretation of reaction thresholds for production of the metal hydride yields metal hydrogen bond energies. A large energy dependent isotope effect is observed in the reaction of Ni^+ with HD (Chapter V).

In Chapters VI-VIII, results for reactions of Co^+ with organic molecules are presented. Chapter VI concerns the formation of $CoCH_2^+$ by reaction of Co^+ with ethene, cyclopropane and ethylene oxide. The bond energy of the cobalt carbene ion is derived. Chapters VII and VIII discuss the reactions of Co^+ with alkanes. The emphasis in Chapter VII is the ion beam instrument as a probe of the potential

energy surface of complex organometallic reactions. Chapter VIII is a comprehensive thermochemical and mechanistic study of the interactions of Co^+ with saturated hydrocarbons. Several bond energies between Co^+ and hydrocarbons are derived and a general mechanism for the reactions proposed.

TABLE OF CONTENTS

CHAPTER I

INTRODUCTION

The last decade has seen the techniques of molecular beam scattering increasingly applied to reactive chemical systems.[1] The result has been a significant expansion in the number and types of reagent species studied.[2,3] The rather wide classes of metal atoms and metal ions, however, have received comparatively little attention. Examples of the former include Mg, Ca, Sr, Ba;[4] Al;[5,6] Sc, Y, La;[7,8] Ti;[6,9] V;[10] Ta;[6] Sn;[11] Hg[12] and U.[13,14,15] Studies of the reactions of metal ions using beam techniques are even rarer, being confined to Al^+,[16,17] Cs^+,[18] and U^+.[19] Included among these is published work of the author.[17,19] The interest in such systems is clear. The fields of organometallic chemistry, surface chemistry and catalysis may all benefit from the fundamental information beam techniques can provide.

A major reason for the lack of investigation of metal systems is that the reactions of such species are typically endothermic.[16-19] Due to the inherently low reaction cross sections of such processes, accurate experimental data are difficult to obtain. As a consequence, the theory needed to interpret experiments on endothermic reactions has been slow to develop.[20] An underlying theme in the following chapters is elucidation of the behavior of cross sections for endothermic reactions as a function of the relative energy. Of particular interest is the extraction of thermochemical data by determining the energy threshold for reaction.

An outline for the ensuing chapters would follow the precept that an understanding of simple, well-characterized systems must precede examination of complex systems previously unstudied. Thus, the

reactions of uranium ions and uranium oxide ions are discussed first (Chapters II and III) because the thermochemistry of molecules containing this element is well established. Chapter II examines both the exothermic and endothermic reactions of U^+ and UO^+ with several small molecules. Good agreement with literature thermochemistry is seen for the exothermic reactions with the exception of UO^+ reacting with CO_2 or COS to yield UO_2^+. Here, a significant energy barrier to reaction is observed. Reasons for this anomalous result, one of the few ion-molecule reactions to exhibit such behavior,[21,22] are discussed. The endothermic reaction of U^+ with CO yielding UC^+ and UO^+ is interpreted using a simple model which gives thresholds in agreement with literature values. Chapter III discusses a particular type of endothermic reaction, collision induced dissociation (CID), for which theory is available. This theory is used to interpret the cross sections for CID of UO^+ and UO_2^+ impacting on Ar. Good agreement between the energy thresholds for reaction and the known bond energies of UO^+ and UO_2^+ is obtained. A decrease is observed in the CID cross section for both species at higher energies, 20-80 eV.

The next two chapters report investigations of the reactions of Ba^+ and Ni^+ with hydrogen to form metal hydrides. Although the thermochemistry of these systems is unknown, the fact that the processes involve only three particles allows detailed analysis of the results. In Chapter IV, the impulsive model of Mahan, Ruska and Winn[23] is extended to include endothermic reactions. The model is used to predict the variation in reaction cross section as a function of

relative kinetic energy. The prediction is compared to the experimental results for the reaction $Ba^+(D_2, D)BaD^+$ and found to account for the behavior observed. Interpretation of the energy threshold for reaction allows the bond energy of BaD^+ to be derived.

In Chapter V, the reactions of Ni^+ with isomeric hydrogen, H_2, HD and D_2, are examined. Using the model of the previous chapter, the energy thresholds for these reactions are obtained and yield bond energies for NiH^+ and NiD^+ which are found to be consistent with one another. Deviations from the model at high energies are observed and discussed. Total reaction cross sections for all three systems are seen to have comparable magnitudes. Although reaction of Ni^+ with HD yields both NiH^+ and NiD^+, a large energy dependent isotope effect is observed. Reasons for this effect are discussed.

Chapters VI-VIII investigate the reactions of Co^+ with a variety of organic molecules. The increased complexity of these systems requires a somewhat different form for the reaction cross section for endothermic processes than that used earlier. A generalized form which includes the result of Chapter IV is proposed and discussed in Chapter VI. Experiments described in this Chapter and Chapter VIII are used to test this model. The proposed form is found capable of fitting the experimental excitation function. More important, the thermochemistry derived from the interpretation of reaction thresholds agrees with that obtained by other means.

Chapter VI presents the reactions of Co^+ with ethene, cyclopropane and ethylene oxide all leading to formation of $CoCH_2^+$.

The thermochemistry derived from these experiments is internally consistent and yields the cobalt carbene ion bond energy. In Chapters VII and VIII, the reactions of Co^+ with saturated hydrocarbons are investigated. The emphasis in Chapter VII is on the ion beam technique as a probe of the potential energy surface of complex reactions. In Chapter VIII, a comprehensive study is made of the thermochemistry and reactivity of Co^+ with alkanes. A reaction mechanism capable of explaining the observed results is proposed and comparisons made between these gas phase studies and solution phase studies of related systems.

References

1. For a general introduction to this technique see R. D. Levine and R. B. Bernstein, "Molecular Reaction Dynamics", Clarendon, Oxford, 1974.

2. For a recent review of neutral-neutral molecular scattering experiments see R. B. Bernstein, Adv. At. Mol. Phys. 15 (1979).

3. For a recent review of ion-neutral molecular scattering experiments see W. R. Gentry, "Gas-Phase Ion Chemistry," ed. M. T. Bowers, Academic Press, New York, 1979; W. R. Gentry, "Kinetics of Ion-Molecule Reactions," ed. P. Ausloos, Plenum Press, New York, 1979.

4. These metal atoms have been reviewed by R. R. Herm, "The Alkali Halide Vapors," P. Davidovits and D. L. McFadden, eds; Academic Press, New York, 1978.

5. R. N. Zare, Ber. Bunsenges. Phys. Chem. 78, 153 (1974).

6. R. B. Cohen, C. E. Young and S. Wexler, Chem. Phys. Lett. 19, 99 (1973).

7. C. L. Chalek and J. L. Gole, Chem. Phys. 19, 59 (1977); J. L. Gole and C. L. Chalek, J. Chem. Phys. 65, 4384 (1976).

8. D. M. Manos and J. M. Parson, J. Chem. Phys. 69, 231 (1978).

9. L. H. Dubois and J. L. Gole, J. Chem. Phys. 66, 779 (1977).

10. R. W. Jones and J. L. Gole, J. Chem. Phys. 65, 3800 (1976).

11. T. P. Parr, R. Behrens, A. Freedman and R. R. Herm, Chem. Phys. Lett. 56, 71 (1978).

12. J. M. Mayer, B. E. Wilcomb and R. B. Bernstein, J. Chem. Phys. 67, 3507 (1977).

Re~~ferences~~ (continued)

13. W. L. Fite, H. H. Lo and P. Irving, J. Chem. Phys. 60, 1236 (1974).

14. C. E. Young, P. M. Dehmer, R. B. Cohen, L. G. Pobo and S. Wexler, J. Chem. Phys. 64, 306 (1976).

15. N. C. Lang and R. C. Stern, ACS Conf., Honolulu, Hawaii, April 6, 1979.

16. J. A. Rutherford and D. A. Vroom, J. Chem. Phys. 65, 4445, (1976).

17. R. V. Hodges, P. B. Armentrout and J. L. Beauchamp, Int. J. Mass Spec. Ion Phys, 29, 375 (1979).

18. S. A. Safron, G. D. Miller, F. A. Rideout and R. C. Horvat, J. Chem. Phys. 64, 5051 (1976); G. D. Miller and S. A. Safron, J. Chem. Phys. 64, 5065 (1976).

19. P. B. Armentrout, R. V. Hodges and J. L. Beauchamp, J. Am. Chem. Soc. 99, 3162 (1977); P. B. Armentrout, R. V. Hodges and J. L. Beauchamp, J. Chem. Phys. 66, 4683 (1977).

20. A bibliography on the interpretation of endothermic reactions is essentially included in Chapter VI.

21. The classic example of such behavior is the reaction $O^+(N_2, N)NO^+$. See C. F. Giese in "Ion-Molecule Reactions in the Gas Phase," ed. P. Ausloos, ACS Washington, D.C., 1966, p. 20, and D. G. Hopper, J. Am. Chem. Soc. 100, 1019 (1978).

22. Other examples include the reactions of Ar^+ with methane, d_0, d_2 and d_4. J. R. Wyatt, L. W. Stratton, S. Chivalek and P. M. Hierl, J. Chem. Phys. 63, 4582 (1975).

References (continued)

23. B. H. Mahan, W. E. W. Ruska and J. S. Winn, J. Chem. Phys. 65, 3888 (1976).

CHAPTER II

REACTIONS OF U^+ AND UO^+ WITH O_2, CO, CO_2, COS, CS_2 AND D_2O

REACTIONS OF U^+ AND UO^+ WITH O_2, CO, CO_2, COS, CS_2 AND D_2O

P. B. ARMENTROUT and J. L. BEAUCHAMP

Arthur Amos Noyes Laboratory of Chemical Physics,

California Institute of Technology, Pasadena, California 91125, USA

Received

Abstract

An ion-beam apparatus has been employed to investigate the reactions of uranium ions and uranium monoxide ions with O_2, CO, CO_2, COS, CS_2 and D_2O. Reaction cross sections as a function of ion kinetic energy are determined and compared to simple models for exothermic and endothermic reactions. With two exceptions, all exothermic reactions exhibit large cross sections which decrease with increasing kinetic energy. Although expected to be exothermic, the reactions of UO^+ with CO_2 and COS to form UO_2^+ exhibit substantial energy barriers. Uranium ions react with CO to yield both UO^+ and UC^+ in endothermic processes. The thresholds for these reactions agree well with literature thermochemistry.

Introduction

Intrinsic interest in uranium relates to the unusual properties and technological importance of this element and its compounds. Uranium atoms undergo associative ionization reactions, such as

$$U + O \rightarrow UO^+ + e \qquad (1)$$

with a number of atomic and molecular species [1,2], demonstrating the propensity of uranium to form strong bonds. The proton affinity of the uranium atom, 238 ± 4 kcal/mole, is unusually high, exceeding that of many organic bases [3,4]. The electron affinity of uranium hexafluoride, ~ 5 eV, is among the highest of any species determined [5,6]. Studies of the formation and reactions of ionic species containing uranium provide important chemical and thermodynamic data relating to both ions and neutrals. In a previous study, we examined the endothermic reactions of uranium ions with nitrogen, hydrogen, and methane [4]. In the present paper, the reactions of uranium ions and uranium monoxide ions with O_2, CO, CO_2, COS, CS_2 and D_2O are investigated.

There appear to be only two other previous investigations of the reactions of atomic uranium ions and none of the reactions of uranium monoxide ions. Moreland, Rokop and Stevens [7] observed formation of UH^+ and UD^+ from endothermic reactions between U^+ and H_2, O_2, H_2O, D_2O, and H_2S but report no other products. The reaction of uranium ions with oxygen and nitrogen has been studied by Johnsen and Biondi [8]. They find the reaction with oxygen to be exothermic and

report a room temperature rate constant of 8.5 (-1, +4) $\times$ 10^{-10} cm^3 molecule^{-1} s^{-1}.

The energetics of the uranium oxides and their ions are reasonably well established. Other uranium containing diatomics and triatomics have not been as extensively studied. The known thermochemistry of such species, neutrals and ions, is given in Table I. For completeness, several molecules not examined in the present study are also included.

Experimental

The ion beam apparatus shown in Fig. 1 is a highly modified version [9] of an instrument previously described [4]. Ions from a surface ionization source are accelerated and focused into a 60° sector magnet easily capable of resolving uranium ions and the uranium oxides. This mass selected beam is decelerated and focused into a collision chamber containing the reactant gas. Product ions scattered in the forward direction are focused into a quadrupole mass filter and detected using a Channeltron electron multiplier operated in a pulse counting mode. Ion intensities are corrected for the mass discrimination of the quadrupole.

The ion source, previously described [4], comprises a stainless steel oven mounted on a U-shaped repeller plate surrounding a rhenium ionization filament. For these experiments the oven is loaded with UF$_4$. Resistive heating of the filament vaporizes the UF$_4$ which is directed at the filament. There it dissociates and the resulting uranium is ionized [10]. When this source is first operated, enough residual

Table I

Thermochemical data of uranium containing ions and neutrals

Species (M)	$\Delta H^0_{f, 298}(M)$ (kcal/mol)	Ionization Potential (M) (eV)	$\Delta H^0_{f, 298}(M^+)$ (kcal/mol)
U	125.0 ± 3[a]	6.187 ± 0.002[b]	268 ± 3
UH			253 ± 6[c]
UC	187.6 ± 6.2[d]	6.2 ± 0.5[e]	330 ± 18
UN	111 ± 7[f]	7.0 ± 0.6	272 ± 7[c]
UO	8.9 ± 3[a]	5.72 ± 0.06[g]	141 ± 4
US	57 ± 5[h,i]	6.3 ± 0.5[h]	202 ± 16
		$<5.8 \pm 0.1$[j]	$<191 \pm 7$
UO_2	-105.4 ± 3[a]	5.5 ± 0.1[g]	21 ± 5
USO			$<114 \pm 9$[k]
US_2	6 ± 7[h,i]	$<7.3 \pm 1.2$	$<175 \pm 21$[k]
UOH			$89-158$[k]
UO_3	-189.6 ± 3[a]	10.6 ± 0.1[l]	55 ± 5

(a) S. D. Gabelnick, "Ion Reactor Safety and Physical Property Studies," Annual Report, July 1973-June 1974, Chem. Eng. Div., Argonne Natl. Lab., ANL-8120.

(b) G. S. Jones, I. Itzan, C. T. Pike, R. H. Levy and L. Levin, J. Quant. Electron. QE-12, 111 (1976).
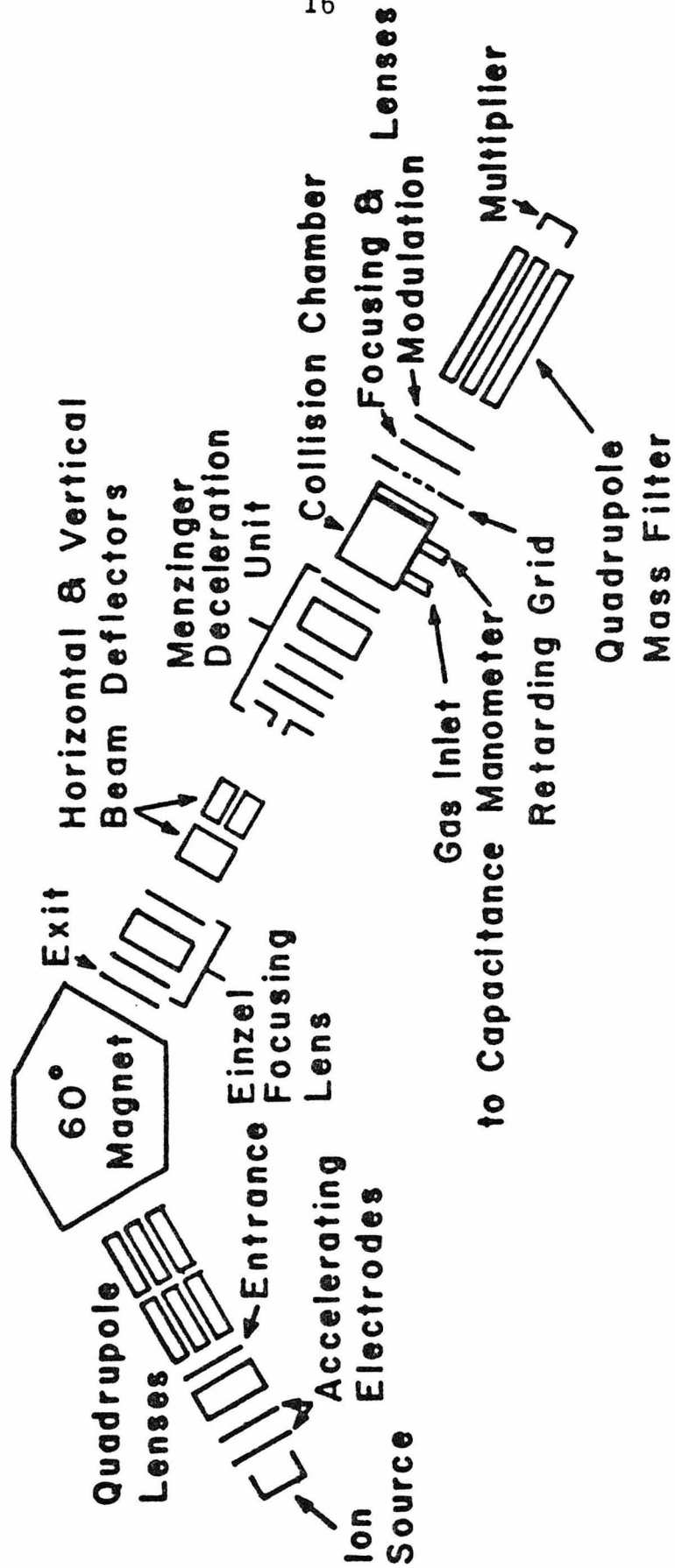
(c) Ref. 4.

(d) S. K. Gupta and K. A. Gingerich, J. Chem. Phys. 71 (1979) 3072.

(e) K. A. Gingerich, J. Chem. Phys. 50 (1969) 2255. Corrected for

(footnotes to Table I continued)

improved IP (U) given above.

(f) K. A. Gingerich, J. Chem. Phys. 47 (1967) 2192.

(g) Ref. 11. These values are in good agreement with those of Ref. ℓ.

(h) D_0^0 (US) = 133.8 ± 2.3 kcal/mol. D_0^0 (US$_2$) = 252 ± 4 kcal/mol.

E. D. Cater, E. G. Rauk and R. J. Thorn, J. Chem. Phys. 44 (1966) 3106.

(i) $\Delta H_{f, 298}^0$ (S) = 66.29 ± 0.01; Ref. 17.

(j) IP (US) $\leq$ D^0(US). W. L. Fite, Private Communication. D^0(US) = 5.8 ± 0.1 eV. Ref. h.

(k) This study.

(ℓ) E. G. Rauh and R. J. Ackermann, J. Chem. Phys. 60 (1974) 1396.

FIG. 1.   Schematic drawing of the ion-beam apparatus.

Quadrupole Lenses

Ion Source

Accelerating Electrodes

Entrance Einzel Focusing Lens

60° Magnet

Exit

Horizontal & Vertical Beam Deflectors

Menzinger Deceleration Unit

Collision Chamber

Focusing & Modulation Lenses

Multiplier

Gas Inlet

to Capacitance Manometer

Retarding Grid

Quadrupole Mass Filter

oxygen (from either air or water) is present that both UO^+ and UO_2^+ are formed preferentially since they have lower ionization potentials than U. This is the source for the UO^+ in these studies. After several hours of operation, the source produces nearly pure uranium ions. At the operating temperature of the filament, several low-lying electronic states of U^+ [11] and UO^+ [1] can be populated. No attempt is made in the present work to account for the presence of excited states.

The energy of the ion beam is taken nominally as the difference in potential between the collision chamber and the center of the filament, the latter being determined by a resistive divider. This energy is verified by use of a retarding field energy analyzer [12]. Agreement is always within 0.3 eV. The energy width of the U^+ and UO^+ beams is determined using the energy analyzer to be 0.7 eV (FWHM). This introduces a negligible uncertainty in the interaction energy. No specific account of this effect is taken in the treatment below.

A more severe problem concerning the actual energy of inter-action is the effect of thermal motion of the reactant gas. For exo-thermic reactions, this has little noticeable effect; but for endothermic reactions, this energy distribution effectively broadens the threshold region. To account for this effect, a proposed excitation function is convoluted with this distribution before comparison with the data using the procedure outlined by Chantry [13].

Reaction cross sections are calculated using

$$I_R = (I_R + I_P) \exp(-n\sigma\ell) \tag{2}$$

which relates the total reaction cross section, σ, the length of the interaction region, ℓ (= 5 mm), and the number density of the target gas, n, to the measured intensities of the reactant ion and the sum of the product ions, I_R and I_P, respectively. In reactions having more than one product, the cross section for a specific product is

$$\sigma_i = \sigma I_i / \Sigma I_i \tag{3}$$

where $\Sigma I_i = I_P$. The greatest uncertainty in these measurements is the ion detection efficiency. In these experiments which involve a heavy incident particle on a light target molecule, the appreciable center of mass velocity results in all products scattered primarily in the forward direction in the laboratory frame. At the lowest energies, < 10 eV in the laboratory frame, a potential of 0.5 eV is placed across the specially designed collision chamber [14] to extract low energy ions. This voltage increases the uncertainty in the interaction energy.

The general method for obtaining excitation functions is to measure the ion intensities for the complete range of energies at a constant pressure. Pressures for these experiments are in the range $1-10 \times 10^{-3}$ Torr. The cross sections calculated from these measurements are verified at several energies by varying the pressure. This ensures that eqs. 2 and 3 are obeyed for the experimental conditions. This procedure also easily reveals those product ions which are due to more than one collision [15]. In general, pressures are kept low enough that more than one collision is unlikely.

Results and Discussion

The reactions of uranium ions and uranium oxide ions examined in the present study are listed in Tables II and III. Included are heats of reaction calculated from the available thermochemical data summarized in Table I. Specific results for each neutral reactant are discussed in detail below, and reaction cross sections are given as a function of relative kinetic energy. Included for comparison are the cross sections predicted using the Langevin-Gioumousis-Stevenson (LGS) model for ion-molecule reactions [16]. In its simplest form, the LGS cross section at a collision energy E is

$$\sigma(E) = \pi \, e(2\alpha/E)^{\frac{1}{2}} \tag{4}$$

where e is the electronic chanrge and α is the rotationally averaged polarizability of the neutral reactant. Table IV lists the value of α used for species examined in this study.

Reactions with O_2

Experimental results for the reactions

$$U^+ + O_2 \rightarrow UO^+ + O \tag{5}$$

and

$$UO^+ + O_2 \rightarrow UO_2^+ + O \tag{6}$$

are shown in Figs. 2 and 3, respectively. Both processes are expected to be exothermic, Tables II and III, and indeed, the data reveal no barrier to reaction. The experimental results shown in

Table II

Reactions of uranium ions

Reaction	$\Delta H_{r,\,298}$ (kcal/mol)[a]
$U^+ + O_2 \rightarrow UO^+ + O$	-67 ± 7
$U^+ + CO_2 \rightarrow UO^+ + CO$	-59 ± 7
$ \rightarrow UO_2^+ + C$	18 ± 8
$U^+ + COS \rightarrow US^+ + CO$	-59 ± 19 [b]
$ \rightarrow UO^+ + CS$	-39 ± 12
$U^+ + CS_2 \rightarrow US^+ + CS$	-39 ± 24 [b]
$U^+ + D_2O \rightarrow UO^+ + D_2$	-69 ± 7 [c]
$ \rightarrow UO^+ + 2D$	35 ± 7 [c]
$ \rightarrow UOD^+ + D$	< 0 [d]
$U^+ + CO \rightarrow UO^+ + C$	70 ± 7
$ \rightarrow UC^+ + O$	148 ± 21

(a) Calculated using values given in Table I for uranium containing

species. For all other species, values are from Ref. 17.

(b) $\Delta H^0_{f,\,298}(US^+) = 202 \pm 16$ kcal/mol, Table I.

(c) Calculated using values for H_2O, H_2 and H.

(d) This study.

Table III

Reactions of uranium oxide ions

Reaction	$\Delta H_{r, 298}$ [a] (kcal/mol)
$UO^+ + O_2 \rightarrow UO_2^+ + O$	-61 ± 9
$UO^+ + CO_2 \rightarrow UO_2^+ + CO$	-52 ± 9
$UO^+ + COS \rightarrow USO^+ + CO$	<0 [b]
$UO^+ + COS \rightarrow UO_2^+ + CS$	-32 ± 14
$UO^+ + CS_2 \rightarrow USO^+ + CS$	<0 [b]
$UO^+ + CS_2 \rightarrow US^+ + COS$	0 ± 20 [c]
$UO^+ + D_2O \rightarrow UO_2^+ + D_2$	-62 ± 9 [d]
$UO^+ + D_2O \rightarrow UO_2D^+ + D$	<0 [b]

(a) Calculated using values given in Table I for uranium containing species. For all other species, values are from Ref. 17.

(b) This study.

(c) $\Delta H^0_{f, 298}(US^+) = 202 \pm 16$ kcal/mol, Table I.

(d) Calculated using values for H_2O and H_2.

Table IV

Average polarizabilities and dipole moments of neutral reactants.

Species	α Polarizability (10^{-25} cm^3)	μ Dipole Moment (Debye)
O_2	16.0[a]	0[b]
CO	19.5[a]	0.1[b, d]
CO_2	26.5[a]	0[b]
COS	56.9[c]	0.709[d]
CS_2	87.4[a]	0[b]
H_2O	14.5[b]	1.84[b], 1.94[d]

(a) J. O. Hirschfelder, C. F. Curtiss and R. B. Bird, "Molecular Theory of Gases and Liquids," Wiley, New York, 1967, Table 13.2-3.

(b) E. W. Rothe and R. B. Bernstein, J. Chem. Phys. 31 (1959) 1619.

(c) Calculated using Table 13.2-2 in Ref. (a).

(d) C. H. Townes and A. L. Schawlow, "Microwave Spectroscopy", Dover, New York, 1975, Appendix VI.
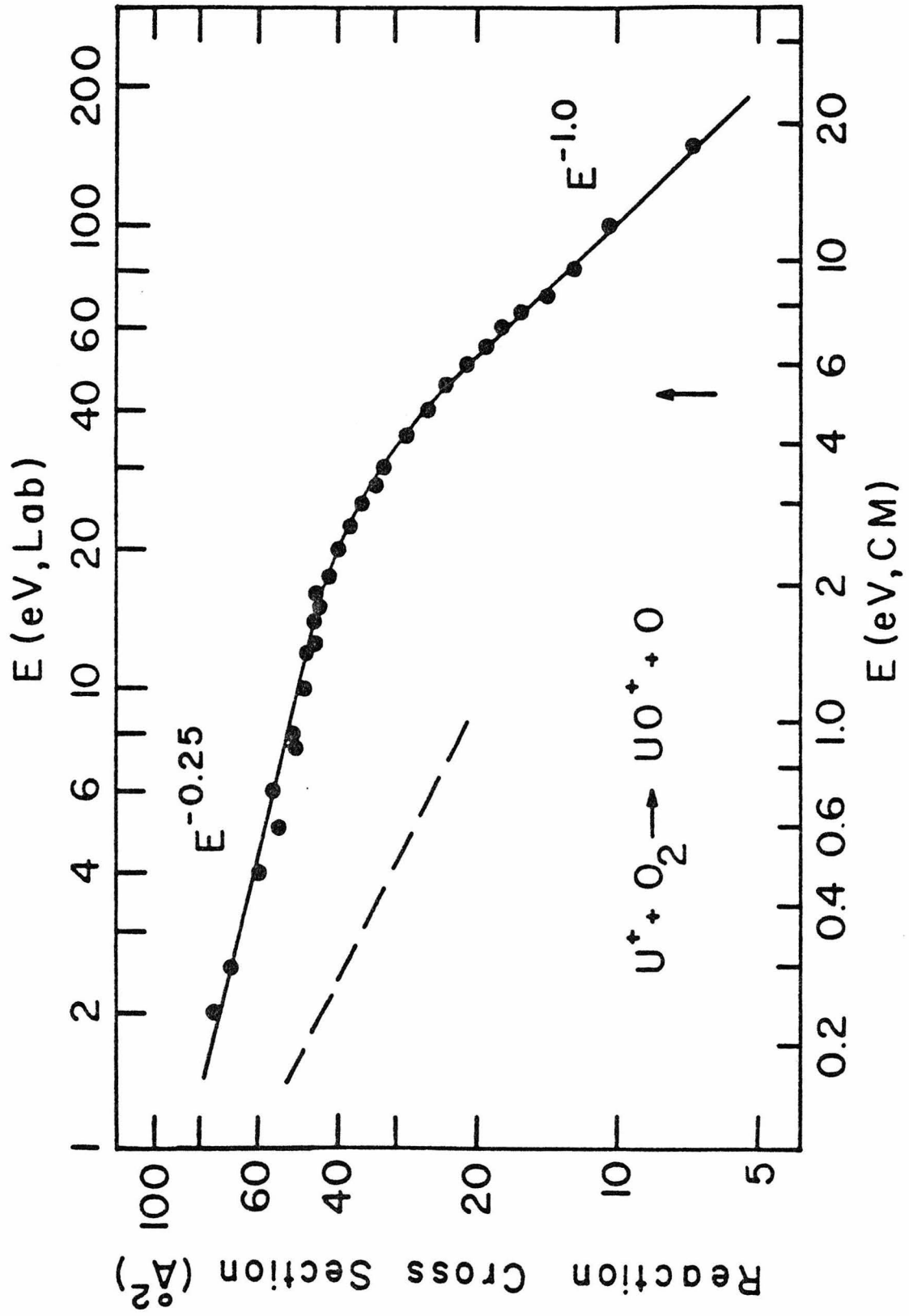
FIG. 2. Variation in cross section for reaction (5) as a function
of kinetic energy in the center of mass frame (lower scale)
and the laboratory frame (upper scale). The dashed line
shows the cross section predicted using the LGS model.
The arrow marks the bond dissociation energy of O_2,
5.16 eV. The slopes of the straight line portions of the
experimental cross section are also given.

$E^{-0.25}$

$E^{-1.0}$

$U^+ + O_2 \longrightarrow UO^+ + O$

E (eV, Lab)

E (eV, CM)

Reaction Cross Section ($\mathring{A}^2$)

FIG. 3. Variation in cross section for reaction (6) as a function
of kinetic energy in the center of mass frame (lower scale)
and the laboratory frame (upper scale). The dashed line
shows the cross section predicted using the LGS model.
The arrow marks the bond dissociation energy of O_2,
5.16 eV. The slopes of the straight line portions of the
experimental cross section are also given.

E (eV, Lab)

Reaction Cross Section ($\mathring{A}^2$)

E (eV, CM)

$E^{-0.55}$

$E^{-1.5}$

$UO^+ + O_2 \rightarrow UO_2^+ + O$
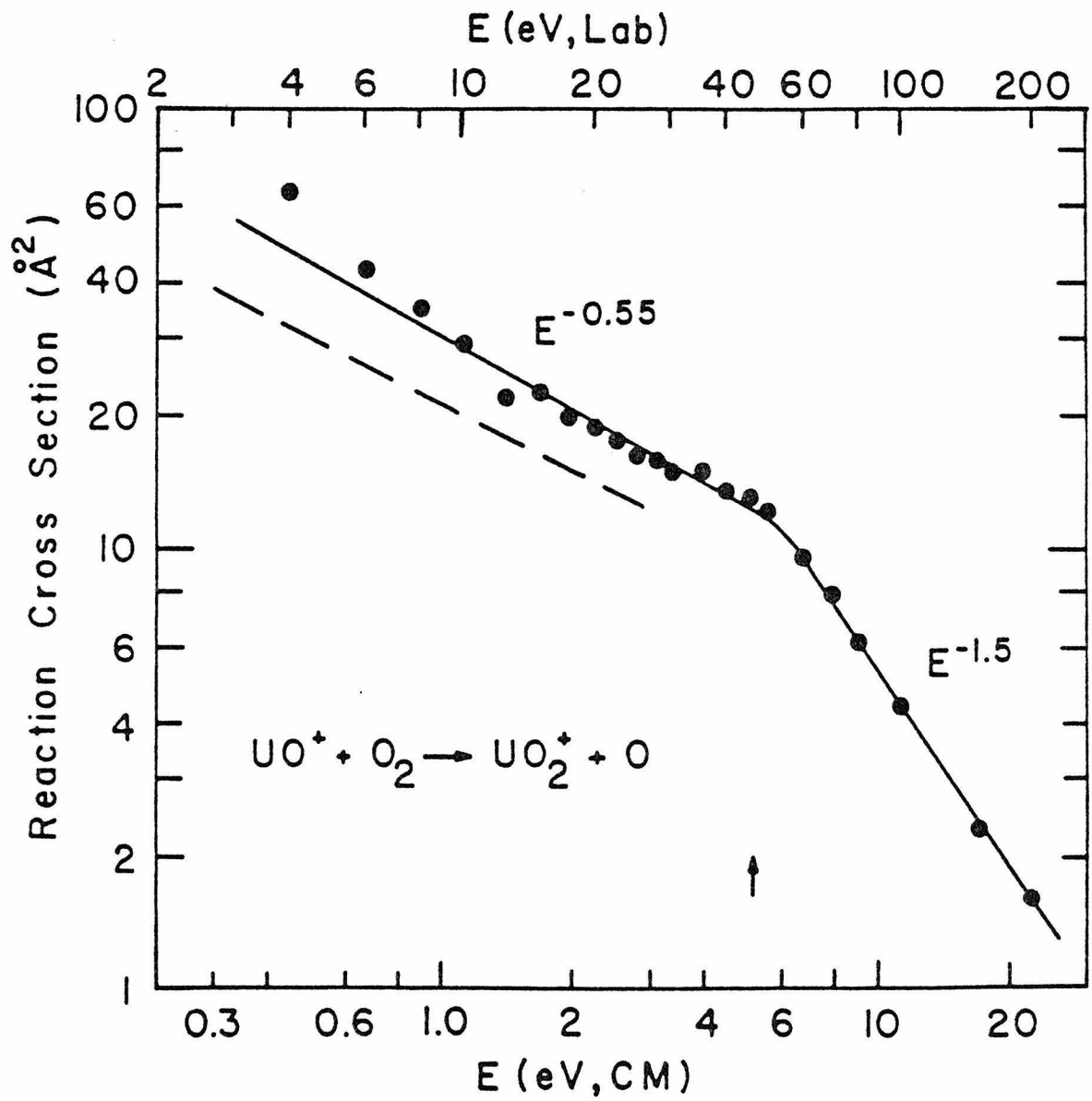
Figs. 2 and 3 represent typical behavior for cross sections of exo-
thermic ion-molecule reactions as a function of kinetic energy. Also
observed in the U^+-O_2 system is the formation of small amounts of
UO_2^+ produced in sequential bimolecular reactions. No UO_3^+ was
observed in either system.

To compare these results for reaction (5) with the rate constant
obtained by Johnsen and Biondi, $k = 8.5 \times 10^{-10}$ cm^3 molecule^{-1} s^{-1} [8],
the cross section must be averaged over a Maxwell Boltzmann distri-
bution of energies. Assuming that the cross section varies as $E^{-\frac{1}{4}}$,
Fig. 2, the rate constant obtained is 5.6×10^{-10} cm^3 molecule^{-1} s^{-1},
in good agreement considering the differing methods.

Reaction of U^+ with CO

Reaction of uranium ions with carbon monoxide yields two
products,

$$U^+ + CO \longrightarrow \begin{cases} UO^+ + C \\ UC^+ + O. \end{cases} \qquad \begin{matrix} (7) \\ (8) \end{matrix}$$

Both these processes are calculated to be endothermic, Table II, and
both exhibit an energy threshold, Fig. 4. The background at low
energies for the UO^+ product is apparently due to a contri bution from
reaction at higher energies outside the collision chamber. For the
UC^+ product, the background is primarily the result of insufficient
resolution from the more intense UO^+ product. Both excitation
functions peak at about the bond dissociation energy of CO, 11.14 eV
[17], and fall off approximately as E^{-3} at higher energies.

FIG. 4. Variation in cross section for reactions 7 and 8 as a
function of kinetic energy in the center of mass frame
(lower scale) and the laboratory frame (upper scale).
The prediction of the LGS model is off scale. Arrows
mark the thermodynamic threshold for reaction (7),
$E_0(UO^+)$ = 3.0 eV, and for reaction (8), $E_0(UC^+)$ =
6.4 eV, and the bond dissociation energy of CO,
11.14 eV. The solid curves are the fits to the data
given in the text convoluted as discussed.
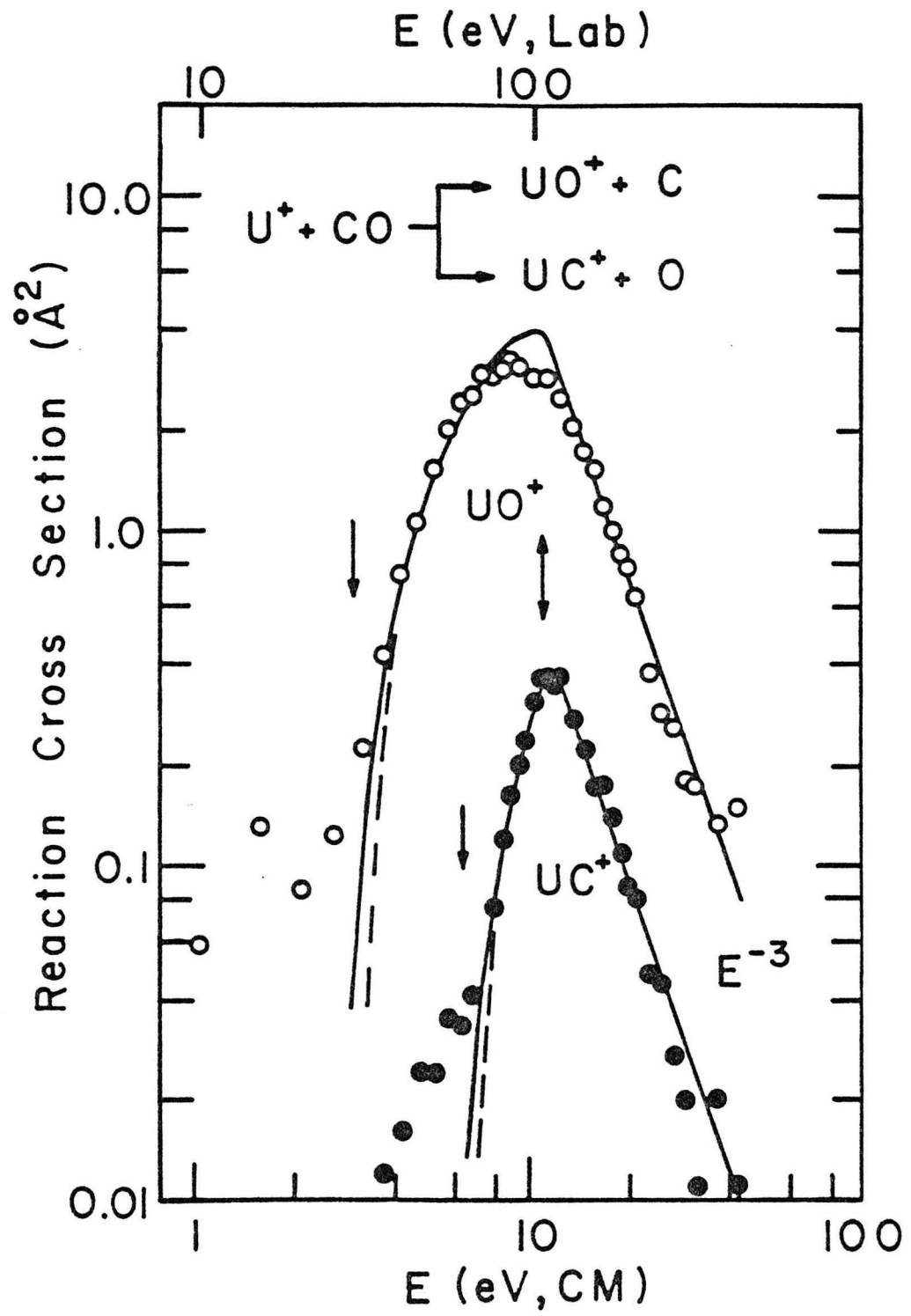
In the threshold region, < 11 eV, the data are fit using an energy-dependent cross section of the form

$$\sigma(E) = \sigma_0 [(E - E_0)/E]^n .\tag{9}$$

In this equation, which has been considered in detail elsewhere [18], E_0 is the threshold energy, σ_0 is an effective cross section independent of energy, and n is a variable parameter. When n equals 2, the data are fit exceptionally well using the literature values for E_0, 3.0 eV for UO^+ and 6.4 eV for UC^+, along with $\sigma_0(UO^+) = 8.6$ Å^2 and $\sigma_0(UC^+) = 1.9$ Å^2. By requiring that $\sigma(E)$ vary as E^{-3} beginning at $D^0(CO)$ and convoluting as described above, the curves plotted in Fig. 4 are obtained. It is interesting to note that the fit to the cross section for UO^+ is noticeably poorer above $E_0(UC^+)$. This is a rather surprising result since it implies that formation of the two products is closely coupled. Ordinarily, these reactions would have been expected to be direct at the elevated kinetic energies necessary for reaction.

Reactions with CO_2

Uranium ions react with CO_2 to form both UO^+ and UO_2^+,

$$U^+ + CO_2 \quad\begin{cases} \longrightarrow UO^+ + CO & (10) \\ \longrightarrow UO_2^+ + C & (11) \end{cases}$$

in an exothermic and endothermic process, respectively, Table II. The results are shown in Fig. 5. It was verified in particular that the UO_2^+ product is formed in a single bimolecular encounter. The peak in the cross section for this product occurs approximately at the thermo-

FIG. 5. Variation in cross section for reactions (10) and (11) as a function of kinetic energy in the center of mass frame (lower scale) and the laboratory frame (upper scale). The dashed line shows the cross section predicted using the LGS model. The arrows mark the bond dissociation energy of CO_2, $D^0(OC\text{-}O) = 5.52$ eV, and the energy required for dissociation to $UO^+ + C + O$ at 8.5 eV. The slopes of the straight line portions of the experimental cross sections are also given.
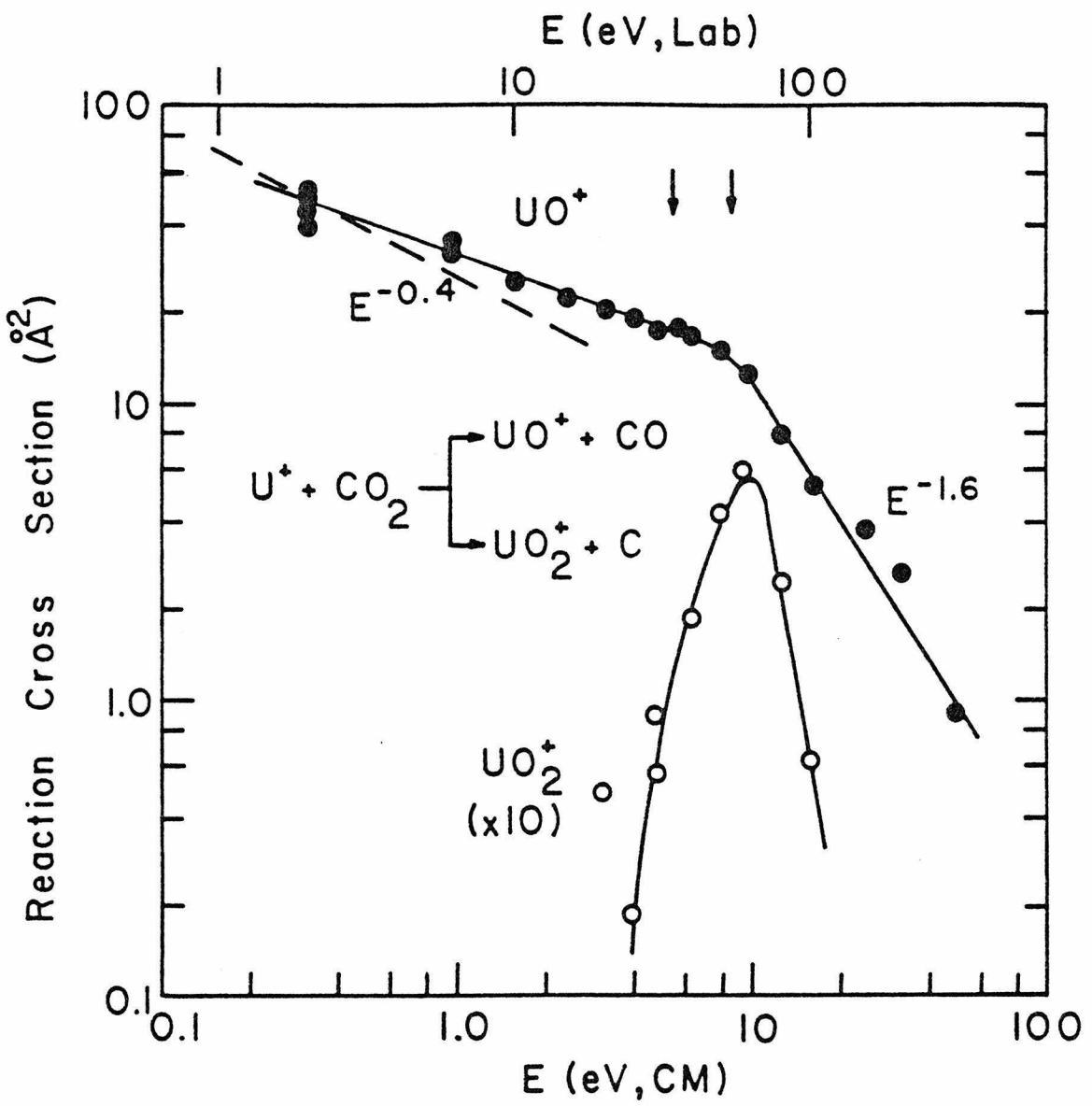
dynamic threshold for dissociation to $UO^+ + O + C$, 8.5 eV. Because reaction (11) is only a minor process in this system, it was difficult to obtain data of sufficient quality to analyze accurately. However, the threshold for this reaction appears to be well above that given in Table II, 0.8 ± 0.4 eV.

The reaction of uranium oxide ions with CO_2,

$$UO^+ + CO_2 \rightarrow UO_2^+ + CO \qquad (12)$$

is calculated to be exothermic by 2.3 eV, Table III. The behavior of the cross section, Fig. 6, however, is more characteristic of an endothermic reaction which suggests a substantial energy barrier. The data are fit using eq. (9) with $\sigma_0 = 7.9$ $\overset{\circ}{A}{}^2$, $E_0 = 1.3 \pm 0.1$ eV, $n = 2$ and by requiring $\sigma(E)$ vary as E^{-2} beginning at 8.9 eV. The curve obtained, convoluted as described above, is plotted in Fig. 6. The background at the lowest energies is again attributed to reaction at higher energies outside the collision chamber.

The reasons for this anomalous behavior are unclear. One possibility, however, is that the ground state reactants and products are not on the same potential energy surface. This is suggested by the fact that ground state CO_2 $(^1\Sigma_g^+)$ dissociates to CO $(X^1\Sigma) + O(^1D)$ rather than to ground state $O(^3P)$ [19]. Because of the many possible states of UO^+ and UO_2^+ [1], it is difficult to detail the states involved in reaction (12). However, UO_2^+ has been observed to undergo collision-induced dissociation with a threshold at the thermodynamic limit [20]. This implies dissociation of UO_2^+ is to ground state $UO^+ + O$ (^3P). Thus, in transferring an oxygen atom from CO to UO^+, a potential

FIG. 6.   Variation in cross section for reaction (12) as a function of
kinetic energy in the center of mass frame (lower scale) and
the laboratory frame (upper scale). The long dashed line
shows the cross section predicted using the LGS model.   The
arrows mark the threshold energy determined empirically,
1.3 eV, and the bond dissociation energy of CO_2, $D^0(OC-O)$ =
5.52 eV. The solid curve is the fit to the data given in the
text and convoluted as discussed. The short dashed line
gives the unconvoluted curve in the threshold region.

$UO^+ + CO_2 \longrightarrow UO_2^+ + CO$

E^{-2}
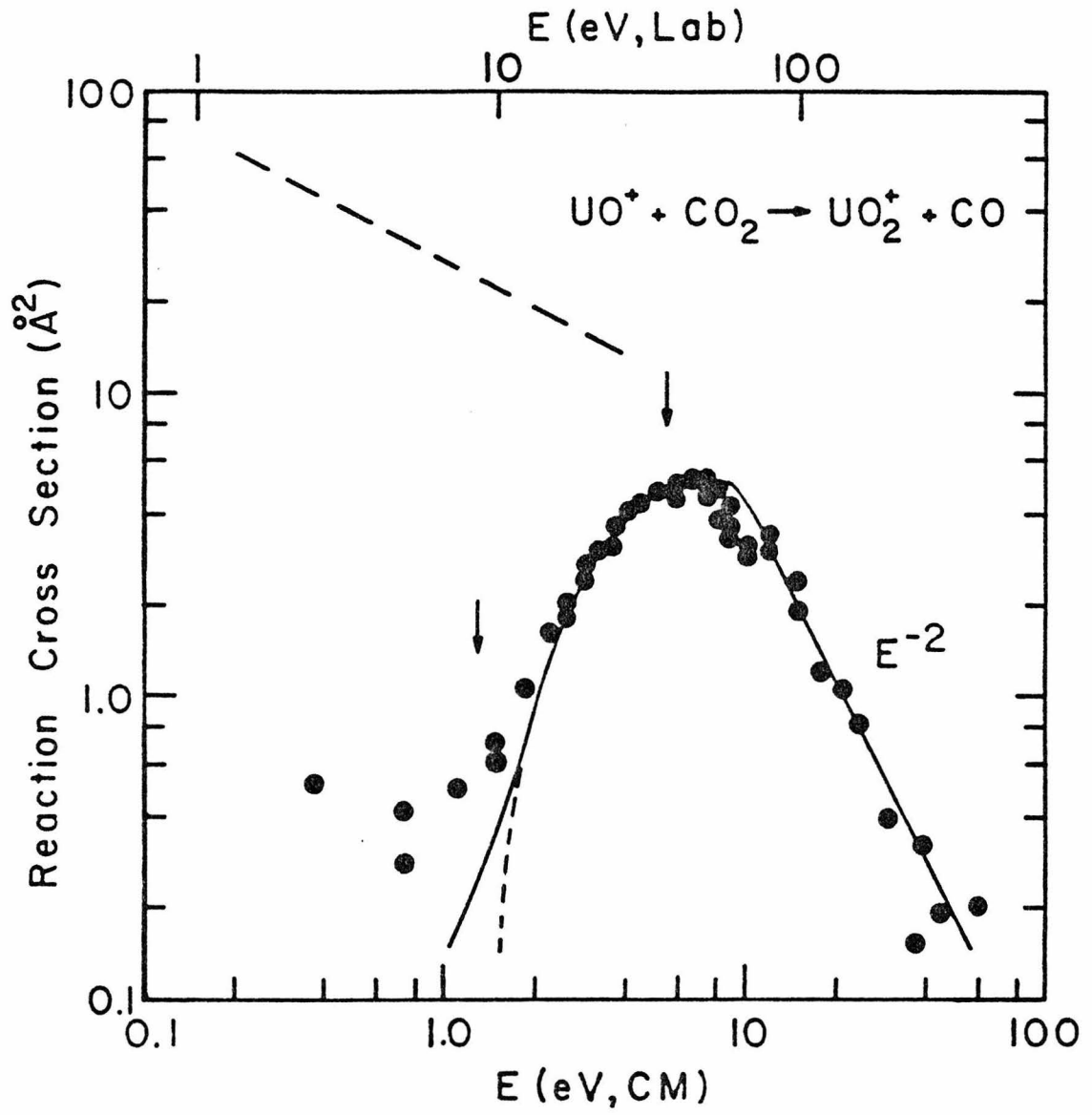
barrier of up to 1.97 eV [21], the excitation energy of the O (^{1}D) state, might be imagined.

It is interesting that an analogous result was obtained for the reaction

$$U + CO_2 \rightarrow UO + CO \tag{13}$$

in crossed neutral beam studies. Although reaction (13) is exothermic by 2.1 eV, the cross section at thermal energies is exceptionally low ($\lesssim 1$ Å^2) compared to that of other oxidants (NO, SO$_2$, O$_2$, and NO$_2$) [22]. It was noted that no correlation between cross sections and reaction exothermixity or electronic state of the reactants could be drawn. A proper explanation would have to also account for the fact that process (10), which is the ionic analog of reaction (13), does not exhibit a barrier to reaction.
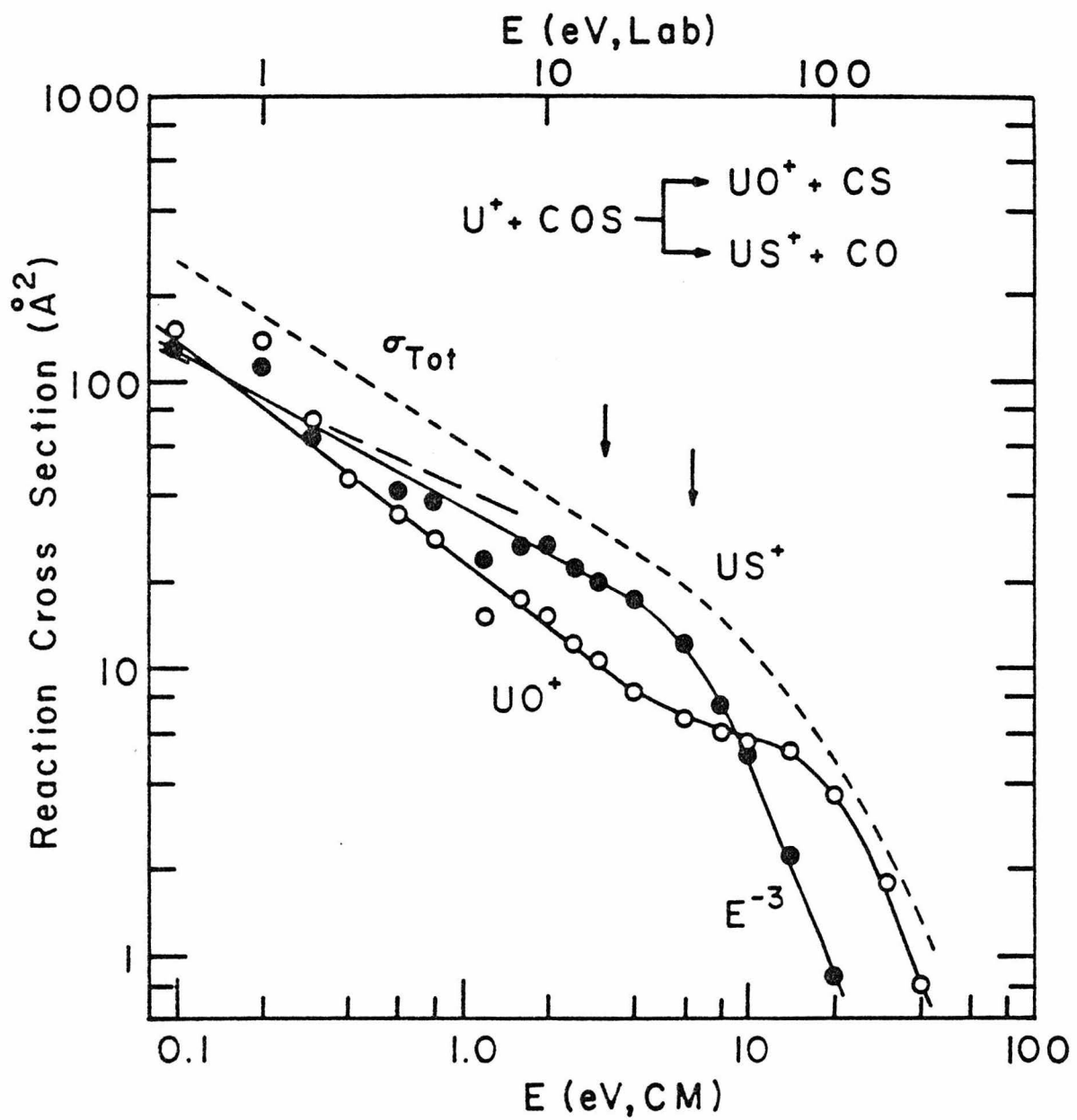
Reactions with COS

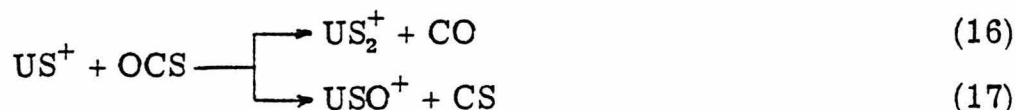Uranium ions react with carbonyl sulfide to yield both US$^+$ and UO$^+$,

$$U^+ + COS \longrightarrow \begin{cases} US^+ + CO & (14) \\ UO^+ + CS & (15) \end{cases}$$
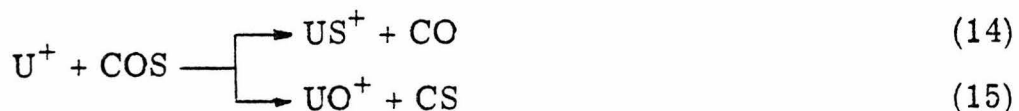
as shown in Fig. 7. The reactions are both observed and predicted to be exothermic (Table II). Also observed are the products, USO$^+$ and US$_2^+$, formed in approximately a 2.7:1.0 ratio at 0.2 eV (CM). Pressure dependence measurements establish that these ions are higher order products formed from reactions of the products of processes (14) and (15),

FIG. 7.   Variation in cross section for reactions (14) and (15) as a
function of kinetic energy in the center of mass frame (lower
scale) and the laboratory frame (upper scale). The dashed
line shows the cross section predicted using the LGS model.
The arrows mark the bond dissociation energies,
$D^{\circ}(OC\text{-}S) = 3.2$ eV and $D^{\circ}(SC\text{-}O) = 6.4$ eV. The slopes of
the straight line portions of the experimental cross sections
are given as well as the total reaction cross section for the
system, σ_{Tot}.

$$US^+ + OCS \longrightarrow \begin{cases} US_2^+ + CO & (16) \\ USO^+ + CS & (17) \end{cases}$$

$$UO^+ + OCS \rightarrow USO^+ + CO. \tag{18}$$

The product UO_2^+ may also be formed in a secondary encounter but is obscured by the primary US^+ product.

The branching ratio for the interaction of uranium ions with COS can be explained qualitatively by two observations. First, formation of US^+, reaction (14) is favored thermodynamically by about 20 kcal/mol, Table II, over formation of UO^+ in reaction (15). Second, carbonyl sulfide has a permanent dipole moment of 0.709 Debye, Table IV, with the oxygen end being most electronegative. Thus, a positive ion will preferentially interact with the oxygen at low enough energies to allow reorientation of the COS molecule. Apparently, these two effects cancel one another at the lowest energies observed and vary differently with kinetic energy to yield an energy-dependent branching ratio. At higher energies, the US^+ product falls off at a lower energy than UO^+. This is explained by noting that the threshold for US^+ product dissociation, 3.2 eV [17], is lower than that for UO^+ dissociation, 6.4 eV [17], where the thresholds correspond to the bond energy of the appropriate bond.

The reactions of uranium oxide ions with COS also yields two products

$$UO^+ + COS \longrightarrow \begin{cases} USO^+ + CO & (19) \\ UO_2^+ + CS. & (20) \end{cases}$$
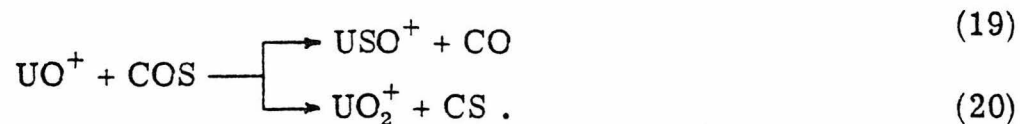
The results are shown in Fig. 8. The observation that reaction (19) is exothermic puts an upper limit on the heat of formation of USO^+ of 134 ± 4 kcal/mol. Reaction (20), in analogy with process (12), exhibits an energy barrier even though exothermic by 1.4 eV, Table III. Interestingly, no such barrier is observed for the abstraction of a sulfur atom, reaction (19). Overall conservation of spin does not seem to be a factor since both CO and CS have $^1\Sigma^+$ ground states [19]. One possibility, in accord with the discussion of process (12), is that the difference in reactivity is a result of the lower energy difference between the ^3P ground state and ^1D excited state of sulfur, 1.15 eV, compared to oxygen, 1.97 eV [21].

Reactions with CS_2

Cross section data for the processes

$$U^+ + CS_2 \rightarrow US^+ + CS \tag{21}$$

and

$$UO^+ + CS_2 \rightarrow USO^+ + CS \tag{22}$$
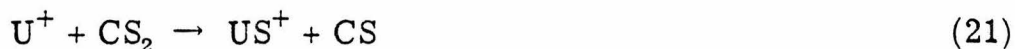
are shown in Fig. 9. The former reaction is calculated to be exothermic, Table II, as observed. The latter reaction, also seen to be exothermic, establishes that $\Delta H^0_{f298} (USO^+) < 114 \pm 9$ kcal/mol, Table I. Also observed in the interaction of U^+ with CS_2 was the secondary process,

$$US^+ + CS_2 \rightarrow US_2^+ + CS. \tag{23}$$

The observation of US_2^+ at low pressures suggests that process (23)
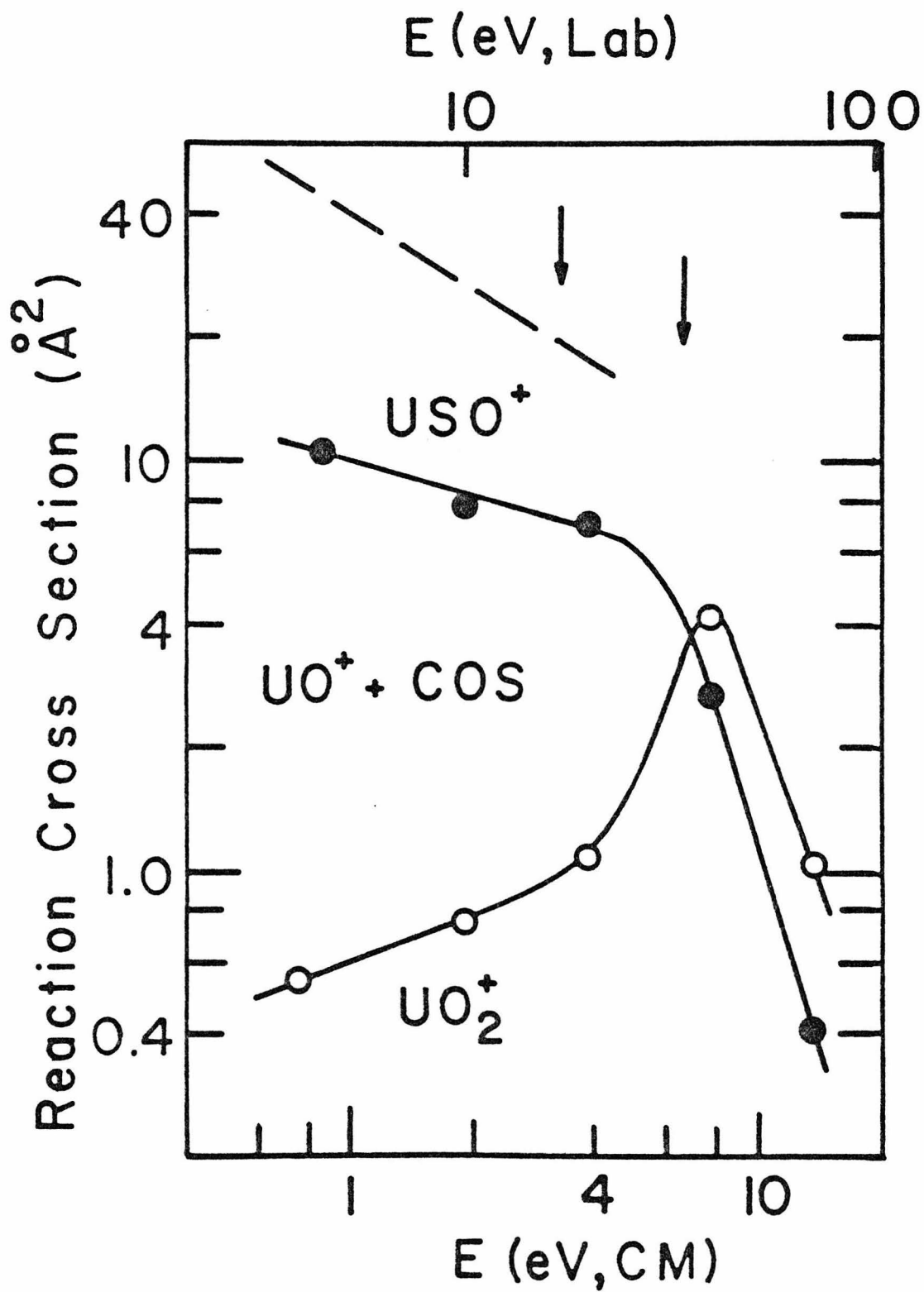
FIG. 8.   Variation in cross section for reactions (19) and (20) as a
function of kinetic energy in the center of mass frame (lower
scale) and the laboratory frame (upper scale). The dashed
line shows the cross section predicted using the LGS model.
The arrows mark the bond dissociation energies,
$D^{0}(OC-S) = 3.2$ eV and $D^{0}(SC-O) = 6.4$ eV.

FIG. 9.   Variation in cross section for reactions (21) and (33) as
a function of kinetic energy in the center of mass frame
(lower scale) and the laboratory frame (upper scale,
approximate). The dashed line shows the cross section
predicted for both systems using the LGS model. The arrow
marks the bond dissociation energy, $D^{0}(SC-S)$ = 4. 0 eV.
The slopes of the straight line portions of the experimental
cross sections are also given.
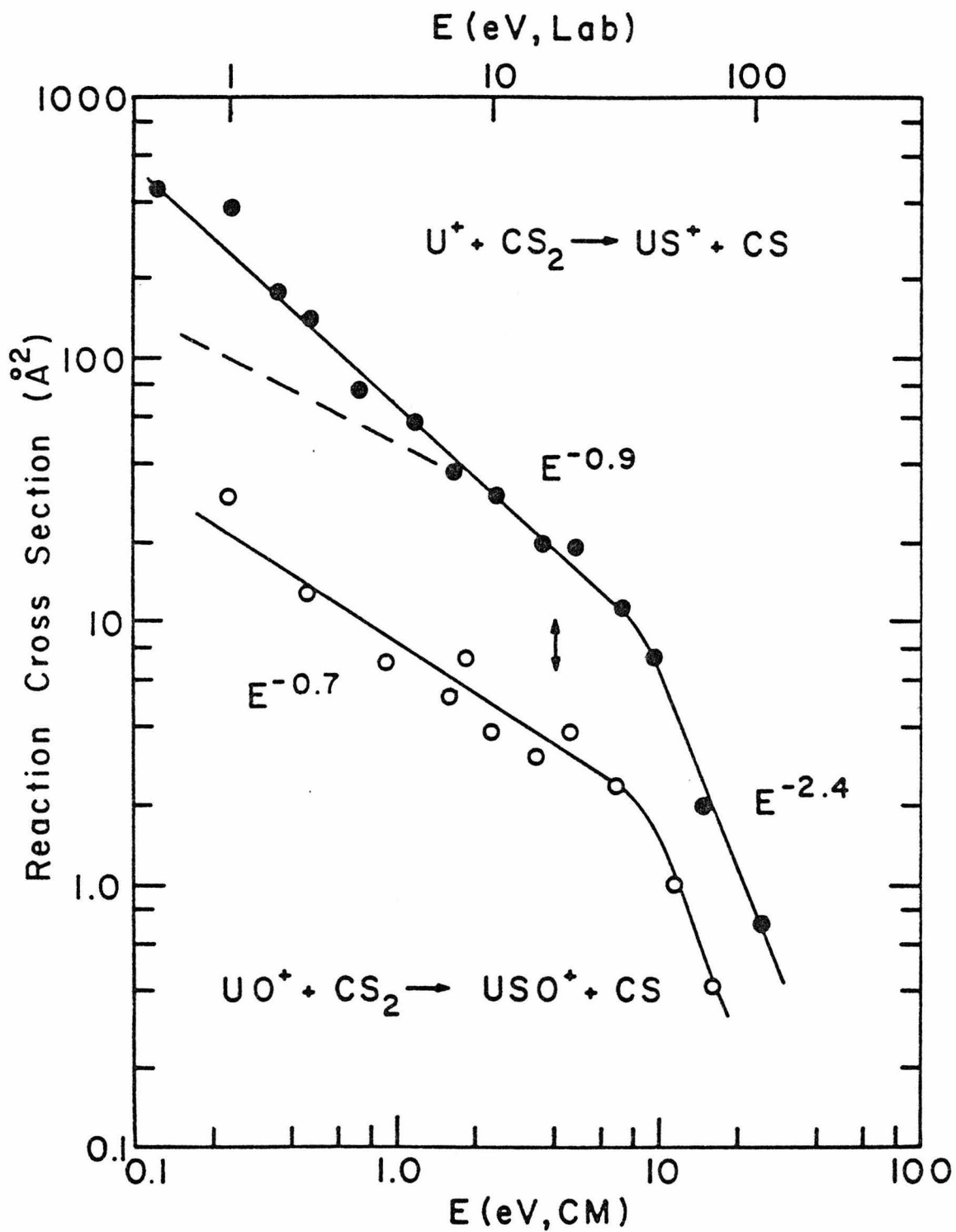
exhibits the large cross section characteristic of an exothermic process. If this is the case, then an upper limit of 175 ± 21 kcal/mol is established for $\Delta H^{\circ}_{f, 298}$ (US_2^+), Table I.

It was of particular interest to see if uranium oxide ions would exchange atoms with carbondisulfide

$$UO^+ + CS_2 \rightarrow US^+ + COS . \tag{24}$$

No evidence of this reaction was observed. Assuming this to be a consequence of the thermodynamics involved, the heat of formation for the uranium monosulfide ion must be greater than 202 ± 4 kcal/mol, in reasonable agreement with the literature values, Table I.
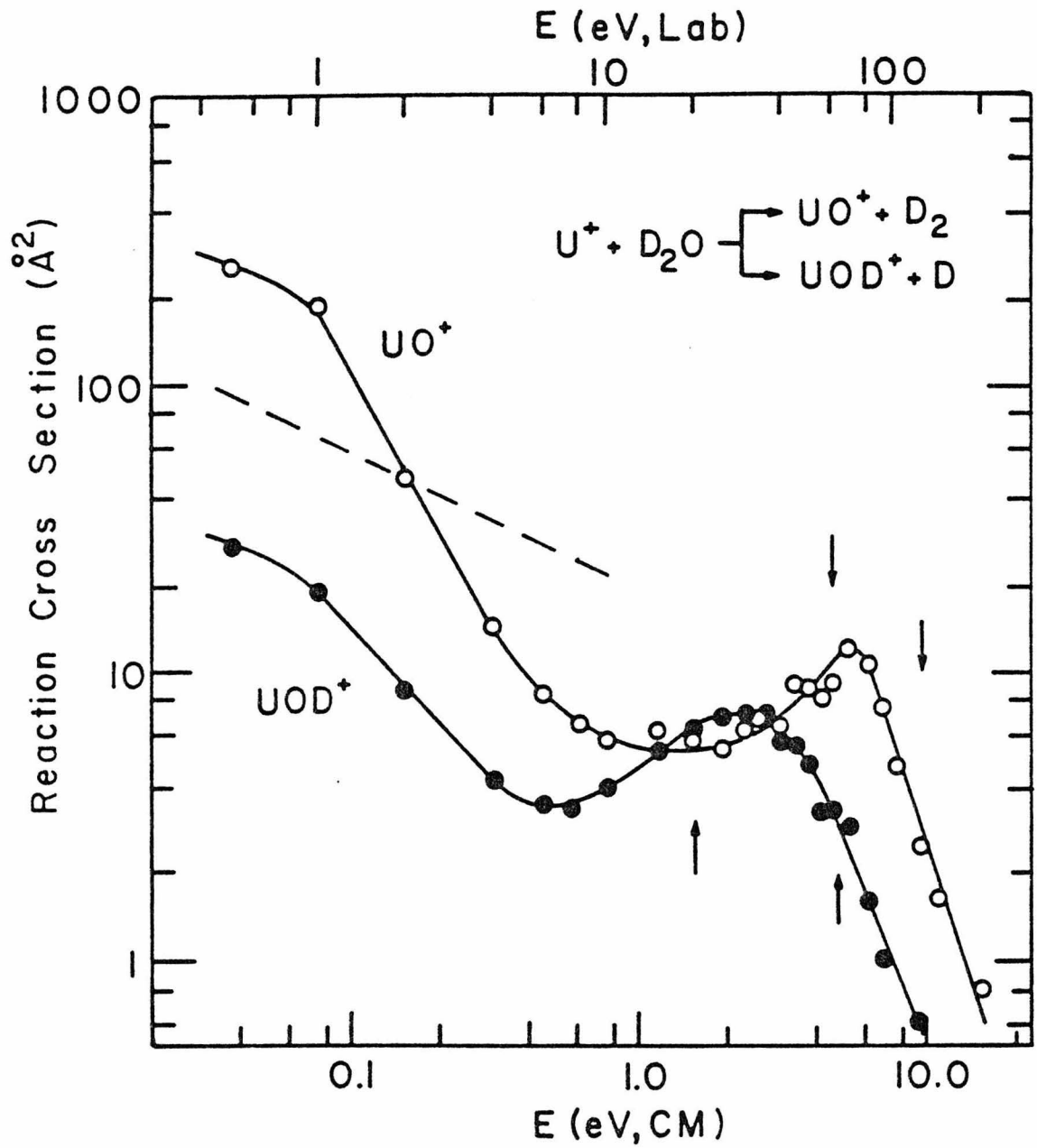
Reactions with D_2O

Uranium ions react with water to yield both uranium oxide ions and deuterated uranium oxide,

$$U^+ + D_2O \longrightarrow \begin{cases} UO^+ + D_2 \\ UOD^+ + D . \end{cases} \tag{25}$$
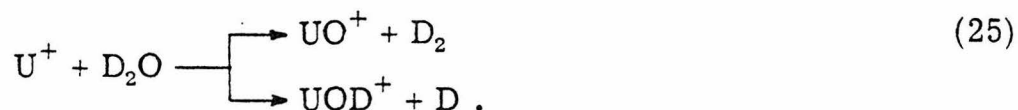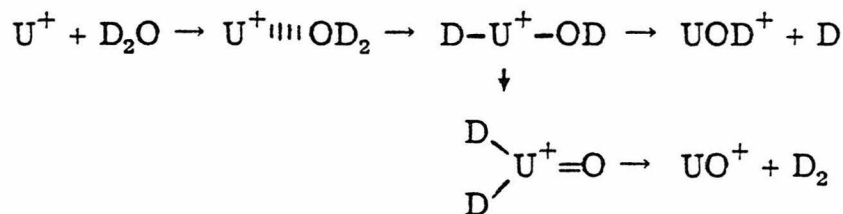
D_2O was used as the reactant to facilitate resolution of the products. The results are shown in Fig. 10. The product, UD^+, which should be formed in a process endothermic by 2.3 eV, was not examined. This process has been previously investigated by Moreland, Rokop and Stevens [7].

The behavior of the cross sections for the U^+-D_2O system is rather complex although not unique [23]. We can imagine that the reaction takes place with the mechanism

FIG. 10. Variation in cross section for reactions (25) and (26) as a
function of kinetic energy in the center of mass frame
(lower scale) and the laboratory frame (upper scale). The
dashed line shows the cross section predicted using the
LGS model. The arrows pointing up mark the thermo-
dynamic thresholds for production of $UO^+ + 2D$, 1.5 eV,
and of $U^+ + OD + D$, 5.2 eV. The arrows pointing down
mark the thresholds for production of $U^+ + O + D_2$, 5.1 eV,
and $U^+ + O + 2D$, 9.6 eV.

$$U^+ + D_2O \rightarrow U^{+\text{IIII}}OD_2 \rightarrow D\text{-}U^+\text{-}OD \rightarrow UOD^+ + D$$

$$\begin{array}{c} D \\ \diagdown \\ \diagup \\ D \end{array} U^+ = O \rightarrow UO^+ + D_2$$

It seems likely that both products proceed through a common intermediate, DU^+OD. Since the UO^+ product predominates at the lowest bond energies, this reaction pathway is probably preferred thermodynamically. However, the bond fission process yielding UOD^+ should have a higher frequency factor [24] and thus competes more effectively as the energy is raised. At still higher energies, a new mechanism corresponding to a direct reaction having a small energy barrier, $\lesssim 10$ kcal/mol, is proposed to account for the increase in UOD^+ formation. The peak of the cross section for UOD^+ at higher energies correlates well with the threshold for dissociation to UO^+ and D, 1.5 eV, rather than to $U^+ + OD$, 5.2 eV. The cross section for UO^+ also increases in this region, peaking at about the energy for dissociation to $U^+ + O + D_2$, 5.1 eV.

Since reaction (26) is exothermic, $\Delta H^0_{f, 298}(UOH^+)$ must be less than 158 ± 3 kcal/mol, neglecting zero point energy differences. If we also assume that the heat of reaction for process 26 is greater than that for process 25, as seems likely, then $\Delta H^0_{f, 298}(UOH^+) >$ 89 ± 10 kcal/mol. From these limits, a proton affinity of uranium monoxide can be calculated to be between 218 ± 7 kcal/mol and 287 ± 14 kcal/mol. This seems reasonable when compared to the proton affinity of uranium, 238 ± 5 kcal/mol [3, 4].

The reactions

$$UO^+ + D_2O \longrightarrow \begin{cases} UO_2^+ + D_2 & (27) \\ UO_2D^+ + D & (28) \end{cases}$$
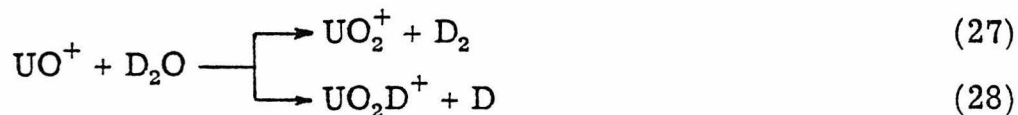
were not studied extensively, however, it was established that both reactions are exothermic. Formed in approximately equal amounts at the lowest energies, ~ 0.1 eV (CM), the predominant product at higher energies is UO_2D^+. Following the analysis used above, the exothermicity of reaction (28) requires $\Delta H^0_{f, 298}(UO_2D^+) < 30 \pm 4$ kcal/mol. A lower limit on the proton affinity of UO_2 is then 232 ± 7 kcal/mol.

Conclusion

Several general observations can be made about the reactions investigated in the present study. The general behavior of the cross sections as a function of energy is quite similar for the various systems. For exothermic reactions, the cross sections decrease slowly with energy, as $E^{-\frac{1}{4}}$ to E^{-1}, at the lowest energies. At higher energies, the dependence is stronger, varying as E^{-1} to E^{-3}. A dependence of $E^{-5.5}$, predicted by Bates, Cook and Smith for energies $\gtrsim 100$ eV (Lab) [25], is not observed. For endothermic reactions and reactions with a barrier, the cross section rises rapidly to a peak and falls off very much like the high energy portion of the exothermic reactions. The peak in the endothermic reactions and the break in the linear portions of the cross sections for exothermic reactions correlate reasonably well with the bond dissociation energy of the neutral bond broken during reaction. Since this energy is the thermodynamic

threshold for product dissociation, the sharp decrease in cross section at higher energies seems attributable to formation of product with sufficient internal energy to decompose.

While generally within an order of magnitude of the absolute cross sections measured, the Langevin-Gioumousis-Stevenson (LGS) model predictions are not in consistent quantitative accord with the present experiments. At low energies, the cross sections rarely follow the $E^{-\frac{1}{2}}$ law but vary as $E^{-\frac{1}{4}}$ to E^{-1}. The unrestricted use of this model has been criticized by Henchman [26] and the present results are another case where inadequacies are exhibited.

It is of interest to speculate, however, on the reasons for the failure of the LGS model. In several instances, elaboration of the LGS model to include quadrupole [26], induced quadrupole and dispersion effects [27] may result in reasonable quantitative agreement. Certainly, for the reactions with COS and H_2O, interactions involving the permanent dipoles of these molecules should be considered [28]. The large differences in reactivity exhibited by U^+ versus UO^+ for the same reactant gas, e.g., Fig. 9, may simply be a consequence of a steric factor. Namely, uranium oxide ions react preferentially when the uranium end approaches the reactant molecule.

Examination of crude potential energy surfaces for several of the reactions is also enlightening. Reaction coordinate energy diagrams are shown in Fig. 11 for the reactions of U^+ and UO^+ with O_2, processes (5) and (6). While the exothermicities of the reactions are similar, 2.9 eV and 2.6 eV, respectively, the potential wells corresponding to the reaction intermediates differ greatly. Such a

FIG. 11. Qualitative reaction coordinate diagrams for the reactions of (a) U^+ with O_2 and (b) the reaction of UO^+ with O_2.

(a)

$U^+ + O_2$

$UO^+ + O$

$10.7\ eV$

$7.8\ eV$

UO_2^+

(b)

$UO^+ + O_2$

$3.7\ eV$

$UO_2^+ + O$

$1.1\ eV$

UO_3^+
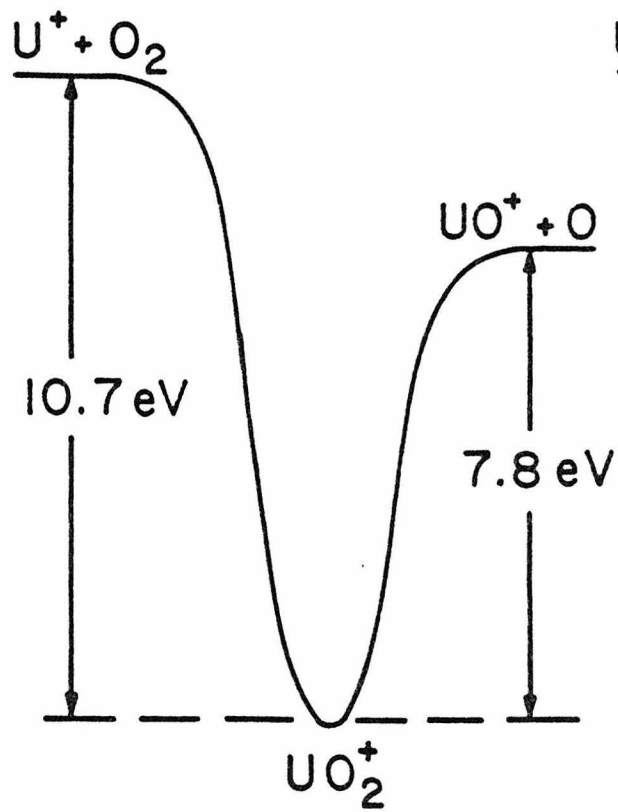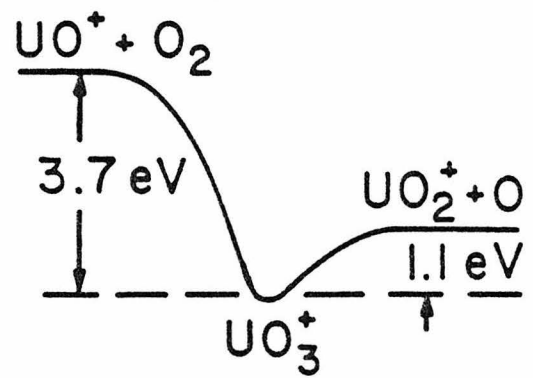
deep well as that for UO_2^+ should greatly influence the reaction dynamics and may explain the rather large cross section observed for reaction (5), Fig. 2. The surface for reaction (6) is more typical and indeed the behavior shown in Fig. 3 is substantially more like the LGS prediction.

Acknowledgment

References

[1] W. L. Fite, H. H. Lo and P. Irving, J. Chem. Phys. 60 (1974) 1236; T. A. Patterson, M. W. Siegel and W. L. Fite, J. Chem. Phys. 69 (1978) 2163; W. L. Fite, H. H. Lo and P. Vasu, Abstracts, IXth International Conference on the Physics of Electronic and Atomic Collisions, Seattle, 24-30 July 1975; M. W. Siegel and W. L. Fite, ibid.

[2] C. E. Young, P. M. Dehmer, R. B. Cohen, L. G. Pabo and S. Wexler, J. Chem. Phys. 64 (1976) 306.

[3] P. Armentrout, R. Hodges and J. L. Beauchamp, J. Am. Chem. Soc. 99 (1977) 3162.

[4] P. B. Armentrout, R. V. Hodges and J. L. Beauchamp, J. Chem. Phys. 66 (1977) 4683.

[5] J. L. Beauchamp, J. Chem. Phys. 64 (1976) 929.

[6] R. N. Compton, J. Chem. Phys. 66 (1977) 4478.

[7] P. E. Moreland, D. J. Rokop and C. M. Stevens, Int. J. Mass Spectrom. Ion Phys. 5 (1970) 127.

[8] R. Johnsen and M. A. Biondi, J. Chem. Phys. 57 (1972) 1975.

[9] P. B. Armentrout and J. L. Beauchamp, J. Chem. Phys., submitted.

[10] G. R. Hertel, J. Chem. Phys. 47 (1967) 133.

[11] J. B. Mann, J. Chem. Phys. 40 (1964) 1632.

[12] R. V. Hodges, P. B. Armentrout and J. L. Beauchamp, Int. J. Mass Spectrom. Ion Phys. 29 (1979) 375.

[13] P. J. Chantry, J. Chem. Phys. 55 (1971) 2746.

References (continued)

[14] H. W. Werner, Int. J. Mass Spectrom. Ion Phys. 14 (1974) 189.

[15] I. Szabo, Int. J. Mass Spectrom. Ion Phys. 3 (1969) 169.

[16] G. Gioumousis and D. P. Stevenson, J. Chem. Phys. 29 (1958) 294.

[17] Calculated using JANF Thermochemical Tables, Natl. Stand. Ref. Data Ser. Natl. Bur. Stand. 37 (1971), and supplements; J. Phys. Chem. Ref. Data 3 (1974) 311, 4 (1975) 1, 7 (1978) 797.

[18] P. B. Armentrout and J. L. Beauchamp, J. Chem. Phys., submitted.

[19] G. Herzberg, "Molecular Spectra and Molecular Structure III" Van Nostrand, N.Y. 1966.

[20] P. B. Armentrout and J. L. Beauchamp, Chem. Phys., submitted.

[21] C. E. Moore, Atomic Energy Leveles, Natl. Bur. Stand., Washington, D.C. 1949.

[22] N. C. Lang and R. C. Stern, ACS Conf., Honolulu, Hawaii, 1979.

[23] C. Lifshitz, R. L. C. Wu and T. O. Tiernan, J. Am. Chem. Soc., 100 (1978) 2040.

[24] P. J. Robinson and K. A. Holbrook, "Unimolecular Reactions" Wiley-Interscience, N.Y., 1972, p. 155.

[25] D. R. Bates, C. J. Cook and F. J. Smith, Proc. Phys. Soc. 83 (1964) 49.

[26] M. Henchman, "Ion-Molecule Reactions", ed. J. L. Franklin, Plenum, N.Y., 1972, p. 101.

[27] R. C. Dunbar, J. Chem. Phys. 47 (1967) 5445.

[28] M. T. Bowers and T. Su, "Interactions of Ions and Molecules" Ed. Pierre Ausloos, Plenum, N.Y., 1974, p. 163.

CHAPTER III

COLLISION-INDUCED DISSOCIATION OF UO^+ AND UO_2^+

COLLISION-INDUCED DISSOCIATION OF UO^+ and UO_2^+

P. B. ARMENTROUT and J. L. BEAUCHAMP

Arthur Amos Noyes Laboratory of Chemical Physics,
California Institute of Technology, Pasadena, California 91125, USA

(Received   )

Abstract

Collision-induced dissociation (CID) of uranium monoxide ion and uranium dioxide ions impacting on argon has been studied. The CID cross section for production of U^+ and UO^+, respectively, has been measured at relative kinetic energies ranging from threshold to 70 eV. No appreciable amounts of other products were observed. The thresholds observed in these studies agree within experimental error with the bond dissociation energies of uranium monoxide ion, $D_0^0(U^+-O) = 8.0$ eV, and uranium dioxide ion, $D_0^0(OU^+-O) = 7.7$ eV. The CID cross section for UO^+ reaches a maximum at about 20 eV and falls off as E^{-4} at higher energies, where E is the relative kinetic energy. In the UO_2^+ system, the maximum cross section occurs at about 14 eV beyond which it decreases as $E^{-2.8}$.

Introduction

Collision-induced dissociation (CID) at low kinetic energies (less than a kilovolt) has been examined both theoretically [1, 2, 3b] and experimentally [3-8]. The form for the CID cross section derived from statistical considerations has been shown to give good agreement with experimental results for energies up to 1 eV above threshold [1, 3]. In this paper, the CID of UO^+ and UO_2^+ impacting on argon is studied. CID cross sections are obtained at relative kinetic energies ranging from threshold to 70 eV for the reactions

$$UO^+ + Ar \rightarrow U^+ + O + Ar \qquad (1)$$

and

$$UO_2^+ + Ar \rightarrow UO^+ + O + Ar . \qquad (2)$$

Experimental

The ion beam apparatus shown in Fig. 1 is a highly modified version [9] of an instrument previously described [10]. Ions from a surface ionization source are accelerated and focused into a 60° sector magnet which can easily resolve uranium ions and the uranium oxide ions. This mass selected beam is decelerated and focused into a collision chamber, maintained at a field free interaction region, containing the reactant gas. Pressure of the gas, measured using an MKS Baratron 90H1, is $6-10 \times 10^{-3}$ Torr for these experiments. Product ions scattered in the forward direction are focused into a quadrupole mass filter and detected using a Channeltron electron

Fig. 1. Schematic diagram of the ion-beam apparatus.
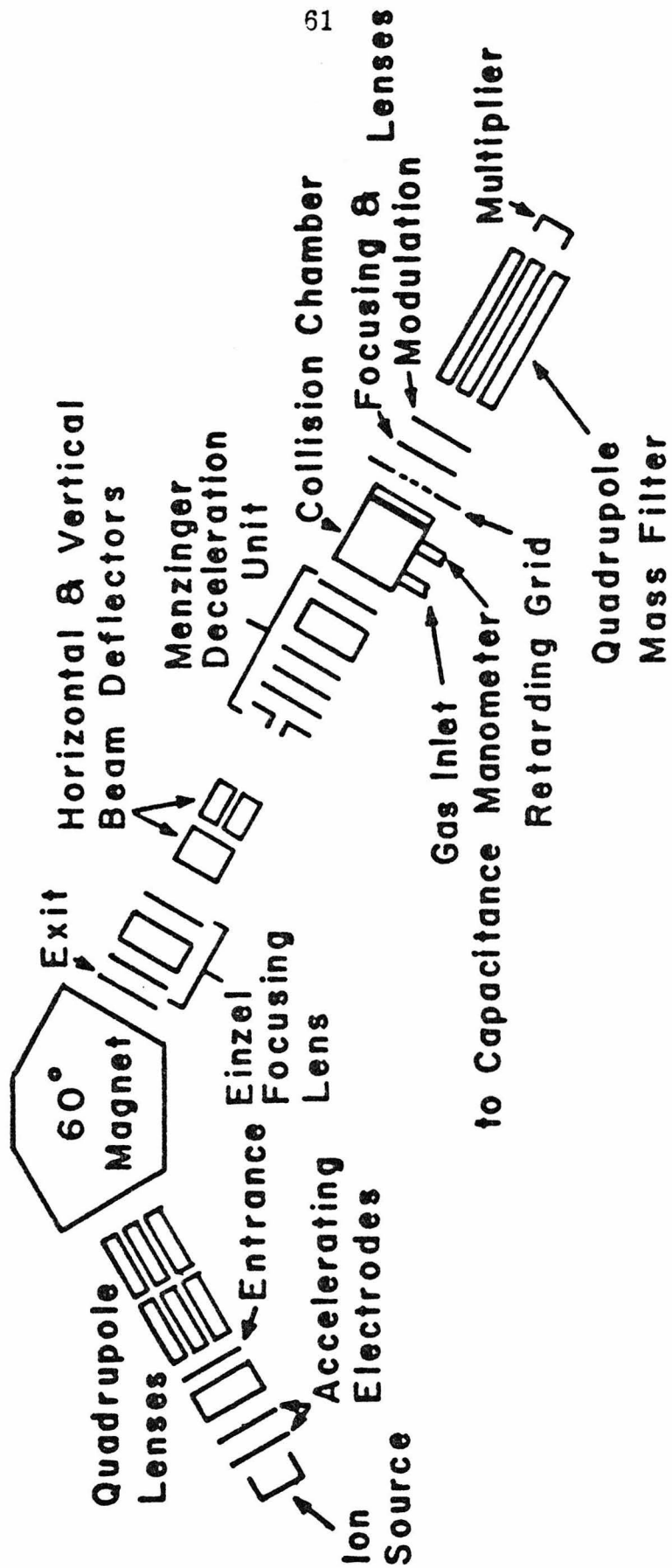
multiplier operated in a pulse counting mode.

The UO^+ and UO_2^+ ions are obtained by making a slurry of uranyl acetate, $UO_2(C_2H_3O_2)_2 \cdot 2H_2O$, in nitric acid. This slurry is put in a coil of rhenium wire. By resistively heating this coil to an estimated 1500° K, large amounts of UO_2^+, UO^+ and U^+ are produced with UO_2^+ predominating. At higher filament temperature, the main ion produced is UO^+. It is expected that several low-lying electronic states of UO^+ and UO_2^+ exist [11] which may be thermally populated at the temperature of the ionizing filament. No attempt is made in the present work to account for the presence of excited states.

The energy of the ion beam is taken nominally as the difference in potential between the collision chamber and the center of the filament, the latter being determined by a resistive divider. This energy is verified by use of a retarding field energy analyzer. Agreement is always within 0.3 eV. The energy width of the UO^+ and UO_2^+ beams is estimated as 0.7 eV (FWHM). In the center of mass frame, this introduces a negligible uncertainty of ± 0.05 eV in the interaction energy.

A more severe problem concerning the actual energy of interaction is the effect of thermal motion of the reactant gas. Using the analysis of Chantry [12], we can calculate that the distribution of the relative kinetic energy at a nominal energy E due to this effect has a full width at half-maximum of approximately 0.5 $E^{\frac{1}{2}}$ eV for the present experiments. This energy distribution prevents observation of any sharp features in the excitation function, including threshold. To account for this effect, the proposed excitation function is convoluted

with the distribution before comparison with the data using the procedure outlined by Chantry [12].

The CID cross section is calculated using

$$I = (I_P + I_R)[1 - \exp(-n\sigma\ell)] \tag{3}$$

which relates the cross section, σ, the length of the interaction region, ℓ (= 5 mm), and the density of the target gas, n, to the measured intensities of the product and reactant ions, I_P and I_R, respectively. The greatest uncertainty in these measurements is the ion detection efficiency. In our apparatus, if reaction of an on-axis ion occurs in the entrance aperture (1.0 mm diameter) it will exit the chamber if the laboratory scattering angle is less than 8.5° (exit aperture, 1.5 mm diameter). Approximate calculations show the maximum laboratory scattering angle of the uranium containing products to be on the order of 8° at several hundred eV and smaller near threshold. This efficient detection is the consequence of the appreciable center of mass velocity which requires the heavy products be scattered in the forward direction in the laboratory frame. Other product ions however, may not be efficiently collected.

Results and Discussion

The only significant product observed for dissociation of UO^+ impacting on argon is the uranium ion, reaction 1. The excitation function measured is shown in Fig. 2. Likwise, uranium oxide ions formed in process 2 are the only appreciable products observed for the UO_2^+-Ar system. The results are shown in Fig. 3. Both CID

Fig. 2. Variation in cross section for reaction 1 with kinetic energy in the center of mass frame (lower scale) and laboratory frame (upper scale). The arrow labeled, E_0, shows the thermodynamic threshold for the process, 8.0 eV. Other arrows indicate thresholds for alternate reactions of UO^+ with Ar listed in Table I. The curve below 19 eV is the fit to the data given inthe text and convoluted as discussed. The rest of the curve is an approximate fit to the data which varies as E^{-4} above 27 eV.
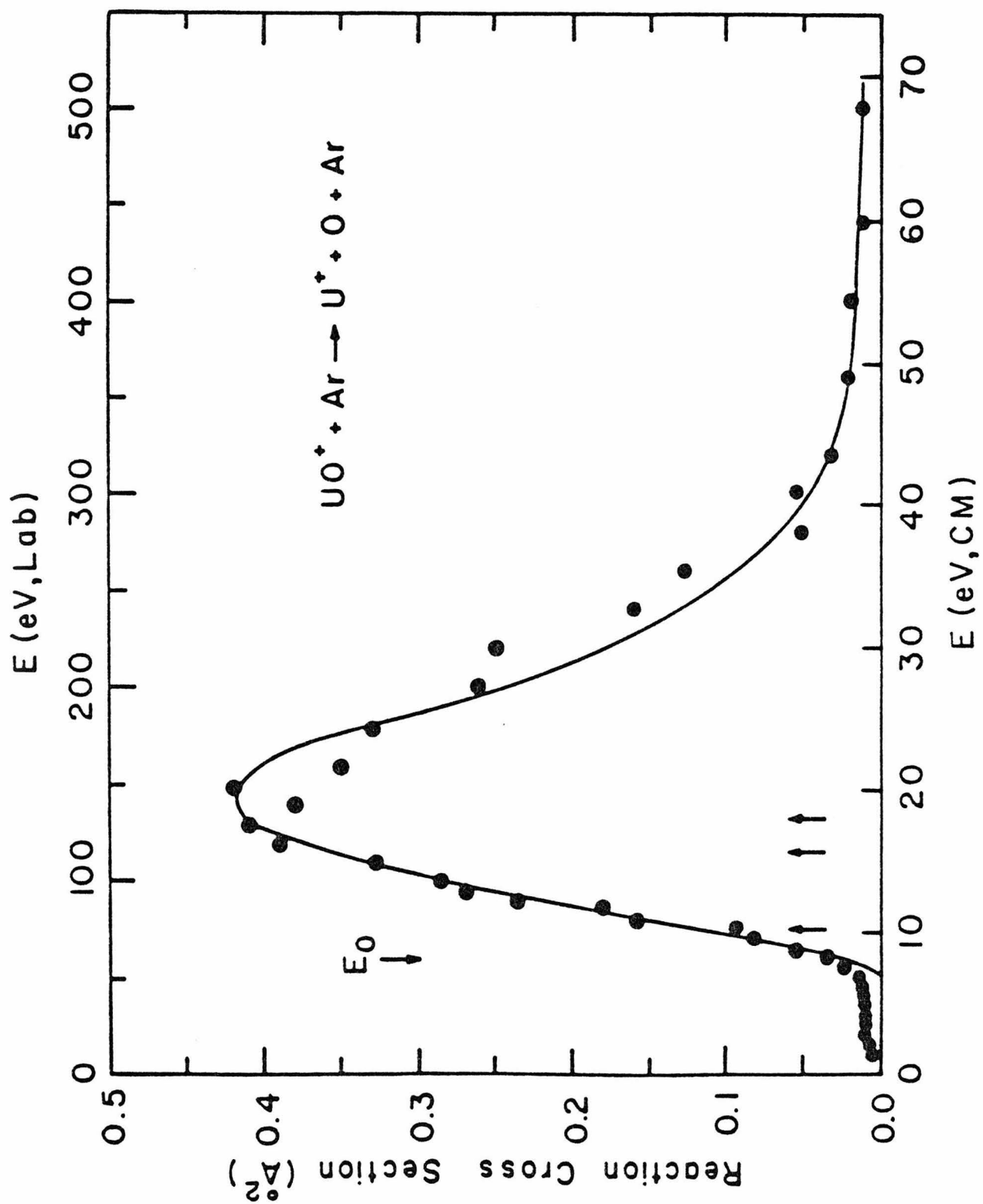
Fig. 3. Variation in cross section for reaction 2 with kinetic energy
in the center of mass frame (lower scale) and laboratory
frame (upper scale). The arrow labeled, E_0, shows the
thermodynamic threshold for the process, 7.7 eV. Other
arrows indicate thresholds for alternate reactions of UO_2^+
with Ar listed in Table I. The curve below 14 eV (dashed
line) is the fit to the data given in the text and convoluted as
disucssed. The full line includes an approximate contri-
bution from sequential bimolecular collisions having a
threshold at 3.6 eV (one half 7.2 eV) and a value for
$A = 0.15 \overset{\circ}{A}{}^2$. The curve given above 14 eV is an approximate
fit to the data which varies as $E^{-2.8}$ above 18 eV.

$UO_2^+ + Ar \longrightarrow UO^+ + O + Ar$
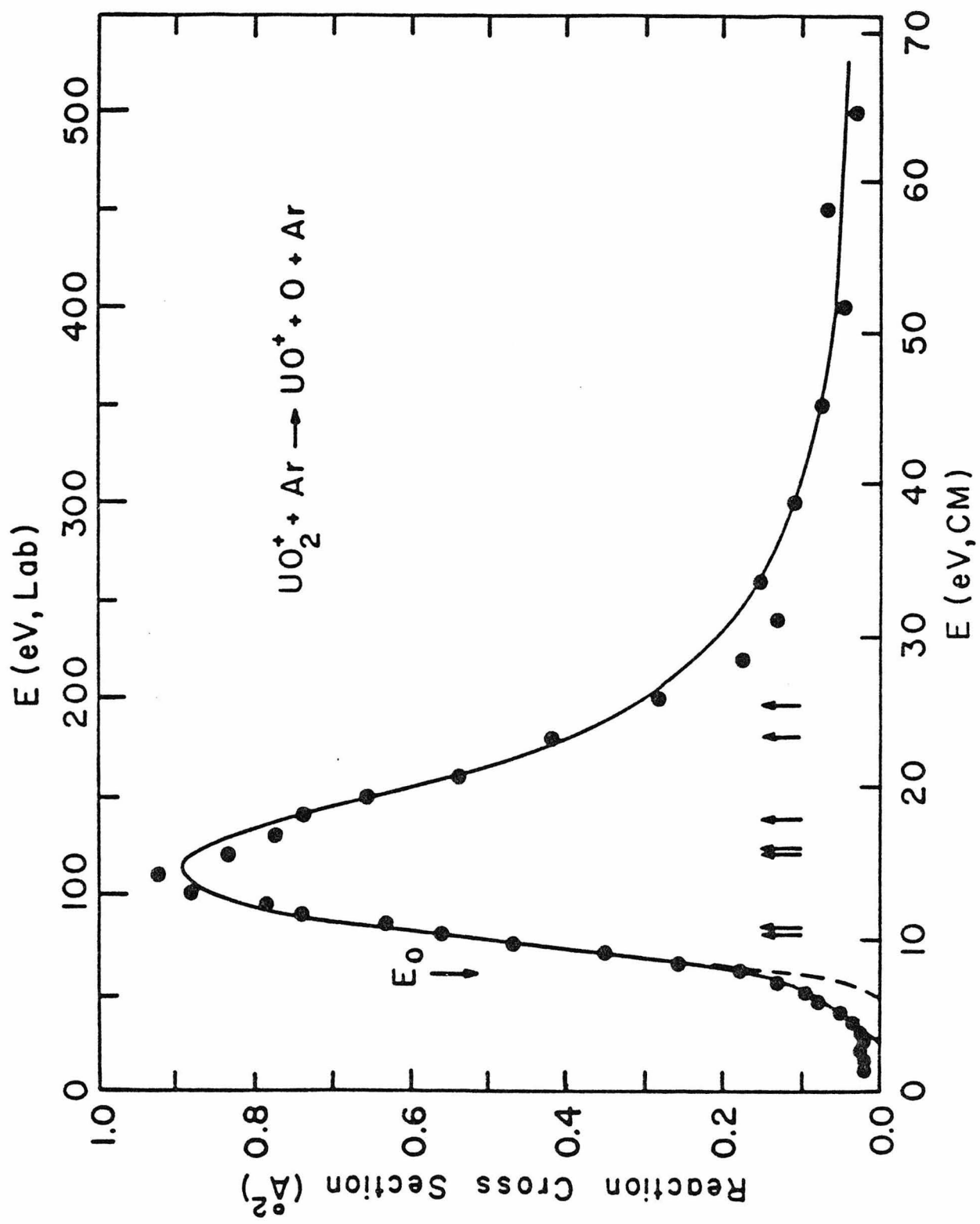
processes have thresholds located approximately at the dissociation energy of the bond being broken (Table I). The cross sections rise until an energy about twice that of threshold and then fall slowly with increasing energy. It is of interest to note that the absolute cross section for CID of UO_2^+ is approximately twice that of UO^+. Classical arguments [3, 13] demonstrate that collisions between an argon atom and the uranium end of UO^+ transfer little energy ($\Delta E/E = 0.036$) while collision with the oxygen end results in efficient energy transfer ($\Delta E/E = 0.89$). Thus, twice as many orientations lead to efficient energy transfer for UO_2^+ as for UO^+.

Statistical theory [2, 3] has shown that the cross section for CID should have the form

$$\sigma = A(E_T - E_0)^n/E \tag{4}$$

where E is the initial relative kinetic energy, E_0 is the threshold for dissociation, and E_T is the total energy available for reaction including any internal energy of the reactants, E_I. The coefficient, A, can generally depend on both E and E_I. An attempt was made to determine the dependence of A on E_I by varying the ionizing filament temperature. However, the range of temperatures which produces a usable ion beam is too narrow to give meaningful results. In the following analysis, A will be assumed to be a constant, the dependence on E being absorbed by variations in n.

As suggested by Rebick and Levine [2c], the parameters of eq. 4 may be determined without prior assumption by plotting $\sigma E/[d(\sigma E)/dE]$

vs. E. This gives a straight line with a slope of $1/n$ and an energy axis intercept of $E_0' = (E_0 - E_I)$. For the UO^+ system, we obtain $n = 1.2 \pm 0.1$, $E_0' = 7.9 \pm 0.3$ eV and $A = 0.47 \, \mathring{A}^2 \, eV^{(1-n)}$. For the UO_2^+ system, we find $n = 1.1 \pm 0.1$, $E_0' = 7.2 \pm 0.3$ eV and $A = 1.65 \, \mathring{A}^2 \, eV^{(1-n)}$. These functions, convoluted as discussed above are plotted in the low energy regions of Figs. 2 and 3. The values for E_0' differ from the appropriate bond dissociation energies, $D_0^0(U^+-O) = 8.0 \pm 0.3$ eV and $D_0^0(OU^+-O) = 7.7 \pm 0.4$ eV, by 0.1 and 0.5 eV, respectively. Since at a filament temperature of $1500°$K, $kT \sim 0.13$ eV, many vibrational, rotational, and electronic states are populated, it seems reasonable that the observed CID threshold is lower than the thermodynamic limit. The more pronounced effect in the case of UO_2^+, could simply be due to the fact that the triatomic has more internal degrees of freedom than UO^+.

The values for n obtained are lower than the typical range of 1.5 to 3 [3,5]. This may reflect the fact that data are considered which are outside the energy range where eq. 4 is supposed to apply (~ 1 eV above threshold). Higher values of n would give higher apparent internal energies. However, this could be compensated for by a dependence of A on E_I.

Previous examinations of CID at low energies have seldom considered energies significantly above threshold. An exception is the study by Piper et al. [14]. They found the cross sections for dissociation to ion-pairs of CsBr by Ar and Xe and NaBr by Ar remained approximately constant at high energies. This behavior contrasts with the marked decrease in CID cross sections as a

function of energy seen in the systems studied here. Other studies [5] have observed an apparent peak in the CID cross section but the data are not reported at energies very much higher than where the peak occurs. Several possible explanations for the decrease in cross section suggest themselves. Experimentally, excessive scattering at the higher energies could reduce the efficiency of collecting product ions. As discussed above, however, calculations suggest that this would not account for the dramatic decrease in cross section observed.

Another explanation is that alternate reaction pathways become the predominant dissociation channels. Some of these alternate processes are listed in Table I with their thermodynamic thresholds. These thresholds, indicated on Figs. 2 and 3, are in the right energy region to possibly account for the decrease in cross section. Although no appreciable amounts of other products are observed, as noted above, the detection efficiency of these ions is suspect.

A third explanation involves the influence of chattering collisions. In this type of event, an argon atom collides with the oxygen end of UO^+ or UO_2^+. The relatively light oxygen atom can then rebound back and forth between the uranium and argon atoms eventually transferring energy back to translational energy of Ar. Theoretical studies [15,16] indicate that such events can greatly affect the energy transferred during collision. Indeed, they suggest the energy transfer efficiency will peak for appropriate mass combinations. It is pertinent to note that such multiple collision events are not as likely in the systems studied by Piper et al. [14] as in the systems examined here.

Table I

Thermochemistry of reactions of UO^+ and UO_2^+ with Ar

Reaction[a]		$\Delta H_r(eV)$[b]
$UO^+ + Ar$	$\rightarrow U^+ + O + Ar$	8.0 ± 0.3
	$\rightarrow UO + Ar^+$	10.04 ± 0.06
	$\rightarrow U + O^+ + Ar$	15.4 ± 0.3
	$\rightarrow U + O + Ar^+$	17.6 ± 0.3
$UO_2^+ + Ar$	$\rightarrow UO^+ + O + Ar$	7.7 ± 0.4
	$\rightarrow UO_2 + Ar^+$	10.3 ± 0.1
	$\rightarrow U^+ + O_2 + Ar$	10.7 ± 0.4
	$\rightarrow UO + O^+ + Ar$	15.6 ± 0.4
	$\rightarrow U^+ + 2O + Ar$	15.8 ± 0.4
	$\rightarrow UO + O + Ar^+$	17.8 ± 0.5
	$\rightarrow U + O + O^+ + Ar$	23.2 ± 0.4
	$\rightarrow U + 2O + Ar^+$	25.3 ± 0.4

[a]All reactions are for ground state species only.

[b]Values derived using Table II.

Table II

Thermochemical Data

Species	$\Delta H^{\circ}_{f,0}$ (kcal/mol)	Ionization Potential (eV)
U	123.4 ± 3[a]	6.187 ± 0.002[b]
UO	7.9 ± 3[a]	5.72 ± 0.06[c]
UO_2	-106.4 ± 3[a]	5.5 ± 0.1[c]
O	58.983 ± 0.024	13.618[e]
Ar	0	15.759[e]

[a]S. D. Gabelnick, "Ion Reactor Safety and Physical Property Studies," Annual Report, July 1973-1974, Chemical Engineering Division, Argonne National Laboratory, ANL-8120.

[b]G. S. Jones, I. Itzan, C. T. Pike, R. H. Levy and L. Levin, J. Quantum Electron. QE-12 (1976) 111.

[c]J. B. Mann, J. Chem. Phys. 40 (1964) 1632.

[d]JANAF Tables, Phys. Chem. Ref. Data, 4 (1975) 1.

[e]C. E. Moore, Natl. Stand. Ref. Data Ser., Natl. Bur. Stand. NSRDS-NBS 34 (1970).

Acknowledgment

References

[1] T. F. Moran and D. C. Fullerton, J. Chem. Phys. 54 (1971) 5231.

[2] (a) R. D. Levine, Chem. Phys. Lett. 11 (1971) 109.

(b) R. D. Levine, Chem. Phys. Lett. 11 (1971) 552.

(c) C. Rebick and R. D. Levine, J. Chem. Phys. 58 (1973) 3942.

[3] (a) E. K. Parks, N. J. Hansen and S. Wexler, J. Chem. Phys. 58 (1973) 5489.

(b) E. K. Parks, A. Wagner and W. Wexler, J. Chem. Phys. 58 (1973) 5502.

(c) E. K. Parks, J. P. Kuhry and S. Wexler, J. Chem. Phys. 67 (1977) 3014.

(d) S. H. Sheen, G. Dimoplon, E. K. Parks and S. Wexler, J. Chem. Phys. 68 (1978) 4950.

[4] R. W. Rozett and W. S. Koski, J. Chem. Phys. 49 (1968) 2691.

[5] (a) T. O. Tiernan and R. E. Marcotte, J. Chem. Phys. 53 (1970) 2107.

(b) C. Lifshitz, R. L. C. Wu, T. O. Tiernan and D. T. Ter-williger, J. Chem. Phys. 68 (1978) 247.

[6] M. H. Cheng, M. Chiang, E. A. Gislason, B. H. Mahan, C. W. Tsao and A. S. Werner, J. Chem. Phys. 52 (1970) 5518.

[7] F. P. Tully, Y. T. Lee and R. S. Berry, Chem. Phys. Lett. 9 (1971) 80.

[8] E. Herbst, K. A. Mulholland, R. L. Champion and L. D. Doverspike, J. Chem. Phys. 67 (1977) 5074.

[9] P. B. Armentrout and J. L. Beauchamp, J. Chem. Phys. submitted.

References (continued)

[10] P. B. Armentrout, R. V. Hodges and J. L. Beauchamp, J. Chem. Phys. 66 (1977) 4683.

[11] W. L. Fite, H. H. Lo and P. Irving, J. Chem. Phys. 60 (1974) 1236.

[12] P. J. Chantry, J. Chem. Phys. 55 (1971) 2746.

[13] R. D. Levine and R. B. Bernstein, "Molecular Reaction Dynamics" (Oxford, New York, 1974) p. 136.

[14] L. G. Piper, L. Hellemans, J. Sloan and J. Ross, J. Chem. Phys. 57 (1972) 4742.

[15] J. D. Kelley and M. Wolfsberg, J. Chem. Phys. 44 (1966) 324; 53 (1970) 2967.

[16] D. Secrest, J. Chem. Phys. 51 (1969) 421.

CHAPTER IV

EXPERIMENTAL AND THEORETICAL STUDIES OF THE
REACTION $Ba^+(D_2, D)BaD^+$: SEQUENTIAL IMPULSE
MODEL FOR ENDOTHERMIC REACTIONS

EXPERIMENTAL AND THEORETICAL STUDIES OF THE REACTION $Ba^+(D_2, D)BaD^+$: SEQUENTIAL IMPULSE MODEL FOR ENDOTHERMIC REACTIONS

P. B. ARMENTROUT and J. L. BEAUCHAMP

Arthur Amos Noyes Laboratory of Chemical Physics,

California Institute of Technology, Pasadena, California 91125, USA

(Received   )

Abstract

The sequential impulse model for direct reactions of Mahan, Ruska and Winn (J. Chem. Phys., 65 (1976) 3888) is extended to include endothermic reactions. The model is outlined and used to predict the variation in cross section with kinetic energy for heavy atom-light homonuclear diatom reactions. The results are found to agree well with experimental data for the reaction $Ba^+(D_2, D)BaD^+$. The bond dissociation energy of BaD^+, 2.5 ± 0.1 eV, and the proton affinity of Ba, 250 ± 3 kcal/mol, are derived.

Introduction

A large body of bimolecular reactions have been shown to proceed by short-lived direct interactions. This is especially true at higher energies where interaction times become much shorter than typical rotational periods. It has been fruitful to examine such reactions in the light of simple models. While not expected to fully account for all features of a reaction, such models often allow a good qualitative understanding of the process. The sequential impulse model of Bates, Cook and Smith [1] has been refined by Suplinskas and George [2, 3] and shown to accurately portray the reaction of Ar^+ with D_2. Gillen, Mahan, and Winn [4] have used a version of this model to interpret the reaction of O^+ wth D_2 and HD at higher energies. In each of these cases, the reactions examined were exothermic or thermoneutral and calculations were performed using a trajectory approach.

Endothermic reactions have received less attention in the past because of the experimental difficulties involved (small cross sections). Phase space theory [5,6] has been applied with success to the reaction $C^+(H_2,H)CH^+$; however, only for about 0.2 eV above threshold [7, 8]. Transition state theory has also been employed to interpret endothermic thresholds [9,10]. Previously, in our laboratories, the endothermic reactions of U^+ with N_2, D_2 and CD_4 were examined [11]. Reaction cross sections as a function of kinetic energy were measured and analyzed using a linear threshold law.

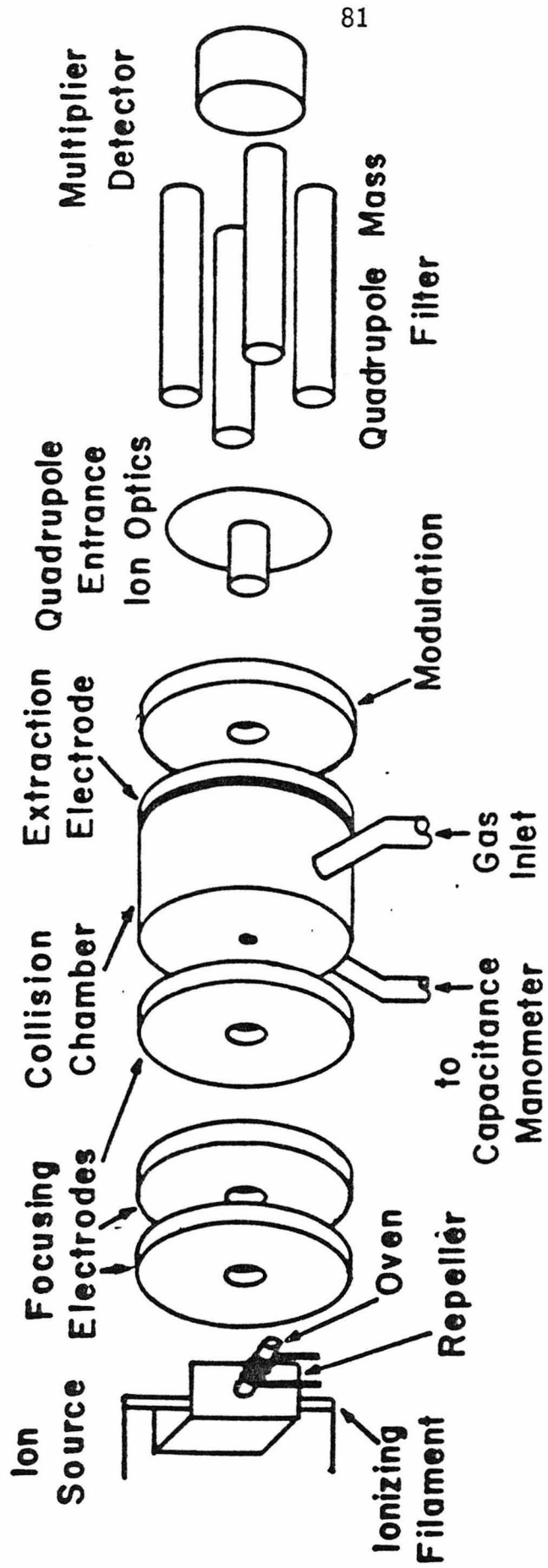In this paper, the approach used by Mahan, Ruska and Winn [12]

(MRW) to deduce product distributions and cross sections for thermo-neutral atom-diatom processes is extended to include endothermic reactions. The model is outlined and used to predict the variation in cross section with kinetic energy for heavy atom-light homonuclear diatom reactions. The results are compared with experimental data for the reaction $Ba^+(D_2, D)BaD^+$. By fitting the theoretical excitation function to the data, the bond dissociation energy, $D^0(Ba^+-D) = 2.5 \pm 0.1$ eV, is derived. From this, the proton affinity of the barium atom is calculated to be 250 ± 3 kcal/mol.

Experimental

The ion beam apparatus has been previously described [11] and is shown schematically in Fig. 1. Ions from a surface ionization source are focused into a collision chamber containing the reactant gas. Ions scattered in the forward direction are collected and focused into an EAI Quad 250B quadrupole mass spectrometer for mass analysis and detection. Resolution of the quadrupole is sufficient to separate BaD^+ (but not BaH^+) from Ba^+, thus dictating use of D_2 as the neutral reactant.

The barium ions source is simply BaF_2 powder held in a rhenium wire coil. Resistively heating the wire causes the BaF_2 to undergo dissociation and surface ionization. At the estimated temperature of the ionization filament, 1600°K, it is calculated that 96% of the beam is $Ba^+(^2S_{\frac{1}{2}})$ and that excited states $Ba^+(^2D)$ comprise less than 4% of the beam. Attenuation experiments [13] show no appreciable concentrations of excited states.

Fig. 1. Schematic diagram of the ion beam apparatus.

Multiplier Detector

Quadrupole Mass Filter

Quadrupole Entrance Ion Optics

Modulation

Extraction Electrode

Gas Inlet

Collision Chamber

to Capacitance Manometer

Focusing Electrodes

Oven

Repeller

Ion Source

Ionizing Filament

The energy of the beam is taken nominally to be the difference in potential between the collision chamber and the center of the filament, the latter determined by a resistive divider. The spread in ion energies is estimated to be 0.7 eV FWHM. As this is only 0.02 eV in the center of mass frame, no specific account of this distribution was taken. The collision chamber is maintained as a field free interaction region. Use of an extraction field did not alter product yields. This verifies calculations which show that the large mass of the ionic reactants and products compared to the neutrals involved results in efficient product ion collection.

The temperature of the collision chamber, as measured by thermistor, is approximately $400°$ K under these operating conditions. Since the capacitance manometer head used to monitor reactant gas pressure is at room temperature, a thermal transpiration correction was applied to the measured pressure. Additionally, the thermal motion of the gas in the chamber broadens the interaction energy distribution. We account for this effect by convoluting a proposed excitation function with the thermal energy distribution using the method outlined by Chantry [14].

Absolute cross sections are calculated using

$$I(BaD^+) = [I(BaD^+) + I(Ba^+)][1 - \exp(-n\sigma\ell)] \tag{1}$$

which relates the cross section, σ, the length of the interaction region, $\ell\,(=5\,mm)$, and the density of the target gas, n, to the measured reactant and product ion intensities, $I(Ba^+)$ and $I(BaD^+)$, respectively. Relative cross sections as a function of energy were very reproducible.

We estimate that the absolute cross sections reported are accurate to a factor of two.

Theory

Our approach to the analysis of endothermic reactions is an extension of the sequential impulse model outlined by MRW. To facilitate comparison, the same terminology shall be used here. It is important to note that all present results reduce to those of MRW as the endothermicity of the reaction goes to zero. For reaction of an atom, particle 1, with a diatom [2,3]

$$[1] + [2,3] \rightarrow [1,2] + [3] \tag{2}$$

the endothermicity, E_0, is equal to $D^0[2,3] - D^0[1,2]$, the difference between the bond dissociation energies of the reactant and product molecules. We consider all atoms to interact pairwise and as hard spheres. The essential features of the model are detailed below.

Particle 1 having mass A and velocity $\underset{\sim}{V_1}$ in the laboratory frame moves toward molecule [2,3] (having masses B and C, respectively) which is at rest. For simplicity, [2,3] is taken to be in its ground vibrational and rotational state. Particles 1 and 2 interact in an impulsive elastic collision about their center of mass, the 1-2 centroid, located at $\underset{\sim}{V_1} A/(A+B)$, Fig. 2. The relative velocity vector of 1 and 2 is thus rotated by an angle χ_1 about their center of mass. The new laboratory velocity of particle 1, $\underset{\sim}{V_1'}$ (the prime denotes one collision has occurred), lies somewhere on a sphere of radius $V_1 B/(A+B)$ centered at the 1-2 centroid. The corresponding

Fig. 2.   A velocity vector diagram for the sequential

impulse model for endothermic reactions.
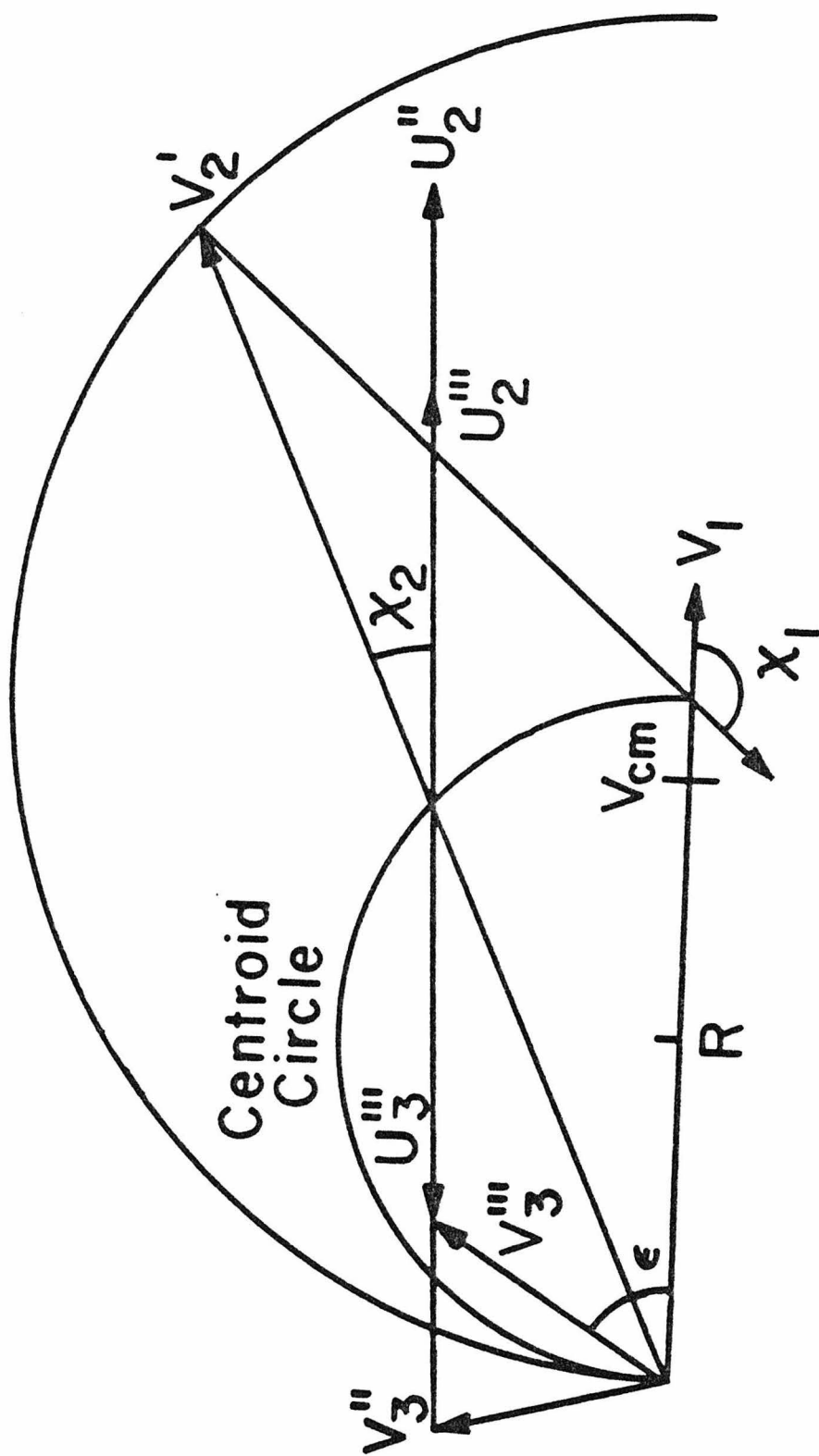
laboratory velocity of 2 lies somewhere on a sphere of radius $V_1 A/(A + B)$ also centered at the 1-2 centroid. The magnitude of V_2' is

$$V_2' = 2 \frac{A}{A+B} V_1 \sin\left(\frac{X_1}{2}\right). \tag{3}$$

The center of mass of the diatom, 2-3, now lies on a sphere (called the centroid sphere) of radius

$$R = \left(\frac{A}{A+B}\right)\left(\frac{B}{B+C}\right) V_1 \tag{4}$$

whose center is at a distance R from the laboratory origin along V_1, Fig. 2. Depending on the orientation of 2-3 relative to V_2', a second collision may occur. If so, it is taken to be elastic and rotates the 2-3 relative velocity vector through an angle X_2 about the 2-3 centroid, Fig. 2. The laboratory velocity of particle 3 after this second collision (denoted by a second prime) is

$$V_3'' = 2\left(\frac{B}{B+C}\right) V_2' \sin\left(\frac{X_2}{2}\right) = 4R \sin\left(\frac{X_1}{2}\right) \sin\left(\frac{X_2}{2}\right). \tag{5}$$

If the orientation of 2-3 is such that no collision takes place, then $X_2 = 0$, the velocities remain unchanged.

Until this point, the discussion is identical to that of MRW. We now require that for reaction to occur, the relative energy in the 2-3 diatom must exceed the endothermicity, E_0. This is a necessary condition for reaction but perhaps not a sufficient condition because orientational and steric factors not considered may reduce the probability of reaction. It is also not a unique condition since

"removal" of the energy E_0 at this point is somewhat arbitrary. Other possibilities include removing the energy as the reactants approach or as the products recede or making the initial collision inelastic. These alternate conditions were explored but did not yield the familiar form for the cross section obtained in the next section, eq. 16.

Having made the requirement stated above, the relative energy of particles 2 and 3 must now be reduced by E_0 to conserve energy. In effect, a third "event" has now occurred such that the magnitude of $\underset{\sim}{U}_3'''$, the final velocity of particle 3 in the 2-3 center of mass system, is

$$U_3''' = 2R\left[\sin^2\left(\frac{\chi_1}{2}\right) - E_1/E\right]^{\frac{1}{2}} \tag{6}$$

but the direction of this vector is unchanged from $\underset{\sim}{U}_3''$, Fig. 2. The magnitude of the velocity, $\underset{\sim}{U}_2'''$, is related to eq. 6 by a mass factor, C/B, and has the opposite direction. The quantity, E_1, is the effective threshold for reaction and is specified by

$$E_1 = E_0/4\cos^2\beta\sin^2\beta \tag{7}$$

where $\cos^2\beta = AC/(A+B)(B+C)$. The mass factor in the denominator of eq. 7 is well known as the fraction of energy transferred from translation to vibration for a collinear atom-diatom collision in the limit of a loose oscillator [16].

We now require (as in MRW) that the relative energy in the 1-2 system not exceed $D^0(1-2)$, that is, that the diatomic product be stable.

This is determined simply by noting whether the tip of $\underset{\sim}{U}_3'''$ lies in a stability zone with limits set by the conditions that the internal energy of the product 1-2 have a value between zero and $D^0(1-2)$. These limits, expressed as values of the translational exoergicity, Q, are spheres with their origins at the center of mass and radii of

$$Q_0 = V_{CM}[(1 - E_1/E)/\cos^2\beta]^{\frac{1}{2}} \tag{8}$$

and

$$Q_{min} = V_{CM}[(1 - D/E)/\cos^2\beta]^{\frac{1}{2}} \tag{9}$$

where $\underset{\sim}{V}_{CM} = \underset{\sim}{V}_1 A/M$, $D \equiv D^0(2-3)$, and $M = A+B+C$.

To facilitate the determination of the stability of the product, it is useful to find the maximum and minimum values of V_3''', the velocity of particle 3 after reaction occurs at a given laboratory angle, ϵ, Fig. 2. The result is

$$(V_3''')_{max} = R(\cos\epsilon + 1) \pm R[(\cos\epsilon + 1)^2 - 4E_1/E]^{\frac{1}{2}} \tag{10}$$

which describes a figure known as a limacon of Pascal. As E_0 approaches zero or as E approaches infinity, the limacon degenerates to a cardioid (as in MRW). A series of these curves is shown in Fig. 3. The three-dimensional maximum surface is generated by rotation of the limacon about the $\underset{\sim}{V}_1$ vector. A corresponding surface also exists which describes the limiting values for the velocity of the product [1,2].

It can be shown that the scattering limacon, given by eq. 10, and

Fig. 3.   The limiting surface, given by eq. 10, for the atomic
product from reaction 2 for a case where A = 12, B = C = 1
at a variety of collision energies in units of E_1, the
effective endothermicity of the reaction. The x's mark
the position of θ_0 given by eq. 11.
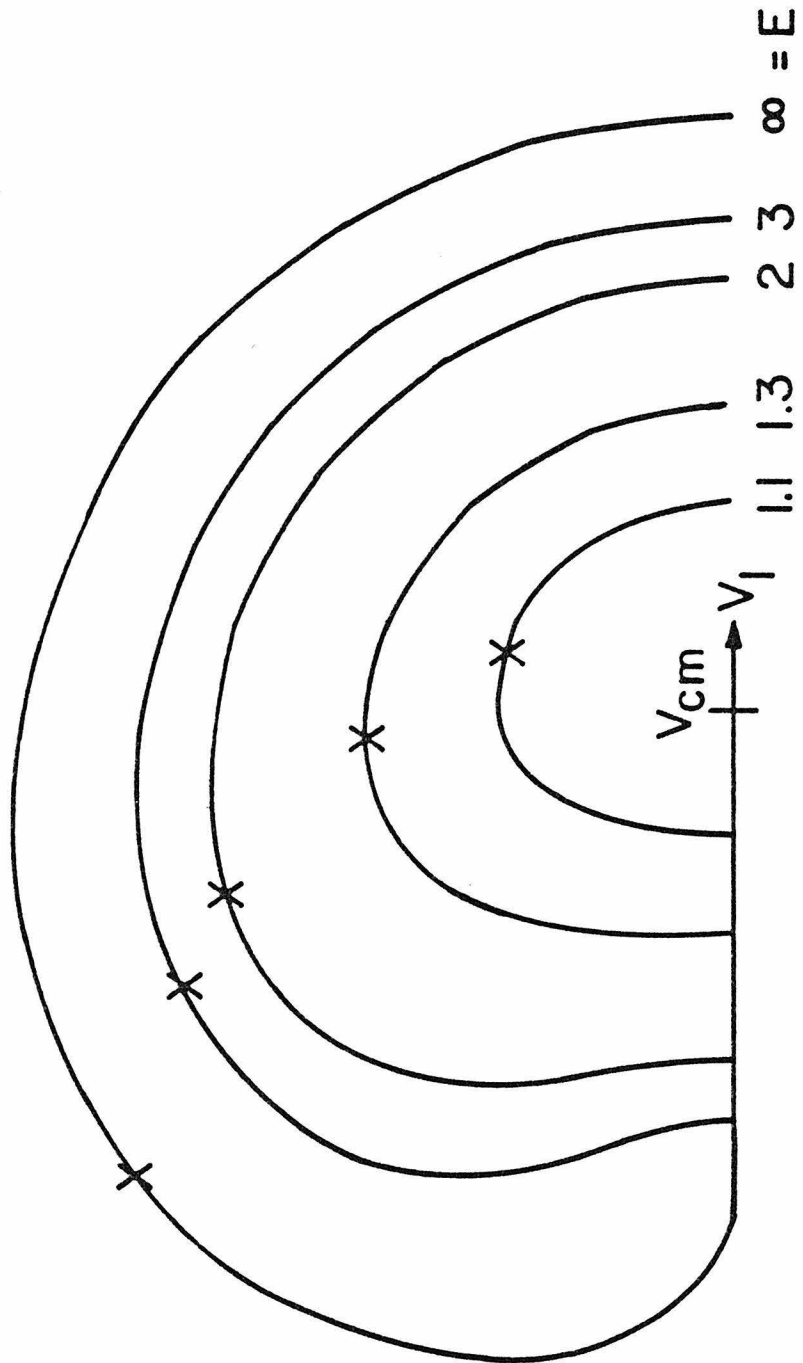
the maximum stability sphere, given by eq. 8, scale with one another as the energy is increased. Indeed, the limacon and sphere are tangent along a circle defined by the barycentric angle θ_0 (Fig. 3) given by

$$\cos \theta_0 = \frac{ABCM + 2A^2C^2 - M^2B^2 - AC(A+B)(B+C)E_0/E}{2AC[AC(A+B)(B+C)(1 - E_0/E)]^{\frac{1}{2}}} \qquad (11).$$

Thus, [1, 2] is located at a laboratory angle θ_L such that

$$\cos \theta_L = \frac{ABCM + 2A^2CM - M^2B^2 - AC(A+B)(B+C)E_0/E}{2A\{MC(A+B)[M(AC-B^2) - AC(B+C)E_0/E]\}^{\frac{1}{2}}} . \qquad (12)$$

This circle, whose plane is perpendicular to $\underset{\sim}{V}_1$, defines the location of all products having no internal energy. Since the scattering limacon lies wholly within the maximum stability sphere, eq. 8, velocities of stable products have as a maximum the limacon, eq. 10, and as a minimum the stability sphere, given by eq. 9, Q_{min}.

Calculation of Reaction Cross Section

To find the reaction cross section at a given energy, $\sigma(E)$, we need to consider all possible collision events. In general, $\sigma(E)$ is given by

$$\sigma(E) = \sigma_{12} P_1 P_2 \qquad (13)$$

where $\sigma_{12} = \pi d_{12}^2$, d_{12} being the sum of the hard sphere radii of particles 1 and 2, P_1 is the probability the collision between 1 and 2 transfers an energy greater than E_1 to the diatom, and P_2 is the

probability that a product molecule, [1,2] is stable. Calculation of $\sigma(E)$ is simplified by considering three energy regions: region I, $E < E_1$; region II, $E_1 < E < D$; and region III, $E > D$. In region I, $\sigma(E)$ equals zero. Insufficient energy is available for reaction to occur. Regions II and III are examined below.

Region II, $E_1 < E < D$

Calculation of $\sigma(E)$ is considerably simplified for this energy region by noting that all products formed are stable. This is apparent since as noted above all scattering occurs within the maximum stability sphere defined by Q_0 and, at these energies, the minimum stability sphere has a radius of zero (eq. 9). Thus, the value of P_2 is unity and we need only calculate P_1.

The probability, P_1, can be expressed in terms of the position of $\underset{\sim}{V_2'}$ which depends on the initial scattering angle χ_1. We know reaction does not occur unless U_3''' is greater than or equal to zero. From eq. 7, this requires that χ_1 exceeds a minimum value given by

$$\chi_0 = 2 \arcsin(E_1/E)^{\frac{1}{2}}. \tag{14}$$

Since the distribution of $\underset{\sim}{V_2'}$ vectors is uniform about the 1-2 centroid,

$$d^2 P_1 = \frac{1}{4\pi} \sin\chi_1 d\chi_1 d\phi' \tag{15}$$

integrated over ϕ' (the azimuthal angle) from 0 to 2π and over χ_1 from χ_1 to π. The result is $P_1 = 1 - E_1/E$ which yields for region II,

$$\sigma(E) = \sigma_{12}(1 - E_1/E). \tag{16}$$

This is the classical line-of-centers hard sphere cross section [16], as might be expected.

At this point, it is fruitful to calculate the partitioning of this reaction cross section into components resulting from a two collision sequence, P_{22}, and those where only a single collision occurs, P_{21}. Here, the sum of P_{21} and P_{22} equals P_2 which is unity in Region II. Following the treatment of MRW, we find

$$d^2 P_{22} = \frac{d_{23}^2}{16\pi r_0^2} \frac{\sin\chi_2\, d\chi_2\, d\gamma}{[1 - (d_{23}\cos(\frac{\chi_2}{2})/r_0)^2]^{\frac{1}{2}}} \tag{17}$$

where d_{23} is the sum of the hard sphere radii of particles 2 and 3, r_0 is the equilibrium bond length of the diatom and γ is the azimuthal scattering angle for particles 2-3, Fig. 4. Integrating over γ from 0 to 2π and χ_2 from 0 to π, we obtain

$$P_{22}^0 = [1 - (1 - d_{23}^2/r_0^2)^{\frac{1}{2}}]/2 , \tag{18}$$

and thus

$$P_{21}^0 = \tfrac{1}{2}(1 - d_{23}^2/r_0^2)^{\frac{1}{2}} . \tag{19}$$

Region III, $E > D$

Once the energy exceeds the bond energy of the diatom, collision sequences in which particle 3 ends within the minimum stability sphere must be excluded. The geometry is shown in Fig. 5. The integration must be performed carefully because there will be values of E and χ_1 for which no intersection of the second collision scattering sphere and

Fig. 4.   The geometry of a sequential impulse collision. The 2-3

bond axis makes an angle α with the velocity vector V_2'.

The impact parameter for the second collision is $b = r_0 \sin\alpha$

where r_0 is the equilibium 2-3 bond distance. (From Ref.
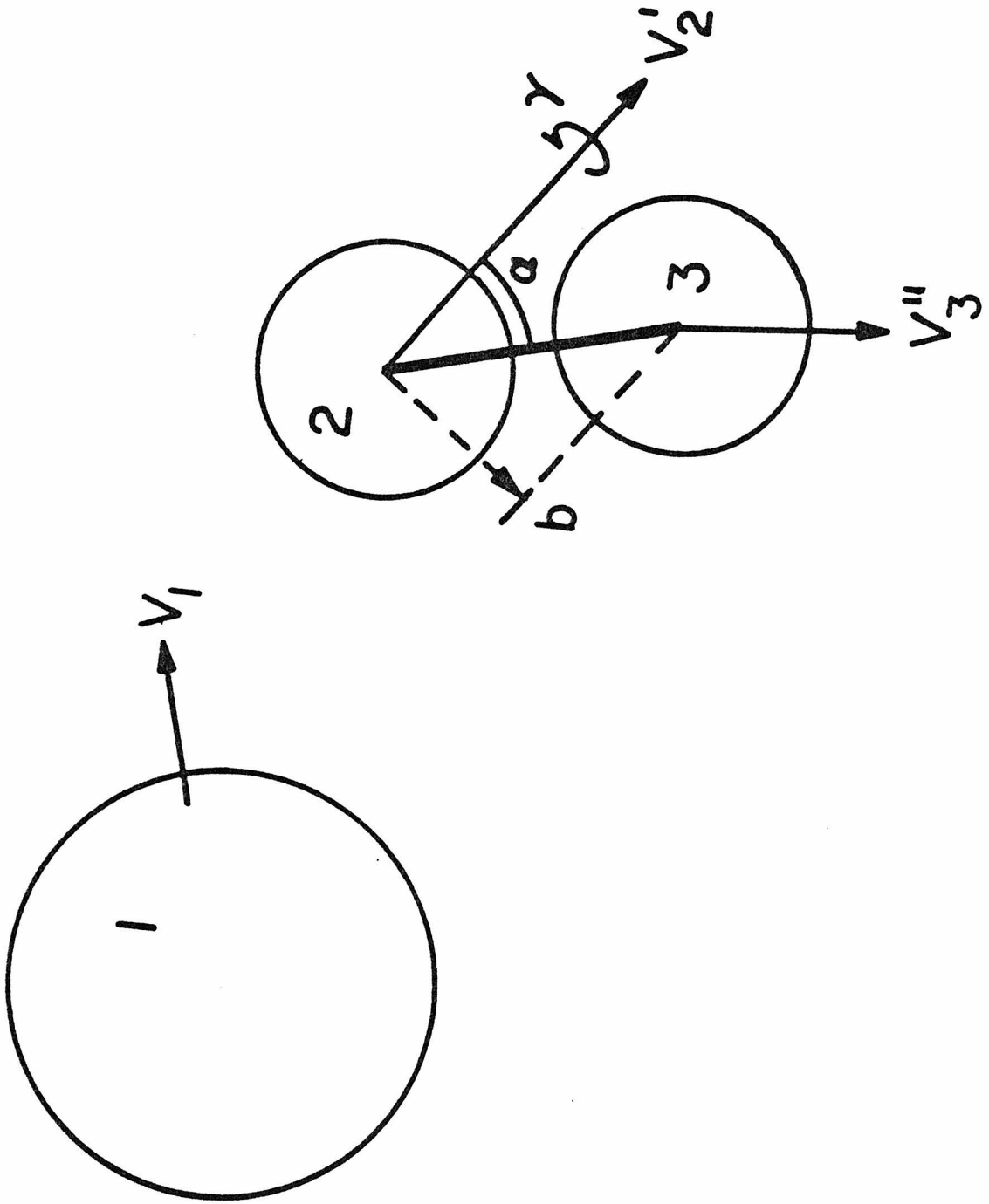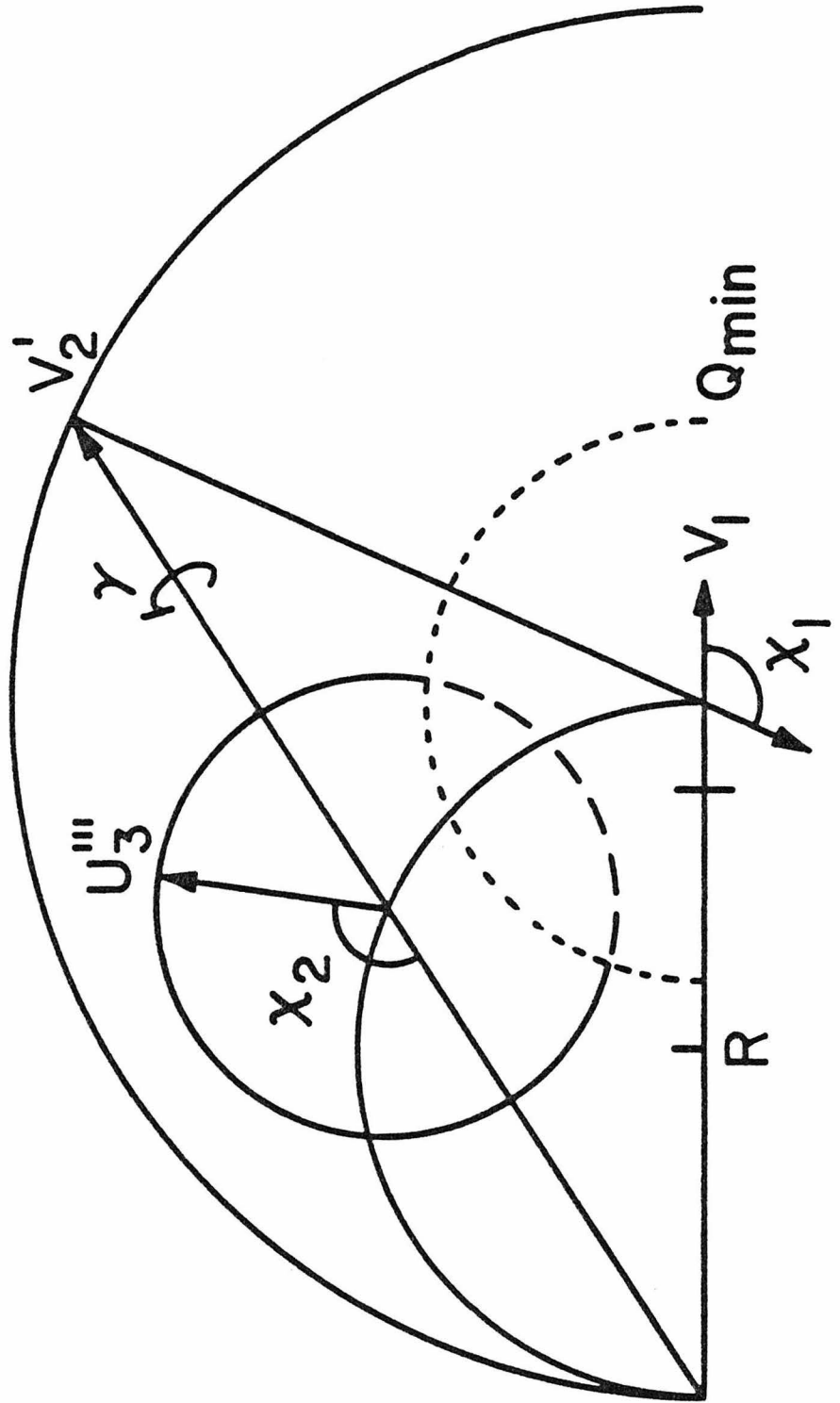
12.)

Fig. 5.   A velocity vector diagram showing the portion of scattering
          events (marked by a long dashed line) which lead to product
          instability for a particular energy and initial scattering
          angle χ_1. In three-dimensional space, both the Q_{min} and
          U_3'' circles are spheres.

the Q_{min} sphere will occur as well as regions where the scattering sphere is entirely within or outside the minimum stability sphere. The general procedure is to solve for P_{22} by integrating eq. 17. The result, which is dependent on χ_1 and E_1 is integrated over x_1, eq. 15, and multiplied by σ_{12}. This cross section when added to the result from a similar treatment of P_{21} yields $\sigma(E)$.

Heavy atom - light diatom limit

Examination of a reaction where $A \gg B, C$ exposes several features of the collision processes. In this limit, the energy at which single collision events result in product dissociation is simply

$$E_s = (D - \cos^2\beta\, E_0)/\sin^2\beta . \tag{20}$$

This energy is substantially less than that predicted by "spectator" stripping [11, 17], $E_s = D/\sin^2\beta$. It is also of interest to note that "knockout" processes where A hits B and reacts with the trailing C atom also result in product dissociation at E_s. When $A \gg B = C$, the geometry of the two-collision process takes a symmetric and simpler form. Consequently, the evaluation of $\sigma(E)$ in Region III is more tractable.

Results and Discussion

Experimental and theoretical results for the reaction $Ba^+(D_2, D)BaD^+$ are shown in Fig. 6. The theoretical curve is obtained by empirically determining σ_{12}, d_{23} and E_0. The values for σ_{12}, 0.98 $\overset{\circ}{A}^2$, and E_0, 2.1 $\pm$ 0.1 eV, are evaluated by fitting the data

Fig. 6.   Variation in experimental cross section with energy in the
center of mass frame (lower scale) and laboratory frame
(upper scale). The short dashed curve gives the cross
section calculated for two-collision events (see text). The
long dashed curve is the total cross section calculated with
includes both one- and two-collision events. This calculated
curve is convoluted as discussed in the text to yield the
solid line. Arrows mark the bond dissociation energy of
D_2, 4.60 eV; the energy above which one-collision events
lead to product dissociation, 7.0 eV, and the energy that
the spectator stripping model predicts for product instability,
9.1 eV.

Ba$^+$ + D$_2$ → BaD$^+$ + D
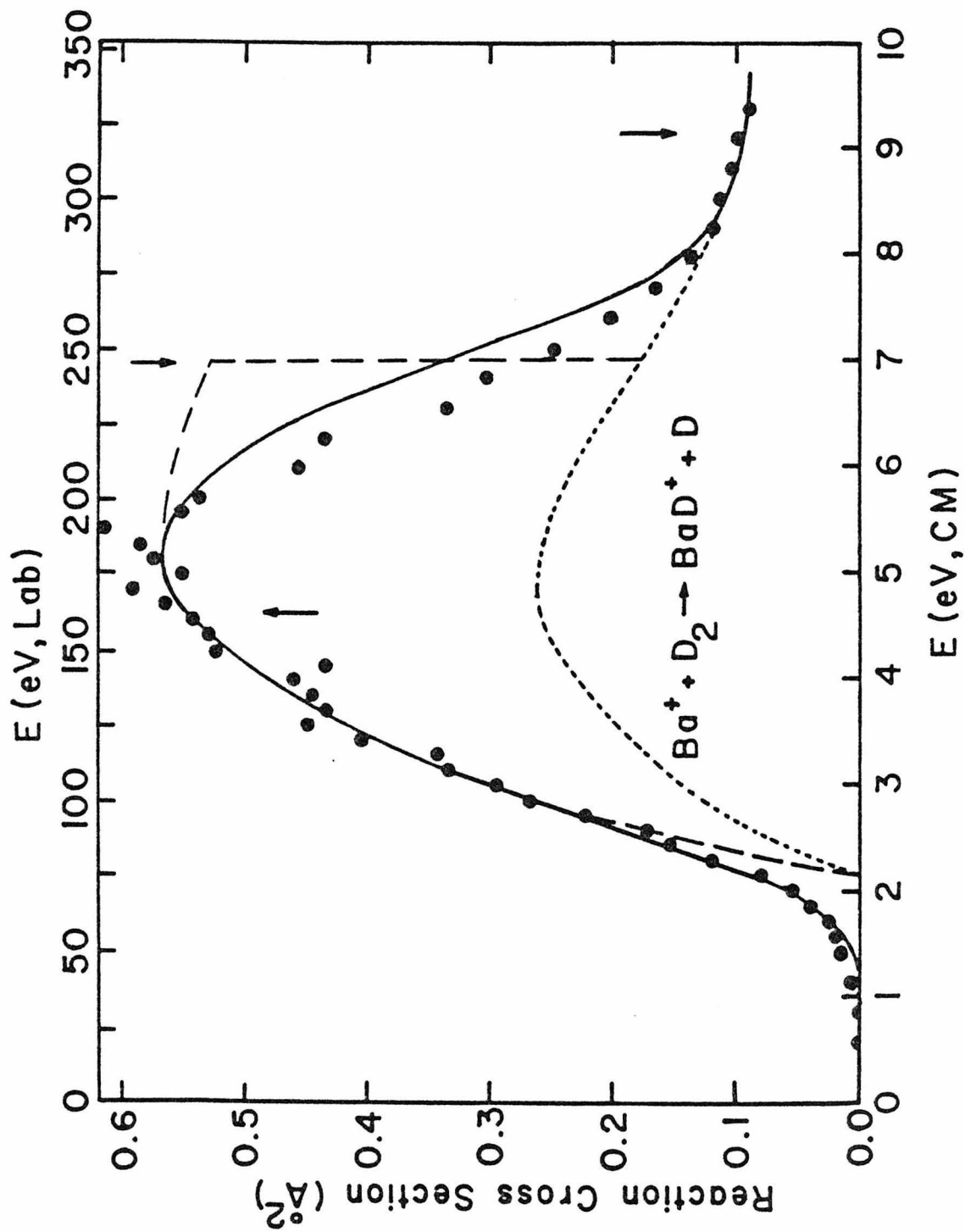
below the bond dissociation energy of D_2, 4.60 eV [18], with the function $\sigma_{12}(1 - E_1/E)$ convoluted as discussed above [14]. The value of d_{23}, which determines the fractions of one- and two-collision events, is evaluated by fitting the two-collision cross section to the data at the higher energies where one-collision events all lead to product dissociation. The fit shown is obtained with $d_{23} = r_0$ such that exactly half the events are two-collision events and half are one-collision events. The one-collision events have a sharp onset for product dissociation at 7.0 eV. This fall-off is also convoluted with the thermal motion of the target gas to yield the solid curve shown in Fig. 6. For comparison, the energy for product dissociation predicted by the spectator stripping model, 9.1 eV, is also shown.

As BaD_2^+, having only three valence electrons, is not expected to be strongly bound, reaction at energies much above thermal will probably proceed via a direct mechanism rather than by complex formation. While σ_{12} is smaller than might be expected a priori, we have not taken into account steric restrictions on the initial collision nor have we included all types of multiple collision sequences (chattering). These considerations would lead to a lower value of σ_{12} than that calculated using known atomic radii.

Using the measured endothermicity of the reaction $Ba^+(D_2, D)BaD^+$, we can calculate several thermochemical values of interest. The bond dissociation energy of the barium deuteride, $D^0(Ba^+-D)$, is found to be 2.5 ± 0.1 eV. This is substantially stronger than the bond energy of the isoelectronic CsH, $D^0(CsH) = 1.8 \pm 0.3$ eV [20]. Combined with the bond energy for neutral BaH, ≤ 1.8 eV [21], we can put an upper

limit on the ionization potential of BaH, IP(BaH) $\lesssim$ 4.5 eV.

The proton affinity of barium can be found using the relation

$$PA(Ba) = IP(H) - IP(Ba) + D^0(Ba^+-H).$$

Making a zero point energy correction of 0.05 eV in $D^0(Ba^+-D)$, we find the proton affinity to be 250 ± 3 kcal/mol [21]. This is easily one of the highest proton affinities of all atomic species for which reasonable thermochemical data are available [11]. It is substantially higher than that of the strongest organic monodentate bases such as NMe_3 and PMe_3 [22], and comparable to the basicity of the alkali hydroxides [23].

Acknowledgment

References

[1] D. R. Bates, C. J. Cook and F. J. Smith, Proc. Phys. Soc. London 83 (1964) 49.

[2] R. J. Suplinskas, J. Chem. Phys. 49 (1968) 5046.

[3] T. F. George and R. J. Suplinskas, J. Chem. Phys. 54 (1971) 1037.

[4] K. T. Gillen, B. H. Mahan and J. S. Winn, J. Chem. Phys. 59 (1973) 6380.

[5] P. Pechukas and J. C. Light, J. Chem. Phys. 42 (1965) 3281.

[6] E. Nikitin, Teor. Eksp. Khim. 1 (1965) 135, 144, 428 [Theor. Exp. Chem. 1 (1975) 83, 90, 275].

[7] D. G. Truhlar, J. Chem. Phys. 51 (1969) 4617.

[8] W. J. Chesnavich and M. T. Bowers, J. Chem. Phys. 68 (1978) 901.

[9] T. M. Mayer, B. E. Wilcomb and R. B. Bernstein, J. Chem. Phys. 67 (1977) 3507.

[10] W. J. Chesnavich and M. T. Bowers, J. Phys. Chem. 83 (1979) 900.

[11] P. B. Armentrout, R. V. Hodges and J. L. Beauchamp, J. Chem. Phys. 66 (1977) 4683.

[12] B. H. Mahan, W. E. W. Ruska and J. S. Winn, J. Chem. Phys. 65 (1976) 3888.

[13] B. R. Turner, J. A. Rutherford and D. M. J. Compton, J. Chem. Phys, 48 (1968) 1602.

[14] P. J. Chantry, J. Chem. Phys. 55 (1971) 2746.

References (continued)

[15] See for example, R. D. Levine and R. B. Bernstein, "Molecular Reaction Dynamics, Oxford University Press, New York, 1974, p. 136.

[16] Ref. 15, p. 46.

[17] A. Henglein, in "Ion Molecule Reactions in the Gas Phase", ed. Pierre Ausloos (ACS, Washington, D.C., 1966) p. 63.

[18] D. de B. Darwent, Natl. Stand. Ref. Data Ser., Natl. Bur. Stand. 31 (1970).

[19] A. G. Gaydon, "Dissociation Energies and Spectra of Diatomic Molecules" (Chapman and Hall, London, 1947).

[20] G. Herzberg, "Spectra of Diatomic Molecules" (Van Nostrand, New York, 1950), Table 39.

[21] IP(H) = 13.598 eV, IP(Ba) = 5.212 eV. C. E. Moore Natl. Stand. Ref. Data Ser., Natl. Bur. Stand. 34 (1970).

[22] J. F. Wolf, R. H. Staley, I. Koppel, M. Taagepera, R. T. McIver, Jr., J. L. Beauchamp and R. W. Taft, J. Am. Chem. Soc. 99 (1977) 5417.

[23] S. K. Searles, I. Ozidic and P. Kebarle, J. Am. Chem. Soc. 91 (1969) 2810.

CHAPTER V

ENDOTHERMIC REACTIONS OF Ni$^+$ WITH H$_2$, HD, AND D$_2$

ENDOTHERMIC REACTIONS OF Ni^+ WITH H_2, HD, AND D_2

P. B. ARMENTROUT and J. L. BEAUCHAMP

Arthur Amos Noyes Laboratory of Chemical Physics,

California Institute of Technology, Pasadena, California 91125, USA

Abstract

An ion beam apparatus is employed to study the reaction of Ni^+ with H_2, HD, and D_2 as a function of kinetic energy. These reactions lead to the endothermic formation of NiH^+, NiH^+ and NiD^+, and NiD^+, respectively. Interpretation of the threshold for these processes yields the average bond energies, $D^0(Ni^+-H) = 1.86 \pm 0.09$ eV and $D^0(Ni^+-D) = 1.90 \pm 0.14$ eV. The total reaction cross sections for all three systems are similar; however, a striking isotope effect is observed for Ni^+ reacting with HD. The dependence of the cross sections on relative kinetic energy is discussed in terms of simple models for reaction.
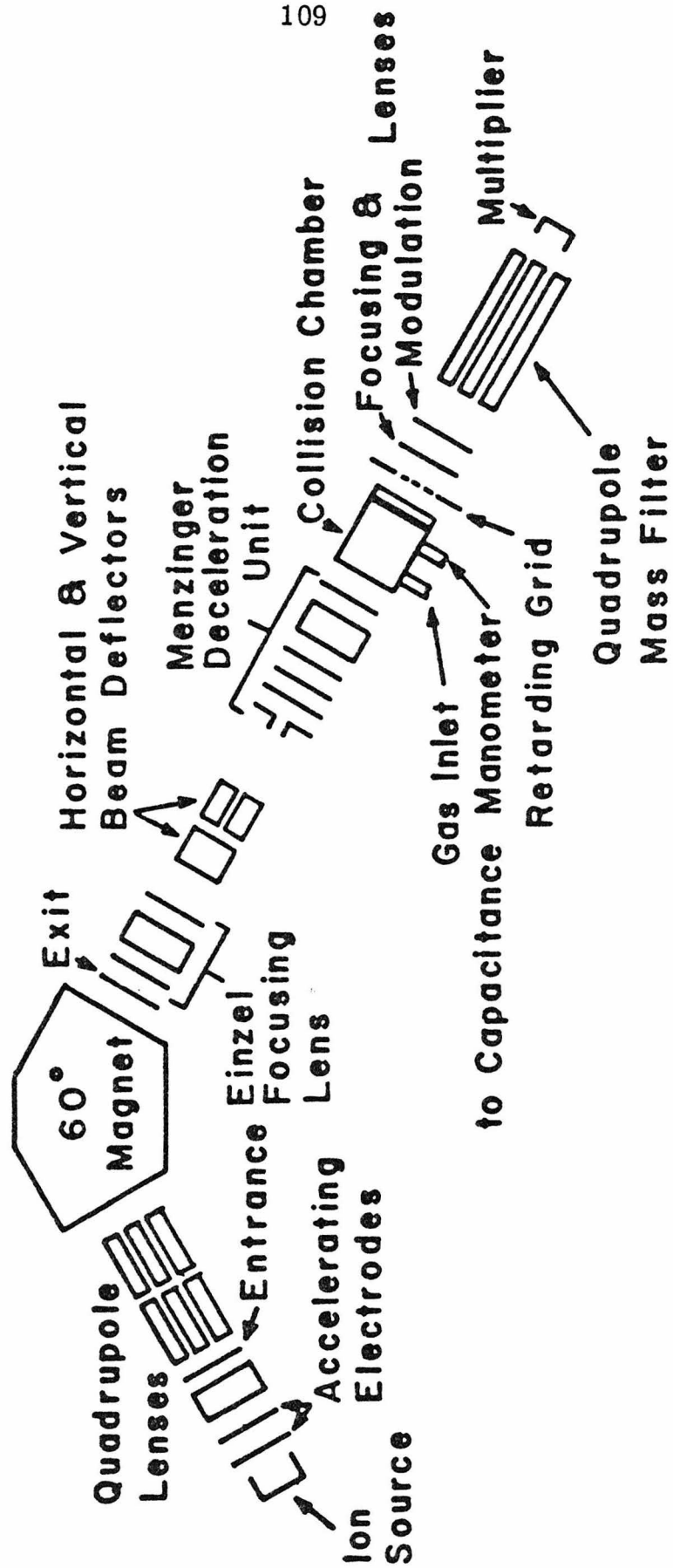
Introduction

Metal hydrides are of increasing interest because of their importance in catalysis, the photochemical generation of H_2 [2], the storage of hydrogen by interstitial alloys [3], and organometallic chemistry [4]. Matrix isolation techniques [5], shock tubes [6], and more conventional means [7] have been used to obtain a variety of spectroscopic information on diatomic metal hydrides. However, spectroscopy is generally not useful in determining the bond dissociation energies of such species [7]. The present study is a continuation of our efforts to investigate the chemistry of metal hydrides in the gas phase [8,9,10]. Using an ion beam apparatus, we have examined the endothermic reactions of nickel ions with hydrogen and its isotopic variants. Interpretation of the threshold for these reactions yields the bond energy for the nickel hydride ion. A striking isotope effect is observed in the reaction between Ni^+ and HD which produces both NiH^+ and NiD^+. Conversely, no isotope effect is seen in comparing the total reaction cross sections of H_2, HD, and D_2.

Experimental

The ion beam apparatus shown in Fig. 1 is a highly modified version of an instrument previously described [8]. Ions from a surface ionization source are accelerated and focused into a 60° sector magnet for mass separation. The ion beam mass selector provides unit mass resolution to greater than 100 m/z. All present results were performed with the ^{58}Ni isotope. This mass selected beam is

FIG. 1.   Schematic drawing of ion-beam apparatus.

Ion Source

Quadrupole Lenses

Accelerating Electrodes

Entrance Einzel Focusing Lens

60° Magnet

Exit

Horizontal & Vertical Beam Deflectors

Menzinger Deceleration Unit

Collision Chamber

Gas Inlet

to Capacitance Manometer

Retarding Grid

Focusing & Modulation

Lenses

Quadrupole Mass Filter

Multiplier

decelerated and focused into a collision chamber containing the reactant gas. The pressure of the gas, measured using an MKS Baratron Model 90H1 capacitance manometer, is in the range of $1-7 \times 10^{-3}$ Torr for the present experiments. Product ions scattered in the forward direction are focused into a quadrupole mass filter, and detected using a Channeltron electron multiplier. Phase sensitive detection is accomplished by modulating the voltage on the final lens element and directing the output of the multiplier to a PAR HR-8 lock-in amplifier, referenced to the modulating frequency.

The ion source, previously described [8], is comprised of a tubular stainless steel oven attached to the side of a U-shaped repeller plate which surrounds a rhenium ionization filament. For these experiments, the oven is loaded with $NiCl_2 \cdot 6H_2O$. The filament generates sufficient heat to dehydrate the nickel complex and vaporize the $NiCl_2$. This vapor is directed at the filament where dissociation and ionization of the resulting Ni takes place. This method of ionization minimizes the production of excited metal ion states. It is estimated that at the filament temperature used, $\sim 2500°K$, over 98% of the Ni^+ ions produced are in the ^2D ground state manifold. Attenuation experiments [11] indicate only a single component in the beam.

The energy of the ion beam is taken nominally as the difference in potential between the collision chamber and the center of the filament, the latter being determined by a resistive divider. This energy is checked by use of a retarding field energy analyzer. Agreement was

always within 0.3 eV. The energy width of the Ni^+ beam was also thus obtained and determined to be 0.7 eV (FWHM). In the center of mass frame, this introduces an uncertainty of ± 0.03 eV and ± 0.05 eV for the reactions with H_2 and D_2, respectively. No specific account of the energy distribution of the ion beam is taken in the treatment below.

A more severe problem concerning the actual energy of inter-action is the effect of the thermal motion of the reactant gas. Chantry [12] has shown that the distribution of the relative kinetic energy at an energy E due to this effect has a full width at half-maximum of

$$W_{\frac{1}{2}} = (11.1 \, \gamma \, kTE)^{\frac{1}{2}} \tag{1}$$

where T is the temperature of the target gas and $\gamma = m/(m+M)$, m and M being the masses of the incident particle and target gas. Thus $W_{\frac{1}{2}} \sim 0.5 \, E^{\frac{1}{2}}$ eV for the present experiments. This energy distribution effectively broadens any sharp features in the excitation function in-cluding threshold. To account for this effect, the proposed excitation function is convoluted with this distribution before comparison with the data using the method outlined by Chantry [12].

Reaction cross sections are calculated using

$$I_R = (I_R + I_P) \exp(-n\sigma\ell) \tag{2}$$

which the total reaction cross section, σ, the length of the interaction region, $\ell \, (= 5 \, mm)$, and the number density of the target gas, n, to the measured intensities of the reactant ion and the product ion, I_R and I_P, respectively. In the case of HD where two products are observed, the

cross section for a specific product is

$$\sigma_i = \sigma I_i / I_p \tag{3}$$

where $I_p = \Sigma I_i$ and the subscript i can refer to either NiH^+ or NiD^+. The greatest uncertainty in such measurements is the ion detection efficiency. Calculation on the maximum scattering angle expected in reactive collisions of the present study indicate all product ions should be collected. This is a consequence of the appreciable center of mass velocity which requires the heavy product be scattered forward in the laboratory frame.

The HD and D_2 were used as obtained from Stohler Isotopes. The purity of the HD was checked by mass spectrometry and found to be about 96% HD with 2% each of H_2 and D_2.

Results

Reaction of Ni^+ with H_2 and D_2

Cross sections measured for the reaction of nickel ions with H_2 and with D_2, shown in Figs. 2 and 3, respectively, are superimposable within experimental error. Qualitatively, these excitation functions are easily understood. The cross section for reaction to form $NiH(D)^+$ $NiH(D)^+$ rises rapidly from threshold. The thresholds for the two systems should be the same except for small differences due to zero point energy effects. At the bond dissociation energy of the neutral reactant, D, the three-body reaction channel

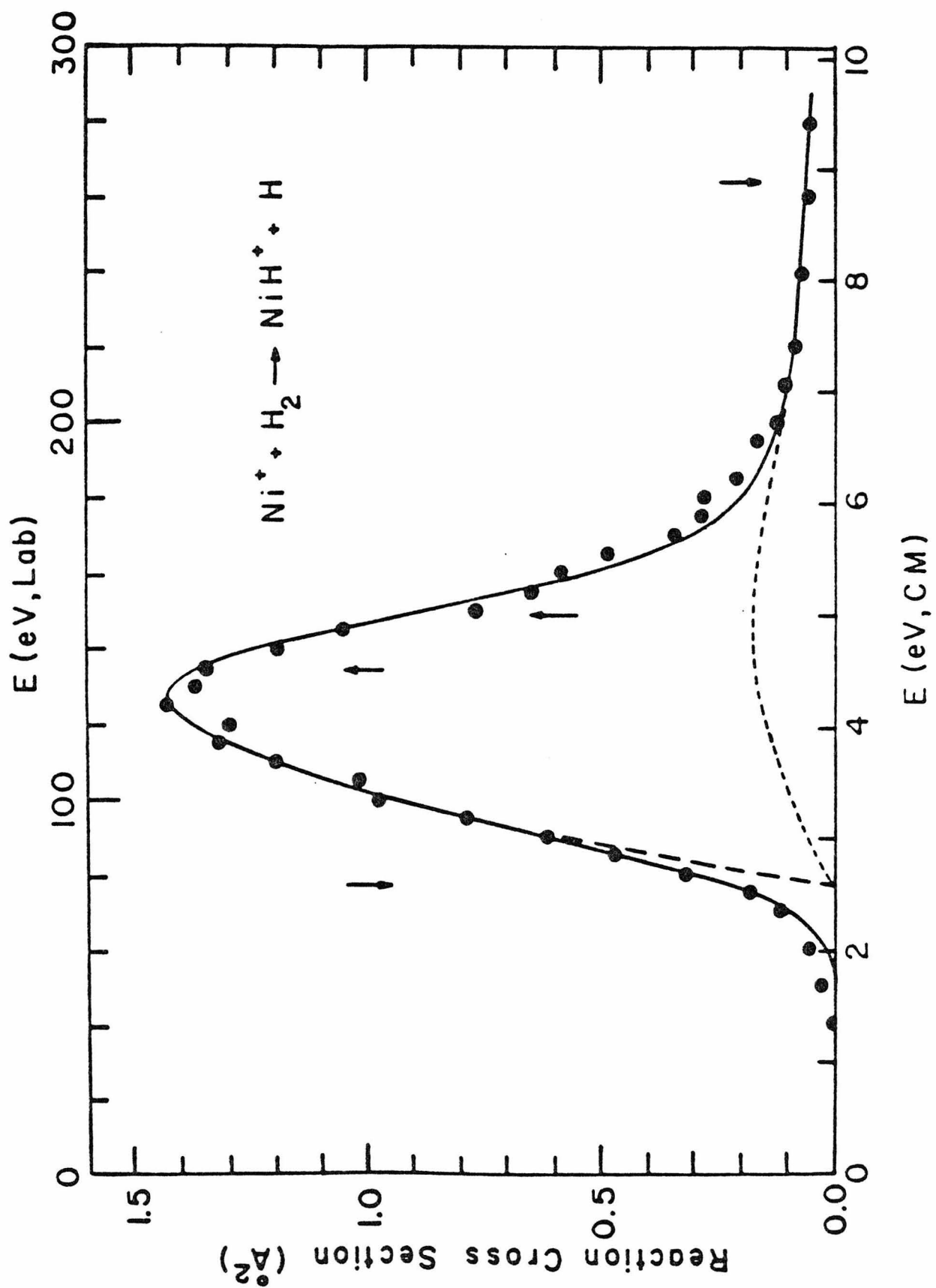$$Ni^+ + H_2(D_2) \rightarrow Ni^+ + 2H(D) \tag{4}$$

FIG. 2. Variation in cross section for the reaction of Ni$^+$ with H$_2$ as
a function of kinetic energy in the center of mass frame
(lower scale) and the laboratory frame (upper scale)
Arrows indicate threshold for reaction, E_0 = 2.60 eV, the
bond energy of H$_2$, D = 4.5 eV, the effective stripping limit
(see text), E_S = 5.0 eV, and the spectator stripping limit,
8.9 eV. The dotted line is the calculated two-collision
contribution to the cross section. The dashed line is the
total cross section in the threshold region calculated using
eq. 5 and parameters in Table I. The solid line is the
calculated total cross section described in the text convoluted
with the energy spread due to the thermal motion of the
reactant gas.

FIG. 3.   Variation in cross section for the reaction of Ni^+ with D^2 as

a function of kinetic energy in the center of mass frame

(lower scale) and the laboratory frame (upper scale).

Arrows indicate threshold for reaction, E_0 = 2.80 eV, the

bond energy of D_2, D = 4.60 eV, the effective stripping limit

(see text), E_s = 5.0 eV, and the spectator stripping limit,

8.9 eV.   The dotted line is the calculated two-collision

contribution to the cross section.   The dashed line is the

total cross section in the threshold region calculated using

eq. 5 and parameters in Table I.   The solid line is the

calculated total cross section described in the text convoluted

with the energy spread due to the thermal motion of the

reactant gas.

$Ni^+ + D_2 \longrightarrow NiD^+ + D$
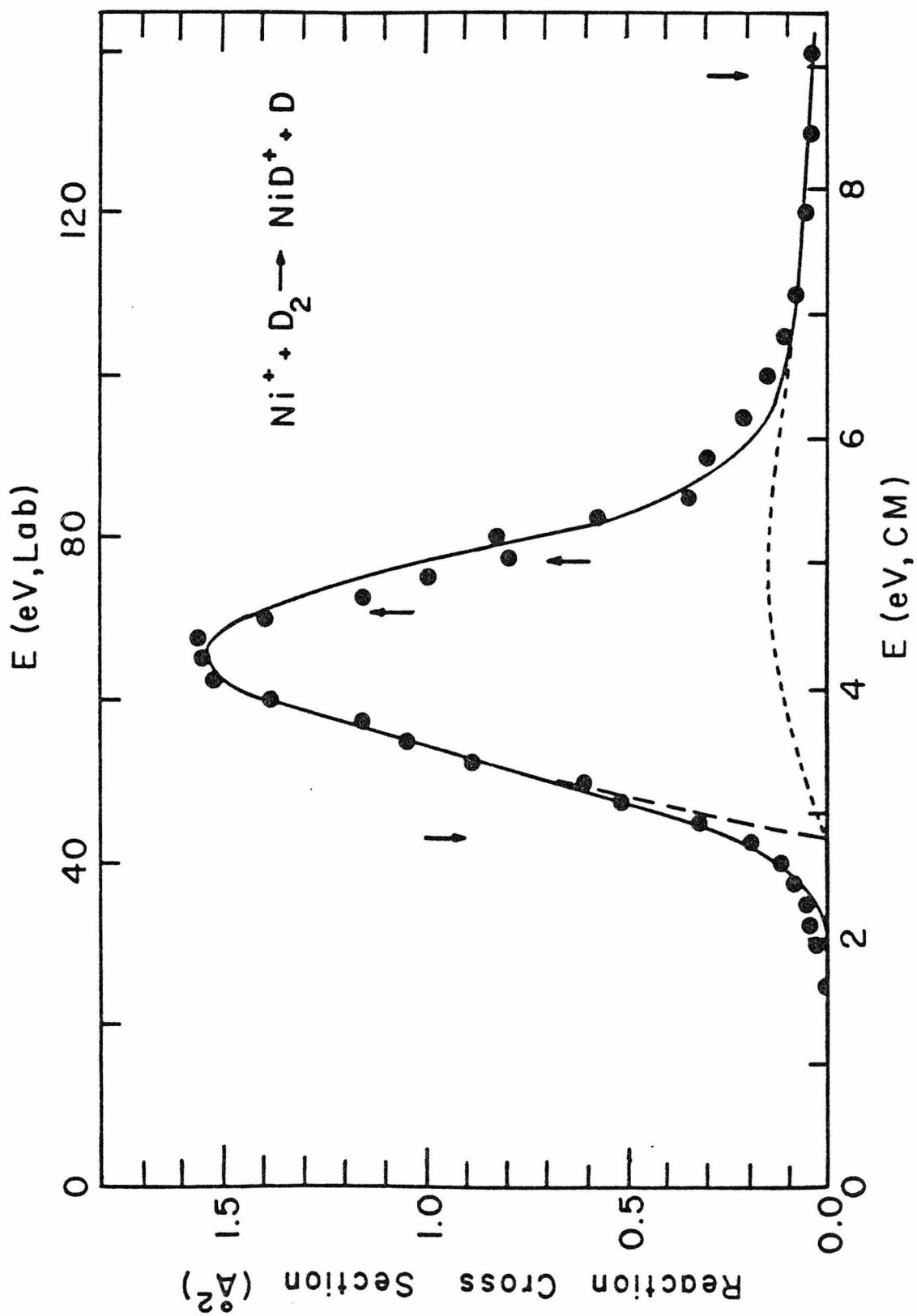
becomes energetically accessible. The result is formation of $NiH(D)^+$ which has sufficient energy to dissociate. As the kinetic energy increases, the fraction of unstable product increases and the cross section drops.

We can attempt to quantify this behavior by using a simple model previously proposed [9, 13]. The sequential impulse model for endothermic reactions examines the reaction A(BC, C)AB classically. All atoms are assumed to interact pairwise in hard sphere collisions. The model shows that the total cross section is composed of contributions from two types of collision events. The first type is a two-collision event where A hits B and then B hits C. Significant energy may be transferred to the neutral product in this sequence. Consequently, stable AB product may be produced even at very high collision energies. The second type of collision event is the stripping collision. Here, A hits B but no secondary collision occurs. However, consideration of the endothermicity of the reaction requires momentum be transferred to C in the bond breaking process. This differs somewhat from the ideal spectator stripping limit where it is assumed no momentum is transferred to the product C regardless of reaction thermochemistry [14].

This model predicts that at energies below D, the bond dissociation energy of BC, the total energy-dependent reaction cross section is given by

$$\sigma(E) = \sigma_0(1 - E_0/E) \tag{5}$$

where σ_0 is the hard sphere cross section for A-B collisions and E_0 is the threshold energy taken equal to the difference between the bond energies of the reactant and product diatoms. At energies above D, two collision events begint to produce unstable product. The fraction of stable product decreases with increasing energy but does persist to high energies. Stripping events have a sharp energy cut-off above which the diatomic product is unstable. This energy is defined by

$$E_S = (D - \cos^2 \beta \, E_0)/\sin^2 \beta \tag{6}$$

where $\cos^2 \beta = m_A m_C / m_{AB} m_{BC}$ and m refers to the mass of the appropriate species. In the spectator limit, this cut-off energy is just $D/\sin^2 \beta$.

Fitting eq. (5) to the data in the threshold regions, convoluted as discussed above, the parameters given in Table I are obtained. The fits are shown in Figs. 2 and 3. Using $D^0(H_2) = 4.52$ eV and $D^0(D_2) = 4.60$ eV [15], bond dissociation energies for NiH^+ 1.92 ± 0.12 eV and for NiD^+ 1.80 ± 0.15 eV are derived. Representing the cross section parameter as

$$\sigma_0 = \pi(r_H + r_{Ni})^2 \tag{7}$$

where r refers to the hard sphere radius of the appropriate species and taking $r_H = 0.25$ Å [16], we can derive an experimental hard sphere radius for Ni^+, $r_{Ni} \approx 1.0$ Å. This value may be compared favorably with the covalent radius of Ni, 1.2 Å [17], and the ionic radius of Ni^{2+}, 0.7 Å [18].

Table I

Parameters used to fit the threshold region of reaction of Ni^+ with H_2, HD and D_2 using eq. 5.

Reaction	Threshold Energy E_0 (eV)	Cross Section σ_0 (Å^2)
$Ni^+ H_2 \rightarrow NiH^+ + H$	2.60 ± 0.1	4.09
$Ni^+ + HD \rightarrow NiH^+ + D$	2.75 ± 0.1	4.02
$\quad\quad\quad\quad NiD^+ + H$	2.55 ± 0.1	1.02
$Ni^+ + D_2 \rightarrow NiD^+ + D$	2.80 ± 0.1	4.87

The sequential impulse model does not accurately portray the cross section behavior at higher energies. Its failure is demonstrated by noting that the rapid decrease in cross section occurs at lower energies than that predicted by eq. 6, $E_s \sim 6.3$ eV. Neglect of product rotational energy which can contribute to dissociation [19] may be the source of this failure. To compensate, E_s is treated as a variable parameter. The data are best fit for both the H_2 and D_2 systems when $E_s = 5.0$ eV. Including a contribution of approximately 10% due to two collision events which account for product formed at high energies, the complete fits, convoluted as discussed, are shown in Figs. 2 and 3.

$Ni^+ + HD$

The experimental results for the interaction of nickel ions and HD are shown in Fig. 4. As can be seen a substantial isotope effect is observed, Fig. 5. In the threshold region, approximately four times as much NiH^+ is produced as NiD^+. As the kinetic energy is raised further, the ratio of hydride to deuteride product goes through a maximum and then returns to a value of about four.

The total reaction cross section in the threshold region is quite comparable to that of the H_2 and D_2 systems. Again interpreting the energy thresholds using eq. 5, the parameters given in Table I are obtained. The bond energies derived, using $D^0(HD) = 4.55$ eV [8], are 1.80 ± 0.12 eV for NiH^+ and 2.00 ± 0.13 eV for NiD^+. These values are in reasonable agreement with those obtained from the H_2 and D_2 systems. Table II lists the average bond energies for NiH^+ and NiD^+

FIG. 4. Variation in cross section for the reactions of Ni^+ with HD as a function of kinetic energy in the center of mass frame (lower scale) and the laboratory frame (upper scale). Arrows indicate thresholds for reaction, $E_0(NiD^+) = 2.55$ eV and $E_0(NiH^+) = 2.75$ eV, the bond energy of HD, D = 4.55 eV, the effective stripping limits (see text) for NiD^+, $E_s = 5.5$ eV, and for NiH^+, $E_s = 8.5$ eV, and the spectator stripping limits, 6.7 eV and 13.2 eV, respectively. The dashed lines are the reaction cross sections for the products calculated using eq. 5 and parameters in Table I. The solid lines are the calculated cross sections described in the text convoluted with the energy spread due to the thermal motion of the reactant gas.
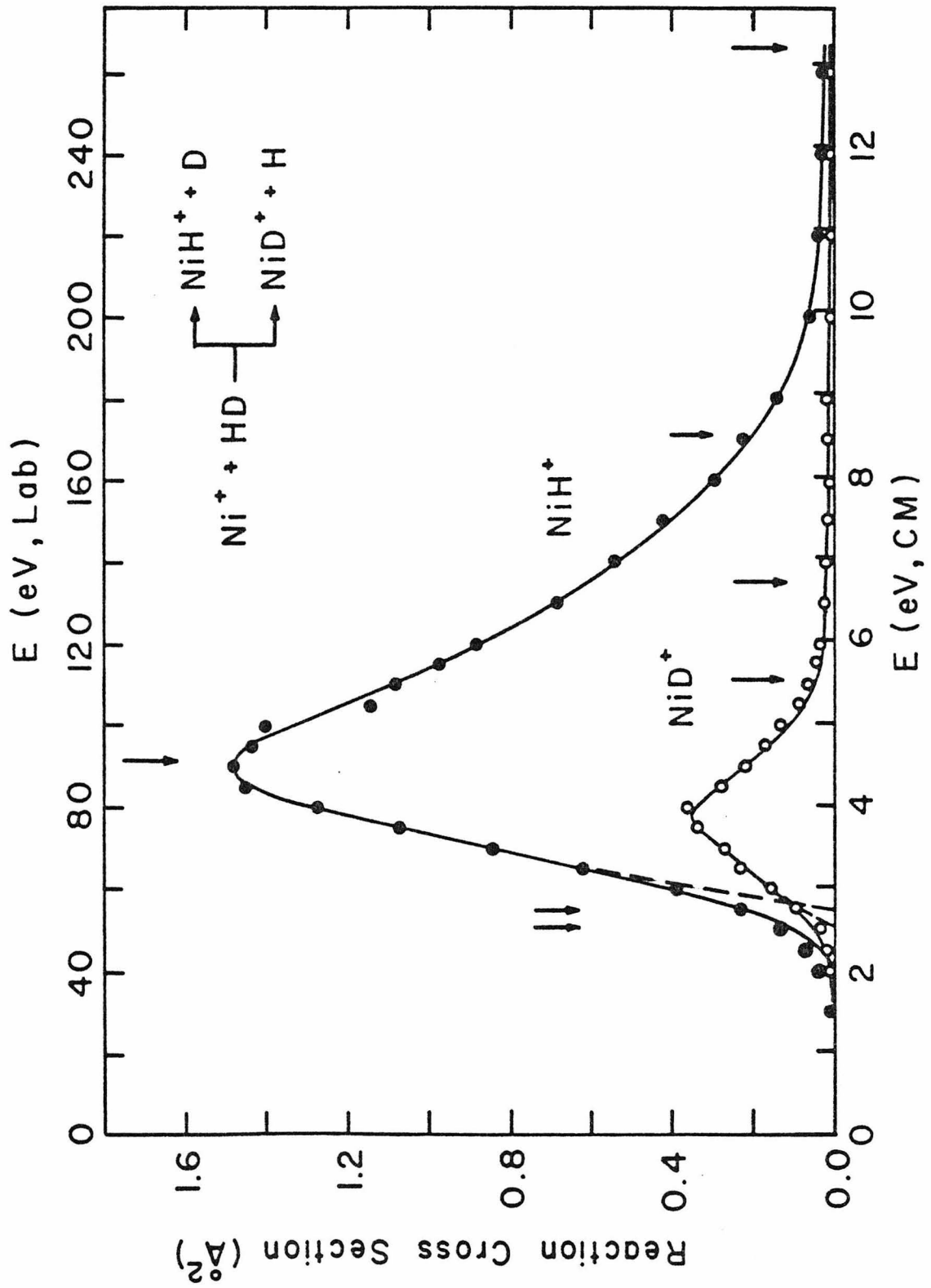
FIG. 5. Isotope effect observed in the reaction of Ni^+ with HD as a
function of relative kinetic energy. Arrows mark same
energies described in Fig. 4. Below 4 eV, the solid curve
and dashed curve correspond to the convoluted and uncon-
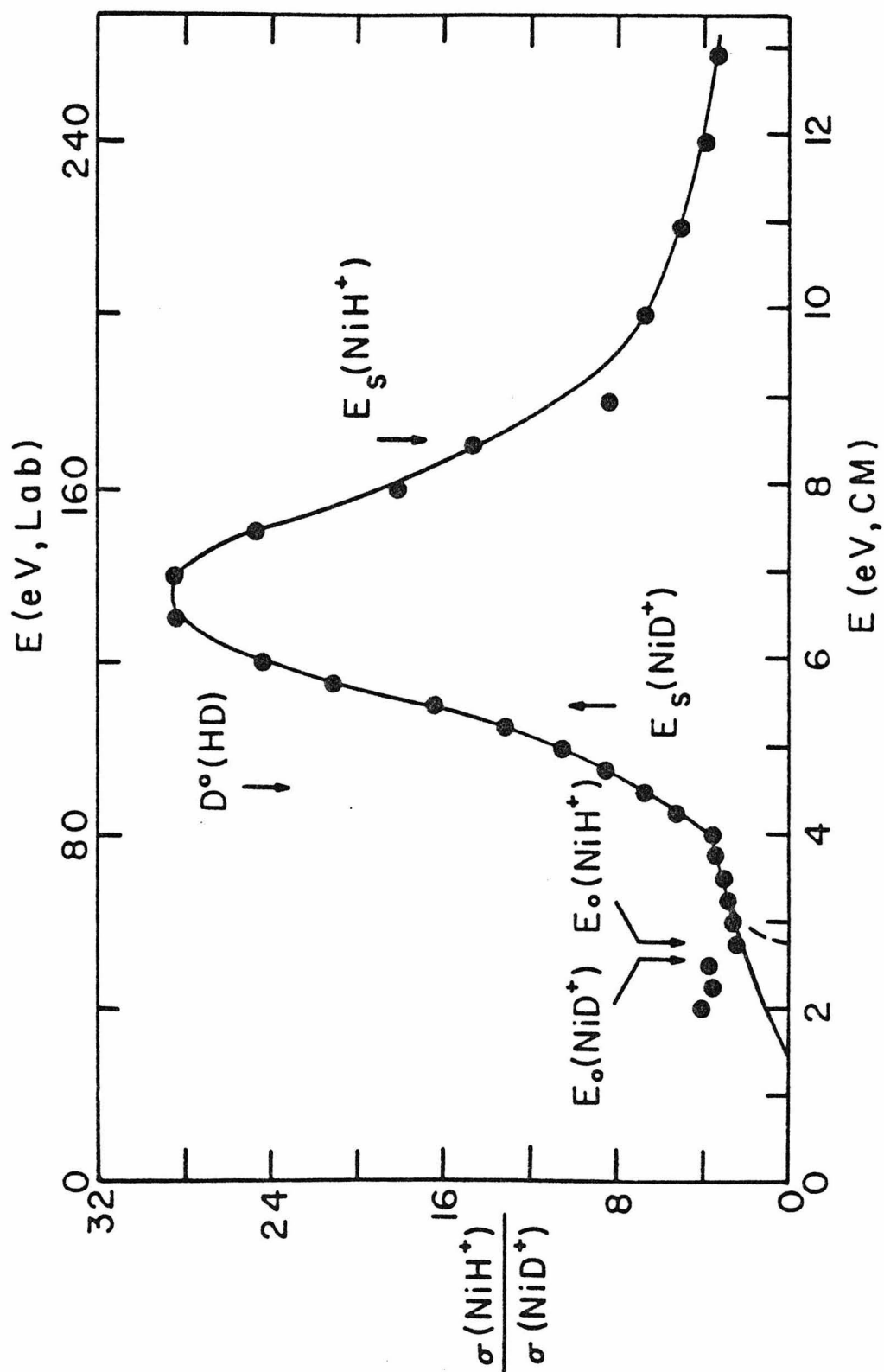voluted fits plotted in Fig. 4.

Table II

Thermochemistry of nickel and cobalt hydrides and their ions.
All values in eV.

Metal (M)	Ionization[a] Potential (M)	Bond Energy (M-H)	Ionization Potential (MH)	Bond Energy (M^+-H)
Ni (H)	7.63	2.1 ± 0.4	7.9 ± 0.3[b]	1.86 ± 0.09[c]
		2.6 ± 0.3[d]	8.4 ± 0.4	
(D)				1.90 ± 0.14[c]
Co	7.87	1.7 ± 0.5	7.3 ± 0.3[e]	2.25 ± 0.17[e]

(a) Ref. 27.

(b) Ref. 26.

(c) This study.

(d) Ref. 28.

(e) Ref. 10.

determined in this study.

It may be noted that the impulse model discussed above predicts that the energy at which product is first observed, an effective threshold, is

$$E_1 = E_0/4\cos^2\beta \sin^2\beta . \tag{8}$$

In the H_2 and D_2 systems, the values of $4\cos^2\beta \sin^2\beta$ are very nearly unity (within 0.1 %); but for HD, the value for both products is 0.90. Correcting the experimental thresholds by this factor, we obtain $D^0(NiH^+) = 2.07$ eV and $D^0(NiD^+) = 2.32$ eV. These values do not agree as well with the bond energies derived in the H_2 and D_2 systems as the uncorrected energies.

Qualitatively, the behavior of the excitation functions at high energies, $E > D$, is a direct consequence of the difference in mass involved. Examination of the ideal spectator stripping model is elucidating. For the present case where $m_{Ni} \gg m_H$, m_D, the center of mass before and after collision is situated on the nickel atom. By definition, after reaction has occurred, the free atom has zero velocity in the laboratory frame. In the center of mass frame, its velocity is equal to the center of mass velocity regardless of its mass. If the free atom is deuterium, twice as much energy is in translation as if the free atom is hydrogen. Since energy conservation requires the difference be in internal modes, the NiD^+ product is generally formed with more internal energy than the NiH^+ product at the same relative kinetic energy. This effect is quantified using eq. 6 which predicts substantial product dissociation at $E_s(NiH^+) = 8.5$ eV and

$E_s(NiD^+) = 5.5$ eV. As in the systems with H_2 and D_2, product dissociation occurs predominantly at lower energies than those calculated.

As before, only small amounts of product persist to the highest energies, indicating small contributions from 2 collision events. We can fit the NiD^+ cross section using eq. 5 with a cut-off at 4.6 eV. However, no such simple fit can be obtained for the cross section of NiH^+ which decreases approximately as E^{-3} between 5 and 7.5 eV and as E^{-7} between 7.5 eV and 11 eV. The fit shown is a 10% contribution from one-collision events with a cut-off at the predicted energy of 8.5 eV and a 90% contribution from two-collision events where the H-D collision occurs head-on exclusively.

While consideration of product stability qualitatively describes the energy dependence of the ratio $\sigma(NiH^+)/\sigma(NiD^+)$, the explanation for a 4:1 ratio in the threshold region and at the highest energies is still unclear. Certainly, this ratio is highly suggestive of a mass effect since it equals the inverse of the square of the mass ratio. One simple suggestion is that since the center of mass of HD is displaced from the center of the bond, the effective area the H atom can present to an incoming nickel ion is four times that of the D atom. In essence, collision with the hydrogen end of the molecule can occur at larger impact parameter than with the deuterium end. Another possible explanation concerns orientation effects based on the displacement of the center of polarizability from the center of mass [20]. This displacement tends to orient the HD molecule with the hydrogen

end towards the incoming ion. However, at the energies necessary for reaction to occur, reorientation is slow compared with collision times. Consequently, it is not expected that this effect can account for the isotope effect observed.

Discussion

It is of interest to compare the present results with those for the reaction of C^+ with H_2, HD, and D_2. Here, too, the total cross sections for reaction with H_2 and D_2 were comparable [21]. However, the isotope ratio, $\sigma(CH^+)/\sigma(CD^+)$, in the HD system was approximately 0.65 from threshold, ~0.4 eV, to 8 eV [22]. Since the intermediate CH_2^+ is a very stable species, -4 eV compared to $C^+ + H_2$ [23], the formation of a long-lived complex is likely and will greatly influence the reaction dynamics [24]. While the nickel dihydride ion, NiH_2^+, has been observed in field ionization experiments [25], the present results, assuming $D^0(HNi^+-H) \approx D^0(Ni^+-H)$, suggest this species will not be stable with respect to $Ni^+ + H_2$ by about 0.8 eV. This implies a barrier to reductive elimination of H_2 from NiH_2^+. Speculation on the potential energy surface for the nickel ion-hydrogen system is shown in Fig. 6. Thus, even though a well may exist along the reaction coordinate, at the energies necessary for reaction, it is likely the reaction is direct. Indeed, the isotope effect observed in the Ni^+-HD system suggests this is the case since formation of $HNiD^+$ species should tend to produce equal amounts of NiH^+ and NiD^+ products.

In other studies in our laboratories, the ionization potential of nickel hydride, IP(NiH), has been estimated as 7.9 ± 0.3 eV. Using

FIG. 6.   Approximate potential energy diagram for the Ni^+-H_2 system. The solid line shows the curve for a perpendicular approach of Ni^+ to H_2 and the dashed line shows that for a collinear approach.
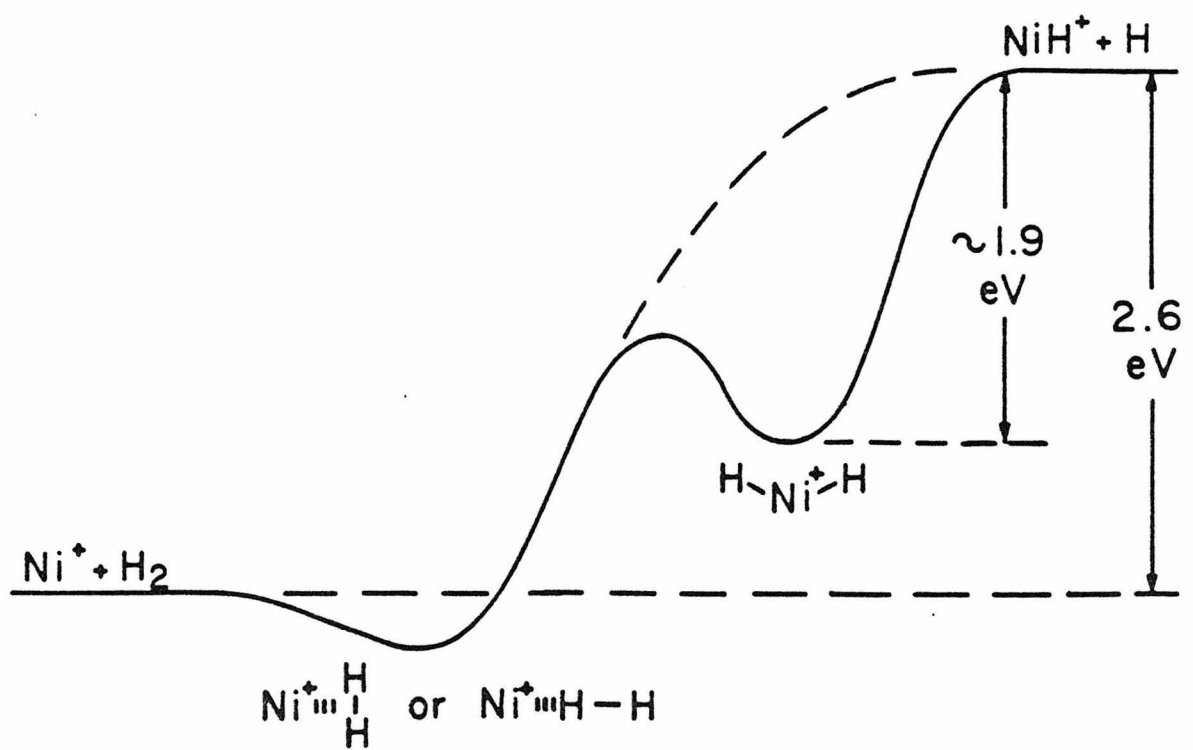
$$D^0(NiH) = IP(NiH) - IP(Ni) + D^0(Ni^+-H) \qquad (9)$$

where $IP(Ni) = 7.63$ eV [27], the bond dissociation energy of nickel hydride neutral is found to be 2.1 ± 0.4 eV in reasonable agreement with Gaydon's value of 2.6 ± 0.3 eV [28]. The proton affinity of the nickel atom can be calculated from

$$PA(Ni) = IP(H) - IP(Ni) + D^0(Ni^+-H). \qquad (10)$$

The value obtained, 180 ± 3 kcal/mol, is comparable to those for other transition metals, $PA(Co) = 184 \pm 4$ kcal/mol [10] and $PA(Fe) < 203$ kcal/mol [29], but well below those of such strong atomic bases as Ba, 250 ± 3 kcal/mol [9], and U, 238 ± 4 kcal/mol [8].

Comparison of the bond energies for the nickel and cobalt hydride ions and neutrals is shown in Table II. Of particular note is the fact that while NiH has a stronger bond than NiH^+, the opposite is the case for cobalt. Examination of the states of the metals suggests possible reasons for this behavior. Calculations have shown that the nickel atom and hydrogen atom form a bond by pairing a Ni 4s orbital with the H 1s [30]. However, the ground states of Ni and Co have s^2d^8 and s^2d^7 configurations, respectively, while Ni^+ and Co^+ have d^9 and d^8 configuration ground states. To excite these metals to an s^1d^n configuration requires 0.03 eV for Ni, 0.43 eV for Co, 1.04 eV for Ni^+ and 0.42 eV for Co^+ [27]. The differences in promotion energy would predict a NiH bond stronger than a CoH bond by 0.4 eV, and a 0.6 eV difference in bond energies for the ions such that the NiH^+ bond is the weaker. The comparison with the observed trend is good;

however, correlation effects and the loss of exchange energy should also be considered.

Acknowledgment

References

[1] See for example, J. K. A. Clarke and J. J. Rooney, Adv. in Catalysis, 25 (1976) 125.

[2] W. C. Trogler, D. K. Erwin, G. L. Geoffroy and H. B. Gray, J. Am. Chem. Soc. 100 (1978) 1160.

[3] a) T. R. P. Gibb, Progress in Inorg. Chem., ed. F. A. Cotton, 3, Interscience, N.Y., 1962;

b) D. G. Westlake, C. B. Satterthwaite and J. H. Weaver, Physics Today, 32 Nov. (1978).

[4] See for example, R. R. Schrock and G. W. Parshall, Chem. Rev. 76 (1976) 243.

[5] W. Weltner, Science 155 (1967) 155; R. J. Van Zee, T. C. DeVore and W. Weltner, J. Chem. Phys. 71 (1979) 2051 and references therein.

[6] R. E. Smith, Proc. Roy. Soc. London A, 332 (1973) 113.

[7] P. R. Scott and W. G. Richards, "Molecular Spectroscopy," ed. by R. F. Barrow, D. A. Long and D. J. Millen, (Specialist Periodical Reports), Vol. 4, (The Chemical Society, London, 1976) p. 70.

[8] P. B. Armentrout, R. V. Hodges and J. L. Beauchamp, J. Chem. Phys. 66 (1977) 4683.

[9] P. B. Armentrout and J. L. Beauchamp, Chem. Phys., submitted.

[10] P. B. Armentrout and J. L. Beauchamp, J. Am. Chem. Soc., submitted.

[11] B. R. Turner, J. A. Rutherford and D. M. J. Compton, J.

References (continued)

Chem. Phys. 48 (1968) 1602.

[12] P. J. Chantry, J. Chem. Phys. 55 (1971) 2746.

[13] B. H. Mahan, W. E. W. Ruska and J. S. Winn, J. Chem. Phys. 65 (1976) 3888.

[14] A. Henglein in "Ion Molecule Reactions in the Gas Phase", ed. Pierre Ausloos, (ACS, Washington, D.C., 1966) p. 63.

[15] B. de B. Darwent, Natl. Stand. Ref. Data Ser., Natl. Bur. Stand., NSRDS-NBS 31 (1970).

[16] K. T. Gillen, B. H. Mahan and J. S. Winn, J. Chem. Phys. 59 (1973) 6380.

[17] W. P. Pearson, "A Handbook of Lattice Spacings and Structures of Metals and Alloys", Pergamon Press, Elmsford, N.Y., 1958.

[18] F. A. Cotton and G. Wilkinson, "Advanced Inorganic Chemistry" 3rd Ed., Interscience, N.Y., 1972, p. 52.

[19] J. T. Muckerman, J. Chem. Phys. 57 (1972) 3388.

[20] P. M. Hierl, J. Chem. Phys. 67 (1977) 4665.

[21] E. Lindemann, L. C. Frees, R. W. Rozett and W. S. Koski, J. Chem. Phys. 56 (1972) 1003.

[22] M. Henchman, "Ion-Molecule Reactions", Vol. 1, ed. J. L. Franklin, Plenum, New York, 1972, p. 244.

[23] B. H. Mahan and T. M. Sloane, J. Chem. Phys. 59 (1973) 5661.

[24] W. J. Chesnovich and M. T. Bowers, J. Chem. Phys. 68 (1978) 901.

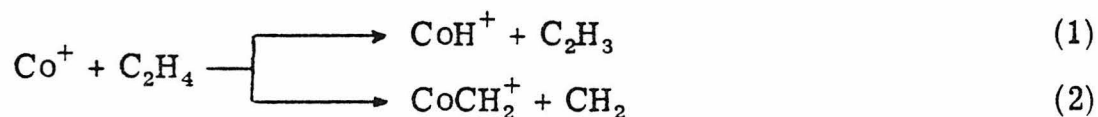[25] S. Kapur and E. W. Muller, Surf. Sci. 66 (1977) 45.

References (continued)

[26] L. F. Halle, P. B. Armentrout and J. L. Beauchamp, to be published. The method used is the same as that of Ref. 10.

[27] C. E. Moore, "Atomic Energy Levels", Natl. Bur. Stand., Washington, D.C., 1949.

[28] A. G. Gaydon, "Dissociation Energies and Spectra of Diatomic Molecules", Chapman and Hall, London, 1947.

[29] J. Allison and D. P. Ridge, J. Am. Chem. Soc. 101 (1979) 4998.

[30] M. J. Sollenberger, M. S. Thesis, California Institute of Technology, 1976; S. P. Walch and W. A. Goddard III, J. Am. Chem. Soc. 100 (1978) 1338.
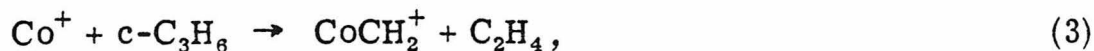
CHAPTER VI

COBALT CARBENE ION: REACTIONS OF Co^+ WITH C_2H_4, cyclo-C_3H_6, AND cyclo-C_2H_4O

Cobalt carbene ion: Reactions of Co^+ with C_2H_4, cyclo-C_3H_6, and cyclo-C_2H_4O

P. B. Armentrout and J. L. Beauchamp

Contribution No. _____ from the Arthur Amos Noyes Laboratory of Chemical Physics, California Institute of Technology, Pasadena, California 91125

(Received   )

Abstract

An ion beam apparatus is employed to study the formation of the cobalt carbene ion, $CoCH_2^+$. This ion is produced in the endothermic reaction of cobalt ions with ethene and cyclopropane and in an exothermic reaction with ethylene oxide. A model is proposed to account for the dependence of experimental cross sections on relative kinetic energy for the endothermic reactions. Using this model to interpret the experimental results, a bond dissociation energy $D°(Co^+-CH_2) = 3.7 \pm 0.3$ eV is derived.
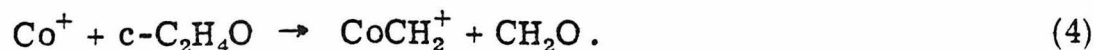
I. INTRODUCTION

Transition metal carbenes have been postulated as intermediates in a variety of reactions, including metal alkyl decomposition,[1] olefin metathesis,[2] polymerization of olefins,[3] olefin homologation,[4] and cyclopropane formation from olefins.[5] Yet, despite their seeming abundance, little is known about metal carbene thermochemistry. Recently, ion cyclotron resonance spectroscopy was used in our laboratories to prepare several ionic carbenes of iron[6] and manganese[7] in the gas phase. These studies included the first experimental determinations of metal carbene bond dissociation energies. The present investigation represents a continuation of our effort to characterize metal carbenes in the gas phase. Specifically, we have studied the endothermic reactions of Co^+ with ethene,

$$Co^+ + C_2H_4 \longrightarrow \begin{array}{l} CoH^+ + C_2H_3 \quad (1) \\ CoCH_2^+ + CH_2 \quad (2) \end{array}$$

and with cyclopropane,

$$Co^+ + c\text{-}C_3H_6 \rightarrow CoCH_2^+ + C_2H_4, \tag{3}$$

and the exothermic reaction with ethylene oxide,

$$Co^+ + c\text{-}C_2H_4O \rightarrow CoCH_2^+ + CH_2O. \tag{4}$$

A complete understanding of the dynamics of such reactions requires knowledge of the potential energy surface. Due to the unavailability of such detailed information, a simple surface

consisting of only the reaction coordinate is often considered. The dynamics of chemical reactions are often dominated by the gross features of such a simplified surface.[8] Speculation on the reaction coordinate diagrams for processes 2-4 reveals important features which distinguish these reactions. In Fig. 1(a), the example of a highly endothermic process, reaction 2, is given. Even though the binding energy of Co^+ to ethene is substantial, giving rise to a potential well,[9] a considerable amount of energy must be provided to surmount the reaction barrier. At these energies, the influence of the well on the reaction dynamics is small, and therefore, we expect the reaction to be direct. The endothermicity of reaction 3, Fig. 1(b), is much less. Based on related studies,[10] the formation of a metallocyclobutane as a reaction intermediate is proposed. The well corresponding to this reaction intermediate should be of comparable magnitude to the heat of reaction. This situation is more conducive to the formation of a long-lived complex which can dissociate in many ways including back to reactants. Finally, we consider a case where the reaction is exothermic, Fig. 1(c). A long-lived intermediate is again expected but now formation of products is much more likely.

In the present study, a particular form for the excitation function of endothermic reactions is proposed. This form is used to analyze the dependence of the cross section for reaction 2 on kinetic energy of the reactant ion. Previously, the analyses of such processes concentrated on interpretation of the threshold region. In this paper, we have extended this analysis to

FIG. 1.   Postulated reaction coordinate diagrams for reaction 2,
part a, reaction 3, part b, and reaction 4, part c. The
heats of reaction are determined in the present study.
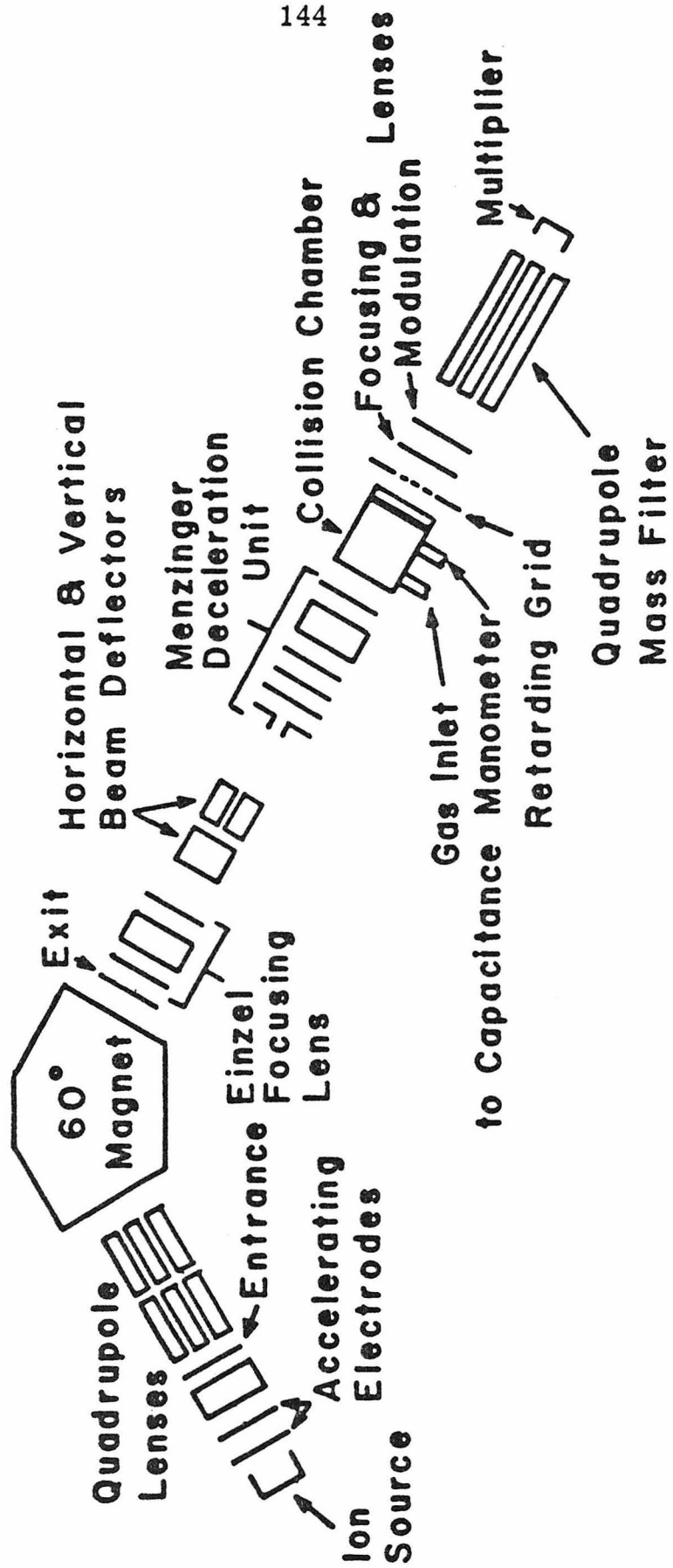The scale of part a is a factor of 6 less than parts b and c.
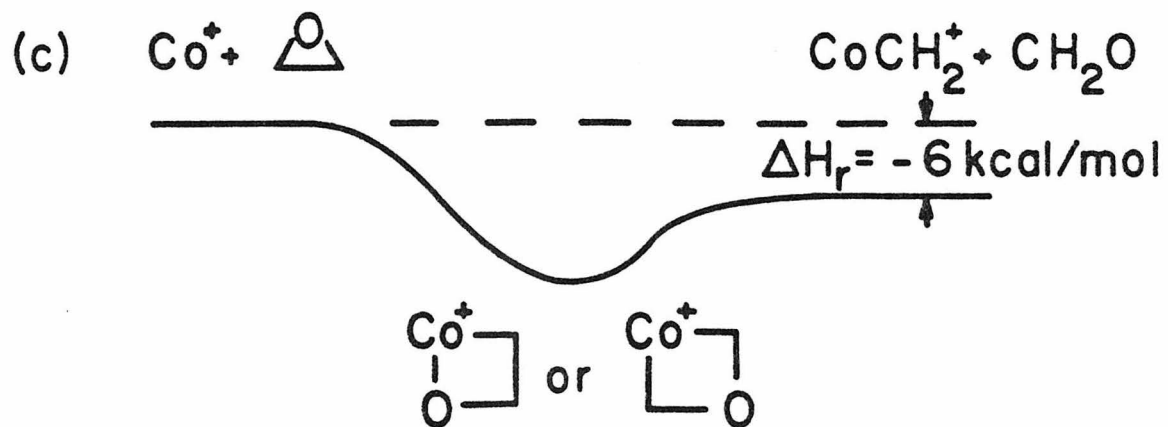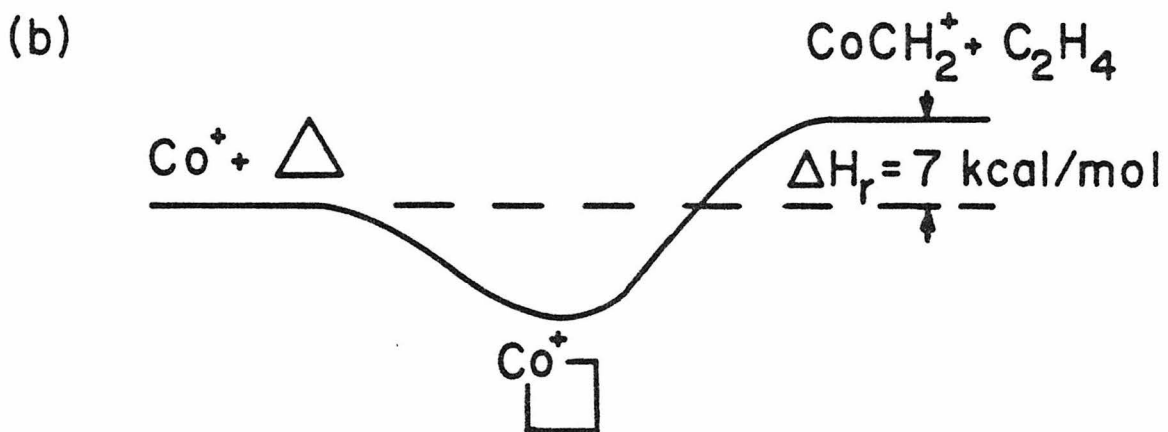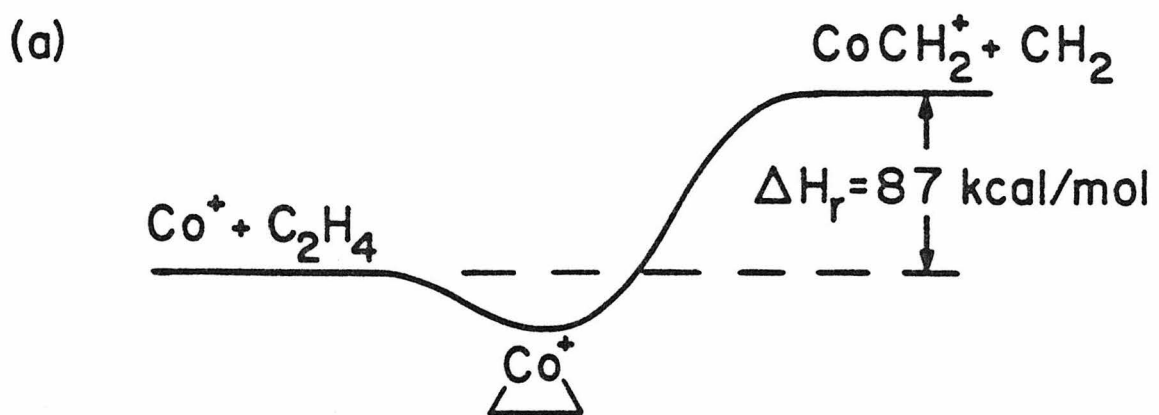
include the energy region where substantial product dissociation may occur.[11] The proposed form for the reaction cross section is shown to fit the experimental results over a large energy range. The threshold measured for reaction 2, using this analysis, allows us to derive the bond dissociation energy, $D°(Co^+-CH_2) = 85 \pm 7$ kcal/mol. This agrees with the upper limit for this bond energy of 92 kcal/mol established by the endothermicity of reaction 3 and with the lower limit of 79 kcal/mol established by the exothermicity of reaction 4. The agreement gives us confidence that the analysis is useful in obtaining accurate thermochemical data.

II. EXPERIMENTAL

The ion beam apparatus shown in Fig. 2 is a highly modified version of an instrument previously described.[12] Ions from a surface ionization source are accelerated (typically to about 700 volts) and focused into a 60° sector magnet for mass separation. The ion beam mass selector provides unit mass resolution to greater than 100 m/z. This mass selected beam is decelerated and focused into a collision chamber containing the reactant gas. Product ions scattered in the forward direction are focused into a quadrupole mass filter and detected using a Channeltron electron multiplier operated in a pulse counting mode. Ion signal intensities are corrected for the mass discrimination of the quadrupole mass filter.

The ion source, previously described,[12] is comprised of a tubular stainless steel oven attached to the side of a U-shaped repeller plate which surrounds a rhenium ionization filament. For these

FIG. 2.   Schematic diagram of the ion beam apparatus.

Ion Source

Quadrupole Lenses

Accelerating Electrodes

Entrance Einzel Focusing Lens

60° Magnet

Exit

Horizontal & Vertical Beam Deflectors

Menzinger Deceleration Unit

Collision Chamber

Gas Inlet

to Capacitance Manometer

Retarding Grid

Focusing & Modulation Lenses

Quadrupole Mass Filter

Multiplier

experiments, the oven is loaded with $CoCl_2 \cdot 6H_2O$. The filament generates sufficient heat to dehydrate the cobalt complex and vaporize the $CoCl_2$. This vapor is directed at the filament where dissociation and ionization of the resulting Co takes place. This method of ionization minimizes the production of excited metal ion states. It is estimated that at the filament temperature used, $\sim2500°$K, 81% of the Co^+ ions produced are in the ^3F ground state manifold and 19% are in the ^5F excited state manifold at 0.42 eV. In order to observe the effects of an excited state, its lifetime must exceed about $10\,\mu s$, the approximate flight time of the ions. An attempt was made to determine the presence of excited ions using an attenuation technique.[13,14] Only a single component was detected, suggesting that excited ions are absent. This assumes that the ^3F and ^5F states have different total scattering cross sections for the collision gases used (O_2, C_2H_4, and C_2H_6).

The energy of the ion beam is taken nominally as the difference in potential between the collision chamber and the center of the filament, the latter being determined by a resistive divider. This energy is verified by use of a retarding field energy analyzer.[15] Agreement was always within 0.3 eV. The energy width of the Co^+ beam was also thus obtained and determined to be 0.7 eV (FWHM). In the center of mass frame, this introduces an uncertainty of ±0.12 eV in the reaction with C_2H_4 and of ±0.15 eV with c-C_3H_6 and c-C_2H_4O. No specific account of the energy distribution of the ion beam is taken in the treatment below.

Despite attempts to make such measurements, we find the present apparatus is not particularly suited to accurate determinations of product ion energies.[15] Severe problems due to focusing effects

preclude an effective analysis on any ion having low intensity and a wide spread in kinetic energy. These effects may be accounted for if the ion is sufficiently intense and nearly monoenergetic (as for the incident ion beam).

A more severe problem concerning the actual energy of interaction is the effect of the thermal motion of the reactant gas. Chantry[16] has shown that the distribution of the relative kinetic energy at an energy E due to this effect has a full width at half-maximum of

$$W_{\frac{1}{2}} = (11.1 \, \gamma kTE)^{\frac{1}{2}} \tag{5}$$

where T is the temperature of the target gas, and $\gamma = m/(m + M)$, m and M being the masses of the incident particle and target gas. Thus, $W_{\frac{1}{2}} = 0.44 \, E^{\frac{1}{2}}$ eV for the reactions with ethene and $W_{\frac{1}{2}} = 0.41 \, E^{\frac{1}{2}}$ for reaction with cyclopropane or ethylene oxide. This energy distribution effectively broadens any sharp features in the excitation function, including threshold. To account for this effect, the proposed excitation function is convoluted with this distribution before comparison with the data using the method outlined by Chantry.[16]

Reaction cross sections for a specific product, σ_i, are calculated from

$$\sigma_i = \sigma I_i / \Sigma I_i \tag{6}$$

where the sum is over all products and I_i refers to a particular measured product ion intensity. The total reaction cross section, σ, is evaluated using

$$I_0 = (I_0 + \Sigma I_i) \exp(-n\sigma\ell) \tag{7}$$

where I_0 is the transmitted reactant ion beam intensity, n is the number density of the target gas, and ℓ is the length of the interaction region. The pressure of the target gas, measured using an MKS Baratron Model 90H1 capacitance manometer, is kept sufficiently low, $1\text{-}5 \times 10^{-3}$ Torr, that attenuation of the ion beam is minimal. The length of the interaction region is 5 mm, and is uncorrected for entrance and exit apparature effects[17] (1.0 and 1.5 mm in diameter, respectively). Our experimental procedure is to take a complete scan of kinetic energy at a single pressure to obtain the excitation function. At several energies, the product yield is measured as a function of pressure to ensure Eqs. (6) and (7) are obeyed. This procedure also readily identifies products formed by more than one collision event.[18]

The greatest uncertainty in measurements of reaction cross sections is the ion detection efficiency. In the present experiments which involve heavy projectile and light target species, efficient detection is assisted by the appreciable center of mass velocity which tends to scatter all products in the forward direction in the laboratory frame. At laboratory energies below about 10 eV, a small field of 0.5 V is placed across the specially designed collision chamber[12] to extract low energy ions. This field introduces an additional uncertainty in the energy of interaction. Relative cross sections are well reproduced and we estimate that the absolute cross sections reported are accurate to a factor of two.

III. THEORETICAL

A key problem in obtaining information from measurements such as those made in the present study is an accurate determination of the true microscopic cross section for reaction, $\sigma(E)$. It has been shown that direct deconvolution of the phenomenological cross section measured does not yield a unique reaction cross section independent of the experimental energy distributions.[19] Thus, a choice for the form of $\sigma(E)$ must be made and eventually shown to be consistent with the data by averaging over the experimental conditions (as above).[16] This choice, however, is not an easy one. No ab initio theory presently exists which derives the correct general form for particle transfer reactions. While trajectory calculations[20] can yield $\sigma(E)$ for a given reaction, this is clearly of no general help to the experimentalist. Simple models,[21] such as hard sphere cross sections, line of centers cross sections, or cross sections determined by the long-range portion of the interaction potential of the reactants, may be used. However, these are primarily useful in defining an encounter but not subsequent events which may or may not lead to reaction. In the past, workers have assumed forms for $\sigma(E)$ which are easy to handle mathematically such as step functions,[22] linear functions,[12,22,23] and exponential functions.[24]

Another approach is to "derive" $\sigma(E)$ from statistical considerations developed for understanding reaction rates such as transition state theory,[25] RRKM theory,[26] and phase space theory.[27,28] However, these theories were developed such that no particular form

for the reaction cross section need be assumed. Consequently, additional assumptions are required to derive a cross section.[25, 29, 30]

1. Form for $\sigma(E)$

The choice we will make for the reaction cross sections is that it has the general form

$$\sigma(E) \propto \left(\frac{E - E_0}{E} \right)^n \tag{8}$$

when we refer to a direct state to state reaction. Here, the reactants have a total energy E and the barrier to reaction is E_0. When $n = 1$, this form reduces to the familiar line of centers model which has often been found to have approximately the correct shape for experimental cross sections.[18] Expression (8) is also familiar as the probability derived by Kassel[31] for one particular oscillator out of a system $n + 1$ oscillators to have an energy greater than E_0 when the total system energy is E. We expect that the problem of determining whether sufficient energy is in a reaction coordinate of a system having $n + 1$ degrees of freedom should be related. The form of (8) can also be viewed as a ratio of numbers of states (in a classical approximation)[26] of a transition state to that of an energized molecule[25] or as the ratio of flux in the reaction product channel relative to the incident flux.[32, 33]

This latter viewpoint suggests several possible refinements which may become warranted as more experiments are done and compared with theory. The first of these refinements is to simply replace (8) by the ratio

$$\sigma(E) \propto N^+(E^+)/N(E) \qquad (9)$$

where $N(x)$ is the number of quantum states of a system with an energy less than or equal to x, $N^+(E^+)$ refers to a transition state with $E^+ = E - E_0$, and $N(E)$, for a direct reaction, refers to the reactants. Now, rather than use classical approximations yielding the form in (8), other means of counting states, such as direct count or semiclassical expressions,[26] may be utilized. These may be more accurate especially near reaction threshold. It can also be noted that expression (9), using a classical approximation, may yield

$$\sigma(E) \propto (E - E_0)^n/E^m \qquad (10)$$

such that n and m are not equal. This could be the case, for instance, if a tight transition state were involved.[34]

The second refinement is the extension to reactions which may proceed via long-lived complex formation. The cross section for reaction is now related to

$$\sigma^\alpha(E) \propto [N^\alpha(E)/\sum_\alpha N^\alpha(E)] \qquad (11)$$

where the sum if over all decomposition paths, designated by α, of the complex (including back to reactants).[34] The expressions (9) and (11) can be identified with the reaction probabilities of Miller's unified statistical theory[33] and thus may be extended to intermediate cases between direct and complex mechanisms.

2. Influence of product dissociation on the form for $\sigma(E)$

The possibility of product dissociation can have a profound influence on the cross section observed for product formation. The thermodynamic threshold for such dissociation is simply the dissociation energy of the bond broken during reaction. However, not all of the available energy will be in the internal modes of the appropriate product. We can estimate that energy assuming that the energy is statistically distributed among the degrees of freedom of the products.[34,35] Treating the problem classically, neglecting angular momentum[36] and remembering that only n internal modes are "active" (excluding the reaction coordinate), it can be shown that the probability of an energy greater than E_v is in internal modes of the products at a total available energy $(E - E_0)$ is just

$$P = [E_v/(E - E_0)]^n . \tag{12}$$

We now assume the product ion dissociates if its internal energy exceeds its bond dissociation energy, D. We define the parameter a as the average fraction of internal energy E_v in the ionic fragment. The dissociation probability (i.e., the probability $aE_v \geq D$) becomes

$$P = [D/a(E - E_0)]^n . \tag{13}$$

If the neutral product is monatomic, a equals unity,[37] and if polyatomic, $0 < a < 1$.

3. Expression to be used for $\sigma(E)$

If we recognize that expression (8) is the reaction probability, P, the final result for $\sigma(E)$ is given by

$$\sigma(E) = 2\pi \int_0^{b_m} P \, b \, db \tag{14}$$

where b is the collision impact parameter and b_m is the maximum value of b for which reaction occurs.[21] Thus, we find

$$\sigma(E) = \pi b_m^2 P = \sigma_0 P. \tag{15}$$

The value of σ_0 may be determined by assuming one of two simple models: one based on the long range intermolecular potential of the reactants[38] and the hard sphere model.[21] The long range inter-molecular potential is given by $-C/r^S$ where r is the distance between reactants. For the specific case of ion-molecule reactions, (s = 4, $C = \alpha/2$, α is the polarizability of the neutral reactant), the result is

$$\sigma_0 = \pi e (2\alpha/E)^{\frac{1}{2}}. \tag{16}$$

This should only be the case until $E = 2\alpha/d^4$ where d is the hard sphere radius.[8] Above this energy, usually less than 1 eV, $\sigma_0 = \pi d^2$, the hard sphere model result.

Summarizing, the form for the reaction cross section below E_0 is zero. For $E_0 < E < E_0 + D/a$, $\sigma(E)$ is given by

$$\sigma(E) = \sigma_0 \left(\frac{E - E_0}{E} \right)^n. \tag{17}$$

For $E > E_0 + D/a$, the cross section is the product of Eqs. (13) and (17) or simply

$$\sigma(E) = \sigma_0 (D/aE)^n . \tag{18}$$

4. Application to experiment

For the reactions in the present study, the total energy E is taken equal to the relative translational energy since under our experimental conditions this energy is much greater than the internal energy of the reactants. We also assume that there is no barrier for reverse reaction (i.e., the transition state is loose). Consequently, E_0 represents the energy difference between products and reactants. We use Eqs. (17) and (18) to fit the data treating σ_0, E_0, n and a as variable parameters. [Note that $D = D^0$ (neutral reactant bond) - E_0.] Determination of these parameters is aided by several techniques of analysis. First, n can be determined from a log-log plot of σ vs. E since the slope of this plot at high energies (after product dissociation commences) is -n. In general, we restrict ourselves to integral and half-integral values of n. Knowing n, σ_0 and E_0 may be determined by plotting $\sigma^{1/n} E$ vs. E for low energies which gives a slope of $\sigma_0^{1/n}$ and an energy axis intercept of E_0. The parameter a is determined by fitting the high side of the excitation function. An alternate means of assessing n and E_0 is to plot $\sigma/[E(\partial\sigma/\partial E)]$ vs. E for low energies which gives an energy axis intercept of E_0 and a slope of $1/nE_0$. Having determined n and approximate values of σ_0 and E_0, we convolute this starting function as discussed above and adjust these parameters until a good

fit is obtained. We also assess how sensitive the fit is to the value of n which fits the best. Often, within experimental error, several sets of parameters fit the data equally well. This, then is how the errors in E_0 are determined.

IV. RESULTS

1. $Co^+ + C_2H_4$

Cobalt ions react with ethene to yield two products, CoH^+, reaction 1, and $CoCH_2^+$, reaction 2. Variation of cross section with relative kinetic energy is shown in Figs. 3 and 4, respectively. The background at low energies in Fig. 3 is apparently due to a contribution from reaction at higher energies outside the collision chamber. The theoretical fit shown in Fig. 3 is obtained using only Eq. (17) with n = 2, σ_0 = 1.81 $\mathring{A}^2$, and E_0 = 2.5 eV. An equally good fit is obtained with n as low as 1.5 and as high as 3.0 giving threshold energies from 2.9 eV to 2.0 eV. The sharp rise in cross section at $\sim$18 eV in Fig. 3 is possibly an indication of a new product channel, perhaps due to formation of electronically excited CoH^+ or C_2H_3.

The data shown in Fig. 4 for reaction 2 are best fit using n = 5, σ_0 = 18.6 $\mathring{A}^2$, E_0 = 3.8 eV and a = 0.80. The data are also fit reasonably well if n = 6 or 4 corresponding to thresholds of 3.5 eV and 4.1 eV, respectively. The background at low energies is believed to be much less than for process 1 since here reaction occurs over a much narrower energy range.
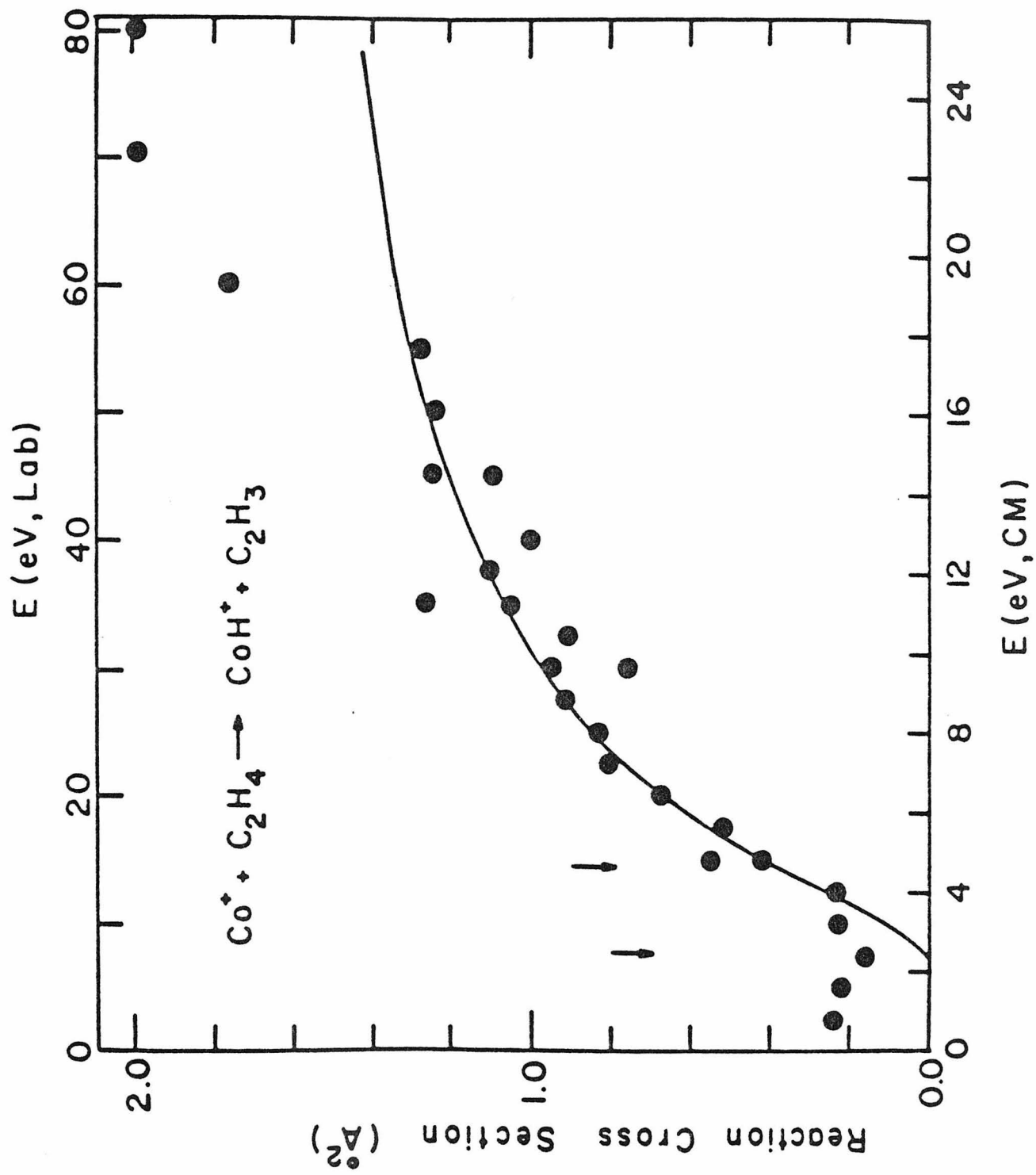
FIG. 3. Variation in experimental cross section with relative kinetic

energy in the center of mass frame (lower scale) and the

laboratory frame (upper scale) for reaction 1. Arrows

indicate the threshold energy for reaction 2.5 eV, and the

lower limit on the $H-C_2H_3$ bond energy, 4.68 eV. The curve

is the fit to the data given in the text convoluted as discussed.

Co⁺ + C₂H₄ ⟶ CoH⁺ + C₂H₃

FIG. 4.   Variation in experimental cross section with relative kinetic
energy in the center of mass frame (lower scale) and the
laboratory frame (upper scale) for reaction 2. Arrows
indicate the threshold energy for reaction, 3.8 eV. and the
carbon-carbon bond energy of ethene, 7.47 eV. The curve
is the fit to the data given in the text convoluted as discussed.

$Co^+ + C_2H_4 \longrightarrow CoCH_2^+ + CH_2$
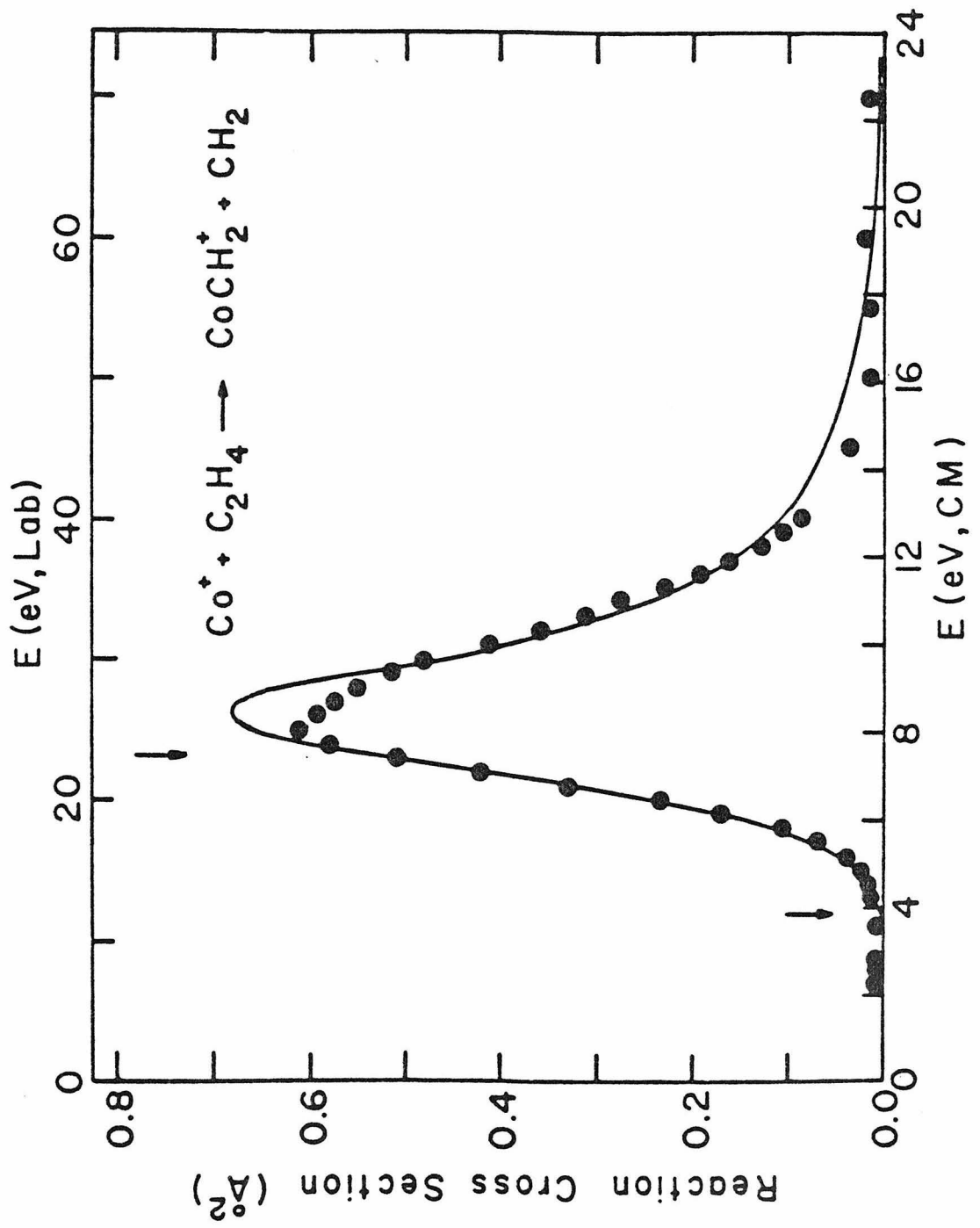
2. $Co^+ + c\text{-}C_3H_6$

While other products are also observed, the primary reaction of cobalt ions and cyclopropane is formation of the metal carbene ion, reaction 3. A crude energy analysis gives the laboratory energy of this product as 1.54 ± 0.80 eV when $E_{Lab}(Co^+) = 3.70 \pm 0.75$ eV, and as 0.83 ± 0.43 eV when $E_{Lab}(Co^+) = 1.5 \pm 0.75$ eV. In both cases, these energies are sufficiently low to suggest the $CoCH_2^+$ ion has the velocity of the center of mass, rather than a velocity resulting from a direct reaction. The former possibility corresponds to $CoCH_2^+$ energies of 1.56 eV and 0.63 eV, respectively, while a spectator stripping model[39] predicts 3.0 eV and 1.2 eV. This observation conforms with the notion that a long-lived intermediate, a metallo-cyclobutane, is formed.

The excitation function shown in Fig. 5 cannot be fit using Eq. (17). This may be due to the influence of the long-lived intermediate, especially since metallocyclobutanes have been postulated as intermediates in the isomerization of cyclopropanes to alkenes.[40] In our particular case, rearrangement of cyclopropane to propene

$$Co^+ + c\text{-}C_3H_6 \rightarrow Co^+ + C_3H_6 \tag{19}$$

is exothermic by 7.8 kcal/mol.[41] In our experiment, we have no means of monitoring such a reaction. The influence this possibility may have on the cross section for reaction 3 is unknown. The fit shown in Fig. 5 utilizes expression (10) for the reaction probability. The parameters used are $n = 3.5$, $m = 5.0$, $\sigma_0 = 46.3$ $\mathring{A}^2 (eV)^{\frac{3}{2}}$,

FIG. 5.   Variation in experimental cross section with relative kinetic
energy in the center of mass frame (lower scale) and the
laboratory frame (upper scale) for reaction 3. Arrows
indicate the reaction threshold at 0.5 eV and the energy
needed to produce methylene and ethene from cyclopropane,
4.0 eV. The curve is the fit to the data given in the text
convoluted as discussed. The inflection point at about 6 eV
marks the energy at which product dissociation begins
according to the model outlined in the text.
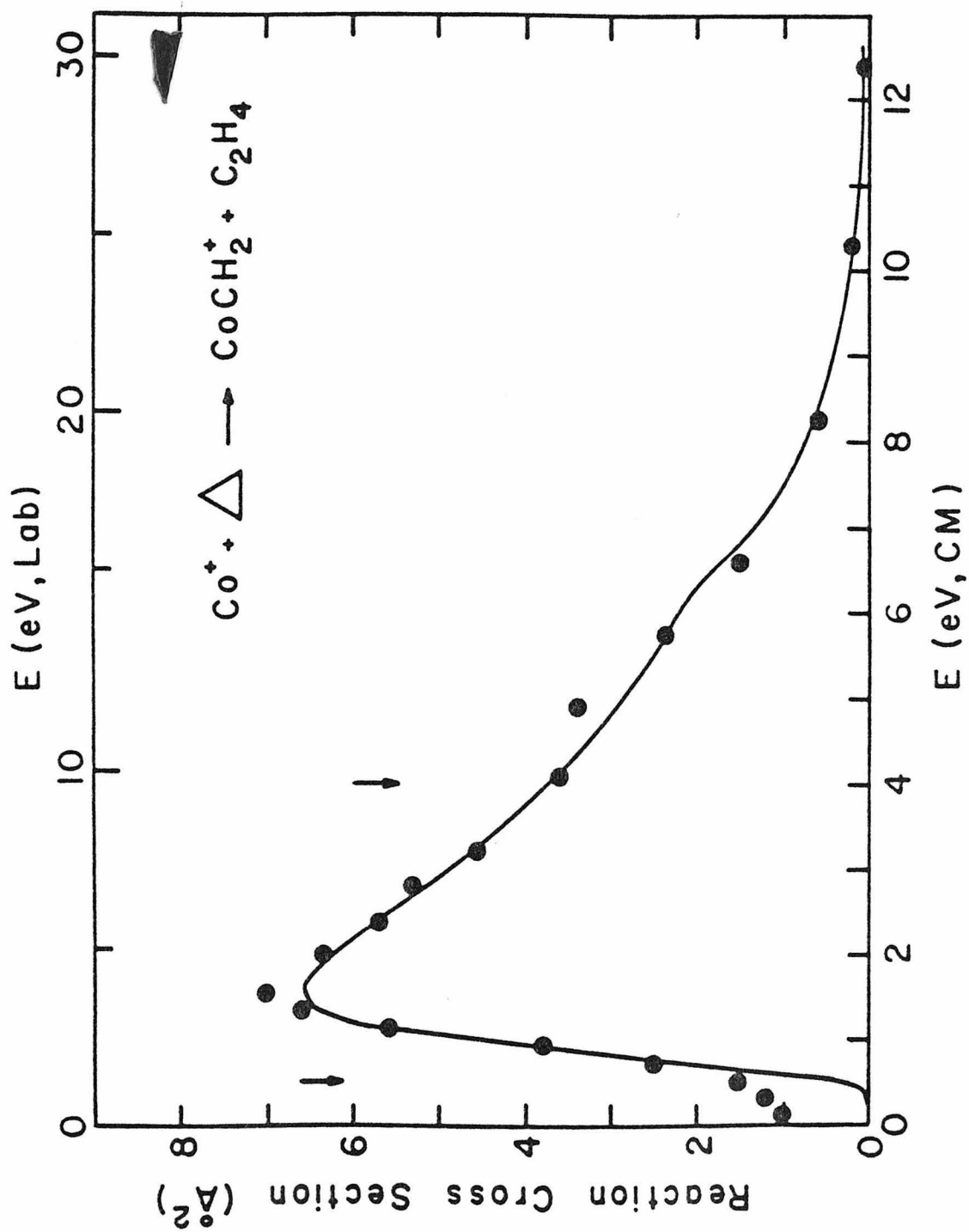
$E_0 = 0.5$ eV and $a = 0.60$.

Other products noted are $CoC_2H_4^+$, $CoC_2H_2^+$, $CoC_3H_4^+$, $C_3H_5^+$, and the adduct, $CoC_3H_6^+$. All but the latter are formed in highly endothermic reactions. Since they cumulatively account for less than 10% of the product yield, no good excitation function data could be obtained for them. The adduct is a collisionally stabilized complex as established by the pressure dependence of its cross section.

3. $Co^+ + c\text{-}C_2H_4O$

The reaction of cobalt ions with ethylene oxide forms a variety of products, Fig. 6. All of these find analogy with the products observed in the cyclopropane system. For present purposes, however, we need only consider the cross section for formation of $CoCH_2^+$. It is observed to decrease monotonically with increasing energy and is considerably larger than the cross sections measured in the other two systems. This clearly indicates that reaction 4 is exothermic. The other major product of an exothermic reaction in this system is $CoCO^+$ which probably results from the rearrangement of ethylene oxide to acetaldehyde followed by decomposition of the latter species.[42] The same product is observed in the reaction of Co^+ with acetaldehyde, where the carbene product is not detected.[43]

V. DISCUSSION

The test of any model is, of course, whether it explains what is observed. It can be seen that for our proposed cross section this is true not just at threshold but throughout the energy range. A more

FIG. 6.   Variation in experimental cross section with relative kinetic
energy in the center of mass frame (lower scale) and the
laboratory frame (upper scale) for reaction of Co^+ with
ethylene oxide. Lines through the data are drawn as an
aid to the reader and have no theoretical significance.
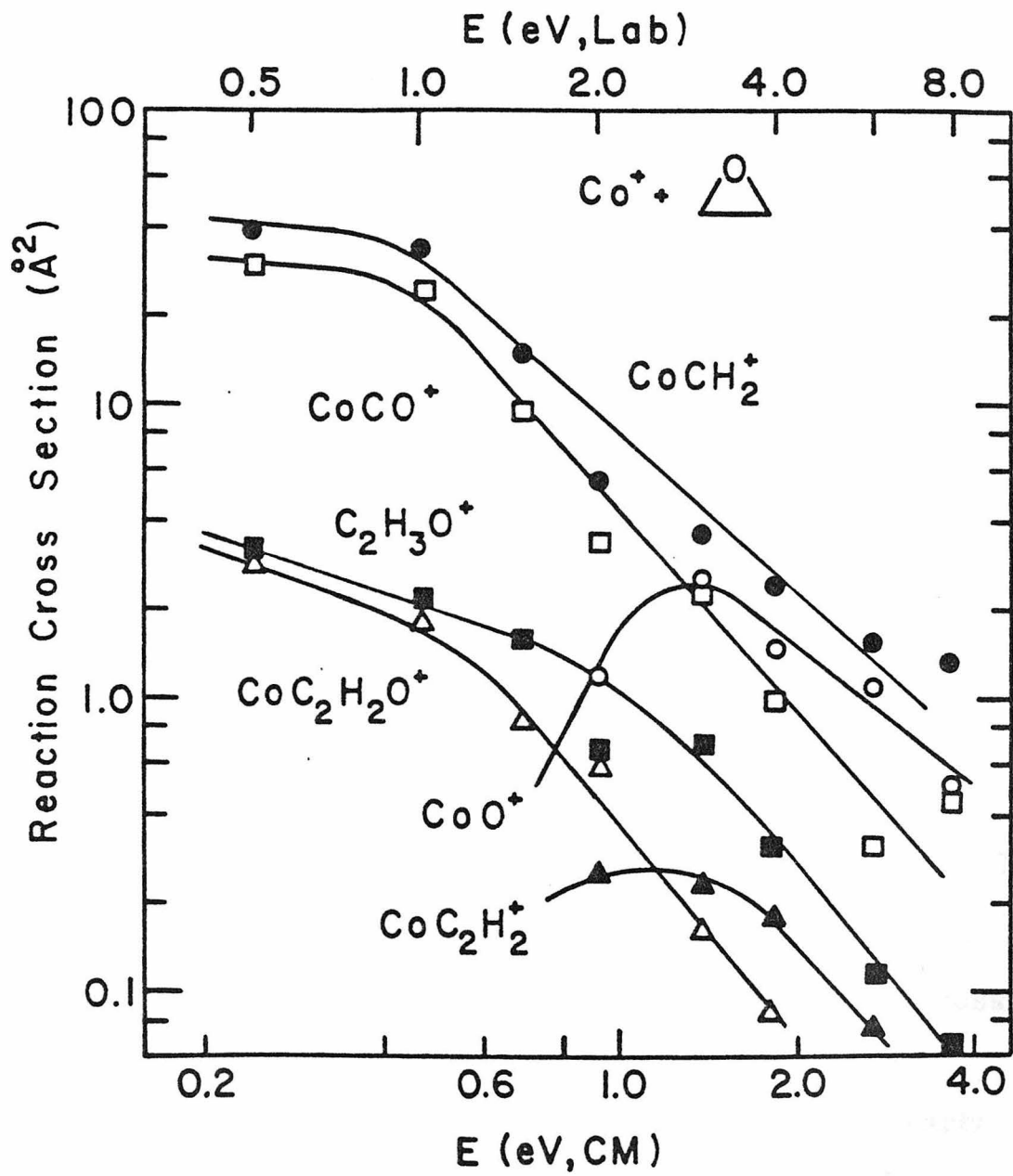
severe test, however, is that the parameters used in obtaining these fits be physically meaningful. This is especially true of E_0 since we would like to extract thermochemical information from our experiments. The thermochemical data inferred from this study are summarized in Table I. The cobalt hydride dissociation energy of $> 2.2 \pm 0.3$ eV (the limit is due to the poorly known C-H bond energy of ethene) compares well with the value 2.3 ± 0.2 eV determined from the endothermic reaction of Co^+ with hydrogen.[44] The agreement between the thermochemical data measured for reactions 2, 3 and 4 is also good. The observation that a straightforward interpretation of the data for reaction 2 yields a bond energy which agrees with limits established by reactions 3 and 4 gives us confidence that this method is a useful means for interpreting the data. While the bond energy derived from reaction 3 is in good accord, 3.5 ± 0.3 eV, the interpretation of this reaction was not straightforward. We therefore choose the result from reaction 2, $D^0(Co^+-CH_2) = 3.7 \pm 0.3$ eV, as the best value. This bond energy is in the same range as limits by other experimental means for $D^0(Mn^+-CH_2)$ of 4.0 to 4.3 eV and $D^0[(CO)_5Mn^+-CH_2] = 3.3$ eV.[7]

Values for the other parameters used to interpret the experimental results also seem reasonable. Certainly, the effective cross sections, σ_0 are on the order of hard sphere interactions. The assumption that such hard sphere cross sections will remain nearly constant over the energy range examined should be good.[45] The observation that the σ_0's used to interpret reactions 1 and 2 are different is consistent with our assumption that these reactions are direct and do not proceed through a common intermediate. The

TABLE I. Thermochemical data.

Species	$\Delta H^{\circ}_{f, 298}$ (kcal/mol)	Reference
CH_2	92.4 ± 1.0	a
C_2H_4	12.54 ± 0.07	b
$c\text{-}C_3H_6$	12.73 ± 0.14	c
CH_2O	-25.95 ± 0.12	c
$c\text{-}C_2H_4O$	-12.58 ± 0.15	b
	D°_{298} (kcal/mol)	
$H\text{-}C_2H_3$	$> 108 \pm 2$	d
$Co^+\text{-}H$	52 ± 4	e
	$> 50 \pm 10$	This work (Reaction 1) [f]
$Co^+\text{-}CH_2$	85 ± 7	This work (Reaction 2) [f]
	$< 92 \pm 1 \ (81 \pm 7)$	This work (Reaction 3) [f]
	$> 79 \pm 1$	This work (Reaction 4)

[a] JANAF Thermochemical Tables, 1975 Supplement, J. Phys. Chem. Ref. Data 4 (1975).

[b] JANAF Thermochemical Tables, Natl. Stand. Ref. Data Ser. Natl. Bur. Stand. 37 (1971).

[c] J. D. Cox and G. Pilcher, "Thermochemistry of Organic and Organometallic Compounds," Academic Press, New York, 1970.

[d] D. M. Golden and S. W. Benson, Chem. Rev. 69, 125 (1969),

[e] Reference 44.

[f] Calculated from the difference between the dissociation energy of the

TABLE I. (Footnotes continued)

neutral bond broken and the measured endothermicity (listed in text).

inclusion of the long-range ion-induced dipole interaction into σ_0 (Eq. (16)) could help explain the behavior observed for reaction 3 at the lowest energies.

The values for paramter a can be understood qualitatively by noting whether the product ion or neutral is likely to have lower vibrational frequencies and thus a higher density of states. For reaction 2, the ionic product would be expected to have lower energy modes and a is correspondingly found to be high, 0.8. The vibrational frequency of CoH^+ is undoubtedly much higher than those of C_2H_3. Consequently, little excitation of this ionic product would be predicted. Since the cross section for production of CoH^+, reaction 1, is observed to increase monotonically from threshold, we take the value of a to be quite low. In reaction 3, both the ionic and neutral products have two heavy atoms. Therefore, it should be an intermediate case, and indeed, a is found to be 0.6.

The identification of expression (8) as a ratio of numbers of states in a classical approximation suggests that n should correspond to the degrees of freedom of the reactants, collision complex or products. The values of n used above are generally much less than the total number of oscillators involved. This is perhaps to be expected since for a direct process, it is not clear whether any mixing of energy among modes should occur. However, this extreme assumption seems unrealistic. While not expected to be completely statistical, extensive energy may flow between strongly coupled modes of a collision complex, however short-lived. It should be cautioned that regarding n as related to the degrees of freedom is only true in the limit of a classical

approximation. It was observed in the early applications of expression (8) to unimolecular decomposition rates that n + 1 was often half the total number of oscillators.[46] More sophisticated treatments for the numbers of states has led to the conclusion that all oscillators are, in fact, active. Whether this will also be the case for direct endothermic bimolecular reactions, a system well removed from an equilibrium situation, will require further study.

V. CONCLUSION

A form has been proposed for the energy dependence of reaction cross sections which draws extensively from ideas formulated to examine reaction rates. Utilization of his form gives good agreement with data for endothermic bimolecular reactions including the energy region where product dissociation affects the observed cross section. Values of the parameters used to fit the data seem reasonable. Most important, energy thresholds for the reactions observed are substantiated by thermochemical data from other sources. This means of interpretation has allowed us to determine the bond energy for the cobalt carbene ion, $D^0(Co^+-CH_2) = 3.7 \pm 0.3$ eV.

The cobalt carbene ion bond is significantly stronger than the cobalt methyl ion bond, $D^0(Co^+-CH_3) = 2.65 \pm 0.17$ eV.[44] Substantial π-bonding would appear to contribute to this difference. Calculations on $NiCH_2$ and $NiCH_3$ lead to the conclusion that only a weak π-bond exists for the former species.[47] Contraction of the metal d orbitals due to a positive charge will likely change the π-bonding characteristics as will specifics of the electronic structure of the cobalt carbene ion.

Generalized valence bond considerations predict a $^3\Sigma$ ground state for the isoelectronic CoO^+ which does not correlate with ground-state separated species.[48] Since coupling of ground state $Co^+(^3F)$ with ground state $CH_2(^3B_1)$ gives rise to several states which may cross the potential energy curves arising from higher levels of Co^+ and CH_2, the electronic structure of $CoCH_2^+$ is unclear. <u>Ab initio</u> calculations on this system will be of interest now that experimental numbers are available.

Acknowledgment

References

[1] P. J. Davidson, M. F. Lappert and R. Pearce, Chem. Rev. 76, 219 (1976).

[2] (a) R. H. Grubbs, Prog. Inorg. Chem. 24, 1 (1978).

(b) T. J. Katz, Adv. Organometal. Chem. 16, 283 (1977).

(c) R. J. Haines and G. J. Leigh, Chem. Soc. Rev. 4, 155 (1975).

[3] K. J. Ivin, J. J. Rooney, C. D. Stewart, M. L. H. Green, R. Mahtab, J.C.S. Chem. Comm. 604 (1978).

[4] (a) F. N. Tebbe, G. W. Parshall and G. S. Reddy, J. Am. Chem. Soc. 100, 3611 (1978).

(b) R. R. Schrock, Accts. Chem. Res. 12, 98 (1979).

[5] (a) P. W. Jolly and R. Pettit, J. Am. Chem. Soc. 88, 5044 (1966).

(b) C. P. Casey and T. J. Burkhardt, J. Am. Chem. Soc. 96, 7808 (1974).

[6] Amy E. Stevens and J. L. Beauchamp, J. Am. Chem. Soc. 101, 245 (1979).

[7] Amy E. Stevens and J. L. Beauchamp, J. Am. Chem. Soc., submitted.

[8] R. Wolfgang, Accts. Chem. Res. 2, 248 (1969).

[9] This potential well is expected to be between 24 and 32 kcal/mol. Ref. 44.

[10] (a) P. G. Gassman, T. H. Johnson, J. Am. Chem. Soc. 98, 6057 (1976).

(b) T. H. Tulip and J. A. Ibers, J. Am. Chem. Soc. 101, 4201 (1979) and references therein.

[11] Mayer, Wilcomb and Bernstein (J. Chem. Phys. 67, 3507 (1977))

References (continued)

have studied the endoergic reaction of Hg and I_2 in crossed beams. Their analysis which included a treatment of product dissociation was aided by previous knowledge of parts of the potential energy surface for the reaction and by the detailed angular and energy distributions available from crossed molecular beam experiments.

[12] P. B. Armentrout, R. V. Hodges and J. L. Beauchamp, J. Chem. Phys. 66, 4683 (1977).

[13] B. R. Turner, J. A. Rutherford and D. M. J. Compton, J. Chem. Phys. 48, 1602 (1968).

[14] R. J. Cotter and W. S. Koski, J. Chem. Phys. 59. 784 (1973).

[15] R. V. Hodges, P. B. Armentrout and J. L. Beauchamp, Int. J. Mass Spec. Ion Phys. 29, 375 (1979).

[16] P. J. Chantry, J. Chem. Phys. 55, 2746 (1971).

[17] T. Nenner, H. Tien and J. B. Fenn, J. Chem. Phys. 63, 5439 (1975).

[18] I. Szabo, Int. J. Mass Spec. Ion Phys. 3, 169 (1969).

[19] L. A. Melton and R. G. Gordon, J. Chem. Phys. 51, 5449 (1969).

[20] P. J. Kuntz in "Interactions between Ions and Molecules," Ed. Pierre Ausloos (Plenum, New York, 1975) p. 123.

[21] R. D. Levine and R. B. Bernstein, "Molecular Reaction Dynamics" (Oxford, New York, 1974) Chap. 2.

[22] D. Vogt, W. Dreves, and J. Mischke, Int. J. Mass Spec. Ion Phys. 24, 285 (1977).

[23] W. Frobin, Ch. Schlier, K. Strein and E. Teloy, J. Chem. Phys. 67, 5505 (1978)

References (continued)

[24]R. J. Cotter, R. W. Rozett and W. S. Koski, J. Chem. Phys. 57, 4100 (1972).

[25]K. Morokuma, B. C. Eu and M. Karplus, J. Chem. Phys. 51, 5193 (1969).

[26]P. J. Robinson and K. A. Holbrook, "Unimolecular Reactions" (Wiley, London, 1972).

[27]P. Pechukas and J. C. Light, J. Chem. Phys. 42, 3281 (1965).

[28]E. Nikitin, Theoret. Exptl. Chem. 1, 831 (1965).

[29]R. A. Marcus, J. Chem. Phys. 45, 2138, 2630 (1966).

[30]W. J. Chesnavick and M. T. Bowers, J. Phys. Chem. 83, 900 (1979).

[31]L. S. Kassel, J. Phys. Chem. 32, 225 (1928).

[32]B. C. Eu and W. S. Liu, J. Chem. Phys. 63, 592 (1975).

[33]W. H. Miller, J. Chem. Phys. 65, 2216 (1976).

[34]R. A. Marcus, J. Chem. Phys. 62, 1372 (1975).

[35]S. A. Safron, N. D. Weinstein, D. R. Herschbach, and J. C. Tully, Chem. Phys. Lett. 12, 564 (1972).

[36]Neglecting angular momentum is equivalent to setting $A(E_p)$ of ref. 34 and $A(E_t')$ of ref. 35 equal to unity.

[37]Assuming a loose transition state, the effect of angular momentum conservation on product dissociation may be approximately reproduced by letting $a \approx 0.9$.

[38]G. Gioumousis and D. P. Stevenson, J. Chem. Phys. 29, 294 (1958).

[39]A. Henglein in "Ion Molecule Reactions in the Gas Phase," ed. Pierre Ausloos, ACS, Washington, D.C., 1966, p. 63.

References (continued)

[40] For a recent review see K. C. Bishop, Chem. Rev. $\underline{76}$, 461 (1926).

[41] $\Delta H^{\circ}_{f298}(c\text{-}C_3H_6) = 12.7$ kcal/mol. $\Delta H^{\circ}_{f298}(C_3H_6) = 4.9$ kcal/mol. J. D. Cox and G. Pilcher "Thermochemistry of Organic and Organometallic Compounds" (Academic Press, New York, 1970).

[42] R. R. Corderman and J. L. Beauchamp, J. Am. Chem. Soc. $\underline{98}$, 5700 (1976).

[43] P. B. Armentrout and J. L. Beauchamp, to be published.

[44] P. B. Armentrout and J. L. Beauchamp, J. Am. Chem. Soc., submitted.

[45] I. Kusunoki and Ch. Ottinger, J. Chem. Phys. $\underline{70}$, 710 (1979).

[46] Ref. 26, p. 59.

[47] A. K. Rappé and W. A. Goddard III, J. Am. Chem. Soc. $\underline{99}$, 3966 (1977).

[48] S. Walch, Ph.D. Thesis, California Institute of Technology, 1977.

CHAPTER VII

ION BEAM STUDIES OF ORGANOMETALLIC CHEMISTRY. HIGH
ENERGY "SAMPLING" OF REACTION INTERMEDIATES INVOLVED
IN CARBON-CARBON BOND CLEAVAGE BY TRANSITION METALS

Ion Beam Studies of Organometallic Chemistry. High Energy "Sampling" of Reaction Intermediates Involved in Carbon-carbon Bond Cleavage by Transition Metals.

Sir:

Chemical transformation often involves reactive intermediates which correspond to local minima on a complex potential energy surface. Ordinarily, these species are not revealed in conventional kinetic and mechanistic studies. One approach to the characterization of such intermediates is to deprive them of sufficient energy to continue to react by deposition or formation in a low temperature matrix. An alternative method, described here, relies conversely on providing the intermediate with substantially more energy than needed for reaction. In this paper, we demonstrate the method using as examples the reactions of cobalt ions with alkanes.

A generalized organometallic reaction is shown in Scheme L The low energy pathway consists of association of a metal center with

Scheme I
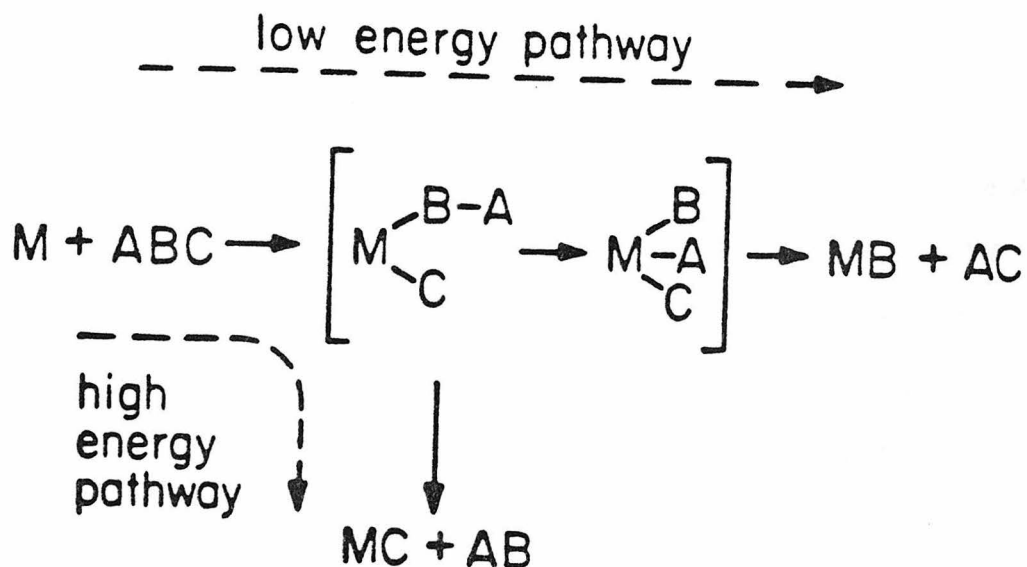
molecule ABC followed by oxidative insertion into the B-C bond, migration of A to the metal, and reductive elimination of AC. As the energy of the system is increased, the lifetimes of the intermediates decrease. At sufficiently high energies, reaction pathways such as simple bond cleavage not accessible at thermal energies may become the dominant decomposition route, since these processes often have favorable frequency factors[1] (Scheme I). Observation of the high energy products, MC and AB, provide evidence for formation of the first intermediate. Hence, species present on the complex energy surface are "sampled."

An ion beam tandem mass spectrometer[2,3] shown schematically in Figure 1 has been utilized in the present studies. In our experiments, singly charged cobalt ions are produced by thermal decomposition of $CoCl_2$ and surface ionization of the resulting Co on a hot ($\sim 2500°K$) rhenium surface[4]. These ions are collimated, mass and energy selected, and allowed to interact with the target gas in a collision chamber. Product ions are monitored using an in-line quadrupole mass filter and electron multiplier. Neutral products are not detected but inferred. These experiments yield reaction cross sections and product distributions as a function of relative kinetic energy.

Results for the reaction of Co^+ with 2-methylpropane are shown in Figure 2. The behavior of the cross sections for the products $CoC_3H_6^+$ and $CoC_4H_8^+$ as a function of translational energy is typical of species formed in exothermic reactions[3]. In light of the discussion above, the observation of species such as CoH^+ and $CoCH_3^+$ at higher

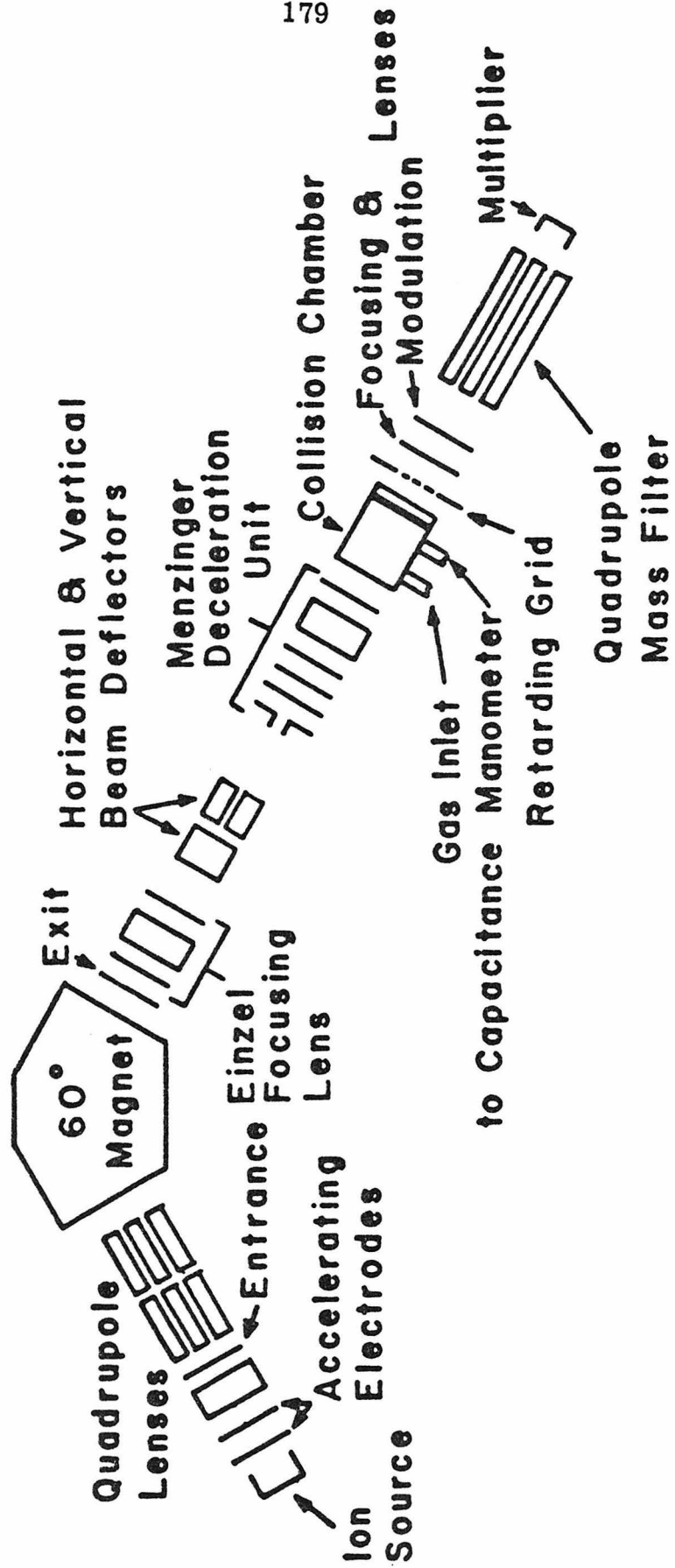FIG. 1.   Schematic drawing of the ion beam apparatus

Ion Source

Quadrupole Lenses

Accelerating Electrodes

Entrance Einzel Focusing Lens

60° Magnet

Exit

Horizontal & Vertical Beam Deflectors

Menzinger Deceleration Unit

Collision Chamber

Gas Inlet

to Capacitance Manometer

Retarding Grid

Focusing & Modulation Lenses

Quadrupole Mass Filter

Multiplier

FIG. 2. Variation in experimental cross section with relative kinetic energy in the center of mass frame (lower scale) and the laboratory frame (upper scale) for the interaction of cobalt ions with 2-methylpropane, showing (a) exothermic channels and (b) endothermic channels. Note change of scale.

181
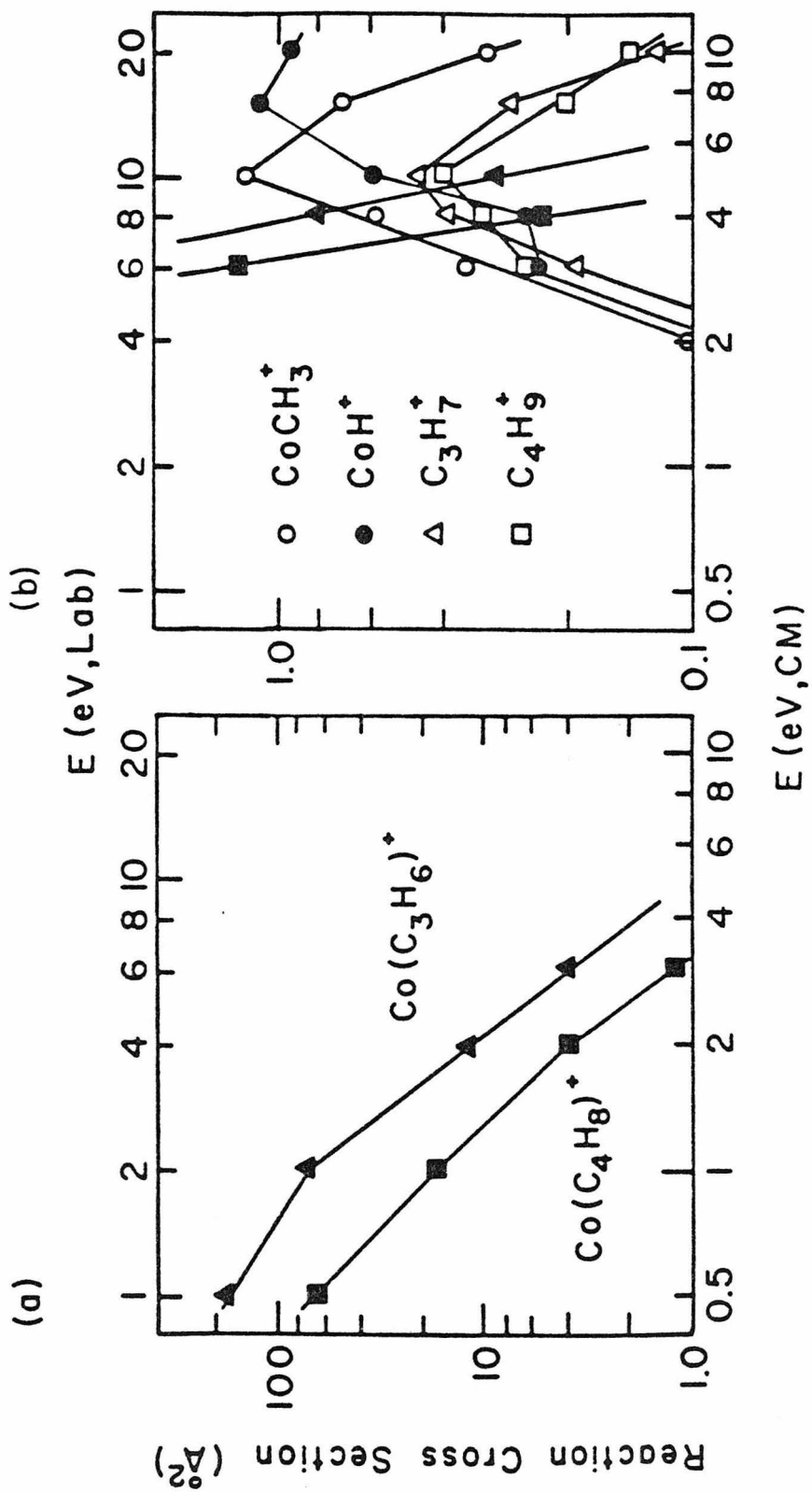
energies suggests that oxidative addition of both C-H and C-C bonds are important reaction steps. Scheme II outlines the low energy mechanism proposed[6]: oxidative addition of of the three types of bonds available in isobutane, followed by β-hydrogen or β-methyl transfer to the metal and reductive elimination of an alkane or hydrogen molecule.

Scheme II
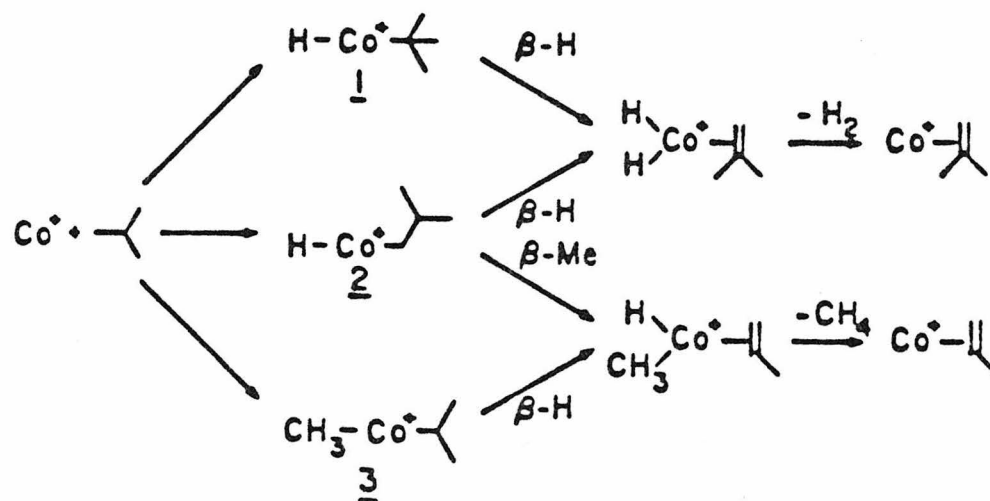
At high energies, intermediates 1 and 2 decompose to yield CoH^+ and $C_4H_9^+$ while 3 gives $CoCH_3^+$ and $C_3H_7^+$.

Additional insights relevant to the proposed mechanisms may be garnered from the reaction of Co^+ and 2, 2-dimethylpropane. Dehydrogenation processes analogous to those proposed in Scheme II are not possible in this system. However, alternative reaction pathways which include formation of alkylidene, 4, or metallocyclobutane, 5, intermediates are still accessible. We observe only $CoC_4H_8^+$ at low energies.

$$
\begin{array}{cc}
\underset{4}{\text{H}\cdots\text{Co}^+\text{=}\overset{\text{\textbackslash}}{\underset{\text{/}}{\text{C}}}\text{R}} & \underset{5}{\text{H}\cdots\text{Co}^+\square\text{R}}
\end{array}
$$

$$R = H, CH_3$$
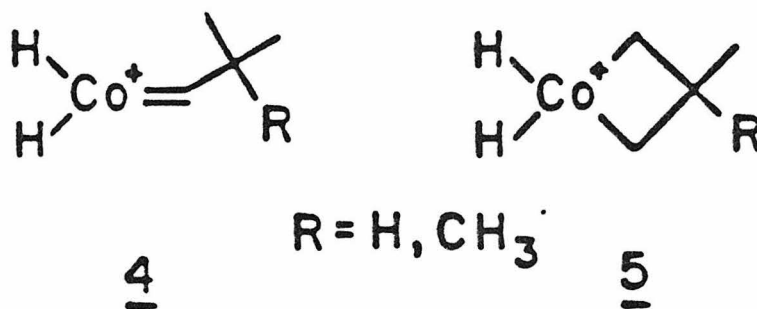
At high energies, the predominant product is $C_4H_9{}^+$. These observations are consistent with a reaction mechanism analogous to Scheme II. Since 4 and 5 would be expected to eliminate hydrogen, we conclude that such species are unimportant in the systems examined.

In the studies detailed above, a quantitative assessment of the fragmentation of reaction intermediates can provide thermodynamic data. In the dissociation of a charged collision complex, such as 3, the preferred ionic product is the fragment having the lower ionization potential (IP)[7]. The observation that the cross section for production of $CoCH_3{}^+$ is always greater than that of $C_3H_7{}^+$, Figure 2, implies that $IP(CoCH_3) < IP(\text{iso-}C_3H_7) = 7.36\ eV$[9]. A similar analysis of the 2,2-dimethylpropane system establishes $IP(CoCH_3) > IP(\text{tert-}C_4H_9) = 6.70\ eV$[9]. The behavior of the other products in Figure 2, CoH^+ and $C_4H_9{}^+$, may also be understood using analogous considerations.

In addition, measurement of the thresholds for the endothermic processes observed at high energies provides bond energies of the products. Preliminary data for the endothermic reactions of Co^+ with hydrogen and ethane indicate that $D^0(Co^+\text{-}H) = 52\pm4\ kcal/mol$ and $D^0(Co^+\text{-}CH_3) = 61\pm4\ kcal/mol$[10]. Combined with the ionization potentials,

184

IP(CoH) = 7. 3±0. 1 eV and IP(CoCH$_3$) = 7. 0±0. 3 eV, derived as discussed above, we find the neutral bond dissociation energies, D^0(CoH) = 39±6 kcal/mol and D^0(CoCH$_3$) = 41±10 kcal/mol.

To our knowledge these are the first investigations of organo-transition metal reactions using ion beam techniques. Such studies provide a wealth of thermochemical data and mechanistic insights. The above results provide substantial evidence for the viability of a mechanism for carbon-carbon bond cleavage of alkanes which involves direct insertion of a metal into the carbon-carbon bond as a first step. Thermochemical data indicating strong metal-carbon bonds corroborate this hypothesis. Further studies are underway in our laboratories to extend this technique to other systems.

References and Notes

(1) Robinson, P. J.; Holbrook, K. A. "Unimolecular Reactions", Wiley-Interscience: New York, 1972.

(2) (a) Armentrout, P. B.; Hodges, R. V.; Beauchamp, J. L. J. Chem. Phys. 1977 66, 4683.

(b) Armentrout, P. B.; Beauchamp, J. L. J. Chem. Phys., submitted.

(3) For a general review of this type of instrument see M. Henchman in Franklin, J. L., Ed. "Ion-Molecule Reactions", Plenum Press: New York, 1972.

(4) This method of ionization minimizes the production of excited states. Attenuation experiments[5] showed no evidence of appreciable amounts of such states.

(5) a) Cotter, R. J.; Koski, W. S. J. Chem. Phys. 1973 59, 784.

b) Turner, B. R.; Rutherford, J. A.; Compton, D. M. J. J. Chem Phys. 1968 48, 1602.

(6) Similar schemes have been proposed by Remick, R. J.; Asunta, T. A.; Skell, P. S. J. Am. Chem. Soc. 1979 101, 1320 and Allison, J.; Freas, R. B.; Ridge, D. P. J. Am. Chem. Soc. 1979 101, 1332.

(7) Sometimes referred to as Stevenson's Rule[8], this observation is a straightforward conclusion of RRKM theory[1].

(8) Stevenson, D. P. Disc. Faraday Soc. 1951 10, 35.

(9) Houle, F. A.; Beauchamp, J. L. J. Am. Chem. Soc. 1979 101, 4067.

(10) This value agrees with the range of 56 kcal/mol $< D°(Co^+-CH_3)$ < 69 kcal/mol reported by Allison, J.; Ridge, D. P. J. Am. Chem. Soc. 1979 101, 4998.

186

P. B. Armentrout and J. L. Beauchamp

Contribution No. _____ from the Arthur Amos

Noyes Laboratory of Chemical Physics,

California Institute of Technology,

Pasadena, California 91125

(Received) _____

Abstract   The gas-phase reactions of Co^+ with 2-methylpropane and 2,2-dimethylpropane have been investigated using an ion-beam apparatus.   Significantly, the major process at near thermal energies in both systems is carbon-carbon bond cleavage to yield methane and propene or isobutene.   At higher relative kinetic energies, new reaction products are observed.   These are shown to be characteristic of the reactive intermediates present at low energies.   This technique of "sampling" reactive intermediates is used to provide evidence for mechanisms which involve initial insertion of Co^+ into both carbon-carbon and carbon-hydrogen bonds.   In addition, the ability to control the relative kinetic energy of reactants allows the extraction of thermochemical data from endothermic thresholds and product distributions.   The bond dissociation energies $D^0(Co^+-H) = 52\pm4$ kcal/mol, $D^0(Co-H) = 39\pm6$ kcal/mol, $D^0(Co^+-CH_3) = 61\pm4$ kcal/mol, and $D^0(Co-CH_3) = 41\pm10$ kcal/mol are obtained.

CHAPTER VIII

ION-BEAM STUDIES OF THE REACTIONS OF ATOMIC COBALT
IONS WITH ALKANES: DETERMINATION OF METAL-HYDROGEN
AND METAL-CARBON BOND ENERGIES AND AN EXAMINATION
OF THE MECHANISM BY WHICH TRANSITION METALS CLEAVE
CARBON-CARBON BONDS

Ion-Beam Studies of the Reactions of Atomic Cobalt Ions with
Alkanes: Determination of Metal-Hydrogen and Metal-Carbon
Bond Energies and an Examination of the Mechanism by which
Transition Metals Cleave Carbon-Carbon Bonds

P. B. Armentrout and J. L. Beauchamp

Contribution No. _____ from the Arthur Amos Noyes Laboratory
of Chemical Physics, California Institute of Technology,
Pasadena, California 91125.
(Received   )

Abstract: An ion beam apparatus is employed to study the reactions of
singly charged cobalt positive ions with hydrogen and 17 alkanes.
Reaction cross sections and product distributions as a function of
kinetic energy are determined. Exothermic carbon-carbon bond
cleavage reactions are observed for all alkanes but methane and ethane.
A mechanism involving oxidative addition of C-C and C-H bonds to
cobalt as a first step is demonstrated to account for all major reactions
at all energies. Interpretation of several endothermic processes
allows the extraction of thermochemical data. The bond dissociation
energies obtained are $D^0(Co^+-H) = 52 \pm 4$ kcal/mol, $D^0(Co-H) =$
39 ± 6 kcal/mol, $D^0(Co^+-CH_3) = 61 \pm 4$ kcal/mol, $D^0(Co-CH_3) =$
41 ± 10 kcal/mol.

Introduction

A recent article[1] pointed out that the "fuzzy interface between surface chemistry, heterogeneous catalysis, and organometallic chemistry" is the transition metal-organic fragment bond. Despite the importance of such information, little is known about the thermodynamics of such bonds.[2] _Ab initio_ calculations[1,3] are one means of obtaining such information, but experimental numbers are needed. Gas phase studies using ion cyclotron resonance mass spectrometry[4-6] have yielded thermochemical data concerning transition metal carbon bonds. The present study utilizes a different technique for determining gas phase metal hydrogen and metal carbon bond energies which has been presented in brief previously.[7] Using an ion beam apparatus, the reactions of atomic cobalt ions with alkanes ranging in complexity from methane to branched octanes have been examined. By varying the kinetic energy at which the Co^+ interacts with the alkanes, the potential energy surface of these systems is probed. This allows a variety of thermochemical information to be derived.

In addition, the general reactivity of alkanes with Co^+ is assessed. For all alkanes larger than ethane, exothermic cleavage of carbon-carbon bonds is observed. Several recent studies have also shown that metal atoms,[8,9] small metal clusters,[9,10] and atomic metal ions[5,7] cleave hydrocarbons. We provide direct evidence that such reactions occur by oxidative addition of carbon-carbon bonds to the metal. Facile β-hydrogen abstraction by the metal and reductive elimination of hydrogen or a hydrocarbon com-

plete the general mechanism. The reaction of Co^+ with 17 alkanes are shown to be consistent with such a proposal.

Experimental

The ion beam apparatus, described in detail elsewhere,[11,12] is shown schematically in Figure 1. Ions from a surface ionization source are mass analyzed using a 60° sector magnet which provides uint mass resolution to greater than 100 m/z. This mass-selected beam is decelerated to a selected energy and focused into a collision chamber containing the reactant gas. Product ions exit the chamber with the aid of a 0.5 volt extraction field.[13] These ions are focused into a quadrupole mass filter and detected using a Channeltron electron multiplier operated in a pulse counting mode. Ion signal intensities are corrected for the mass discrimination of the quadrupole mass filter.

The source for cobalt ions is described in detail elsewhere.[11,14] Briefly, $CoCl_2$ is evaporated onto a rhenium filament where dissociation and ionization of the resulting Co occurs. This method of ionization minimizes the production of excited metal ion states. It is estimated that at the filament temperature used, $\sim 2500°K$, 81% of the Co^+ ions produced are in the ^3F ground state manifold and 19% are in the ^5F excited state manifold at 0.42 eV. In order to observe the effects of an excited state, its lifetime must exceed about 10 μs, the approximate flight time of the ions. An attempt was made to directly determine the presence of excited ions using an attenuation technique.[15,16] Only a single component was detected,

FIG. 1.   Schematic drawing of the ion beam apparatus.
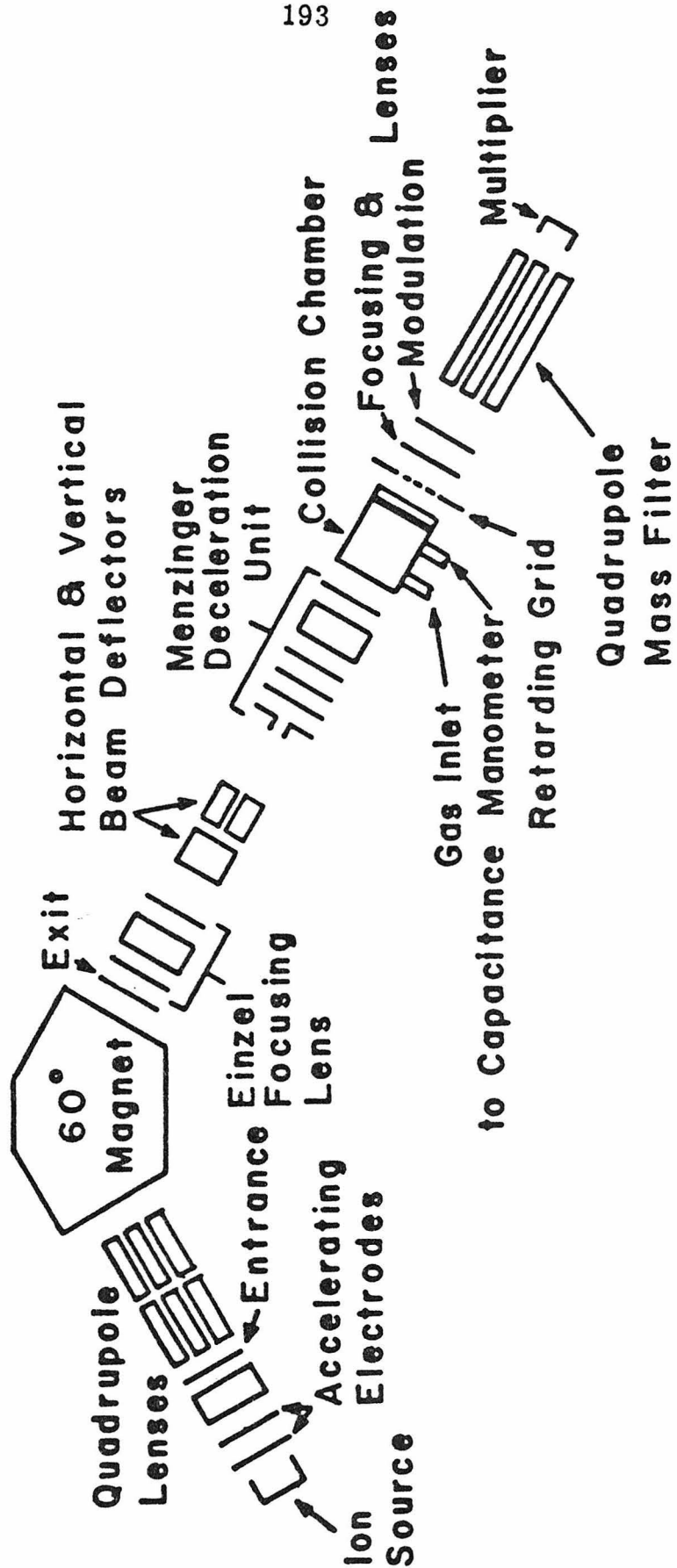
suggesting that excited states are absent. This assumes that the ^{3}F and ^{5}F states have different total scattering cross sections for the collision gases used (O_2, C_2H_4, and C_2H_6).

The nominal collision energy of the ion beam is taken as the difference in potential between the center of the collision chamber and the center of the filament, the latter being determined by a resistive divider. This collision energy is verified by use of a retarding field energy analyzer.[12] Agreement was always within 0.3 eV. Two other factors affect the actual collision energy: energy distribution of the Co^+ beam and the thermal motion of the target gas. The former is determined to be 0.7 eV (FWHM) using the retarding field analyzer. In the present experiments, this effect is sufficiently small compared to the second factor that it will be disregarded.[17] The effect of the thermal motion of the reactant gas in ion beam collision chamber experiments has been discussed in detail else-where.[17,18] The energy broadening due to this motion washes out any sharp features in reaction cross sections. For exothermic reactions, this has little effect on the observed cross sections and branching ratios, and consequently, we report such data without taking this energy distribution into account. For endothermic reactions, the thermal motion obscures the threshold energy for reactions. By convoluting a function form for the reaction cross section, $\sigma(E)$, with the thermal energy distribution, using the method of Chantry,[19] and fitting this new curve to the data, we take specific account of this factor.

The analysis of endothermic reactions to obtain thermochemical data is not a subject without controversy. Our choice for the functional form of the reaction cross section is discussed in detail elswhere.[14] This form, equation (1), has three variable parameters: σ_0, an effective cross section; E_0, the energy threshold for

$$\sigma(E) = \sigma_0 [(E - E_0)/E]^n \qquad (1)$$

reaction (taken equal to the difference in bond energies of the neutral reactant (bond broken) and ionic product (bond formed)); and n. Equation 1 is expected to apply for energies below the threshold for dissociation of the product ion. This threshold corresponds to the energy of the bond broken in the neutral reactant. Detailed treatments of the effect of dissociation on the observed reaction cross section have also been previously discussed.[14,19,20]

Reaction cross sections for specific products, σ_i, are obtained using equations 2 and 3 which relate the total reaction cross section,

$$I_0 = (I_0 + \Sigma I_i) \exp(-n\sigma \ell) \qquad (2)$$

$$\sigma_i = \sigma I_i / \Sigma I_i \qquad (3)$$

σ, the number density of the target gas, n, and the length of the collision chamber, ℓ (5mm), to the transmitted reactant ion beam intensity, I_0, and the sum of the product ion intensities, ΣI_i. The pressure of the target gas, measured using an MKS Baratron Model 90H1 capacitance manometer, is kept low, $< 2 \times 10^{-3}$ Torr, to minimize attenuation of the beam. However, it was found with the

heavier alkanes that total cross sections were not accurately repro-
ducible and were generally much higher than is predicted using the
Langevin-Gioumousis-Stevenson model for ion-molecule reactions.[20]
We attribute this effect to substantial loss of elastically scattered Co^+
from the reactant beam. Relative cross sections of products
(branching ratios) were quite reproducible and the results for the
larger alkanes are reported in this manner.

It is important to point out that in these experiments neutral
products are not detected. However, except at higher energies, the
identity of these products can usually be inferred without ambiguity.
In addition, these experiments provide no direct structural information
about the ionic products. However, straightforward thermochemical
arguments can often distinguish possibilities for isomeric structures.

Results and Discussion

A wide variety of reactions result from interaction of Co^+ with
alkanes. The particular products observed are dependent on the
kinetic energy of the interaction as well as the structure of the alkane.
In the following section, the reactions of cobalt ions with hydrogen,
methane, and ethane are examined first. Detailed analyses of these
reactions, all endothermic, allow a determination of important
thermochemical data, summarized in Table I. Next, the reactions
of Co^+ with propane, butane, 2-methylpropane and 2,2-dimethyl-
propane are presented. Results for these systems establish a general
reaction mechanism which explains the processes observed not only
for these alkanes but for all hydrocarbons examined. Finally, results

Table I. Thermochemistry of Cobalt-Hydrogen and Cobalt-Carbon Bonds Derived in This and Related Studies

R	$D^0(Co^+-R)$ (kcal/mol)	Ionization Potential (eV)	$D^0(Co-R)$ (kcal/mol)
H	52 ± 4[a]	7.3 ± 0.1[b]	39 ± 6
CH_3	61 ± 4[a, c]	7.0 ± 0.3[d]	41 ± 10
CH_2	85 ± 7[e]		

[a]Calculated as described in text.

[b]Ref. 41.

[c]Comparison of the $CoCH_3^+$ product yields to that of other cobalt alkyl ion products suggests that larger alkyls are bonded only a little less strongly than CH_3 to Co^+.

[d]Ref. 38.

[e]Ref. 14.

for larger alkanes up to C_8 species are summarized and discussed.

Reaction of Co^+ with D_2

Cobalt ions react with D_2, used to facilitate mass resolution, to form CoD^+ as given in process 4. The results are shown in

$$Co^+ + D_2 \rightarrow CoD^+ + D \qquad (4)$$

Figure 2. Previous studies of such metal ion-hydrogen systems[11,19] have been interpreted using equation (1) with n = 1. The fit to the data uses equation 1 with $\sigma_0 = 2.3 \text{ Å}^2$ and $E_0 = 2.3 \pm 0.1$ eV, and is shown in Figure 2 both unconvoluted and convoluted as discussed above. The decreasing cross section at high energies is due to CoD^+ dissociation which has a thermodynamic threshold at $D^0(D_2) = 4.60$ eV.[21] The fit shown in Figure 2 above this energy uses an analysis discussed in detail elsewhere.[19]

From the reaction threshold, $E_0 = 2.3 \pm 0.1$ eV, and the D_2 band energy, a value for $D^0(Co^+-D)$ of 2.3 ± 0.14 eV is determined. Making a zero point energy correction of 0.05 eV,[22] $D^0(Co^+-H) = 2.25 \pm 0.17$ eV (52 ± 4 kcal/mol) is obtained.[23] The proton affinity of the cobalt atom, PA(Co), can be calculated using equation 5, in

$$PA(Co) = D^0(Co^+-H) + IP(H) - IP(Co) \qquad (5)$$

which IP(x) is the ionization potential of species x. The value derived,[24] 184 ± 4 kcal/mol, is similar to the proton affinities of Ni, 180 ± 3 kcal/mol,[19b] Fe, < 203 kcal/mol,[5c] and Zn, ~164 kcal/mol,[25] but substantially less than those of such strong atomic bases as Ba,

FIG. 2.   Variation in experimental cross section for reaction 3 as

a function of kinetic energy in the center of mass frame

(lower scale) and the laboratory frame (upper scale).

The solid line is the fit to the data described in the text.

The dashed line is the fit in the threshold region before

convolution. Arrows mark the threshold energy, 2.3 eV,

and the bond energy of D_2, 4.6 eV.

$Co^+ + D_2 \longrightarrow CoD^+ + D$
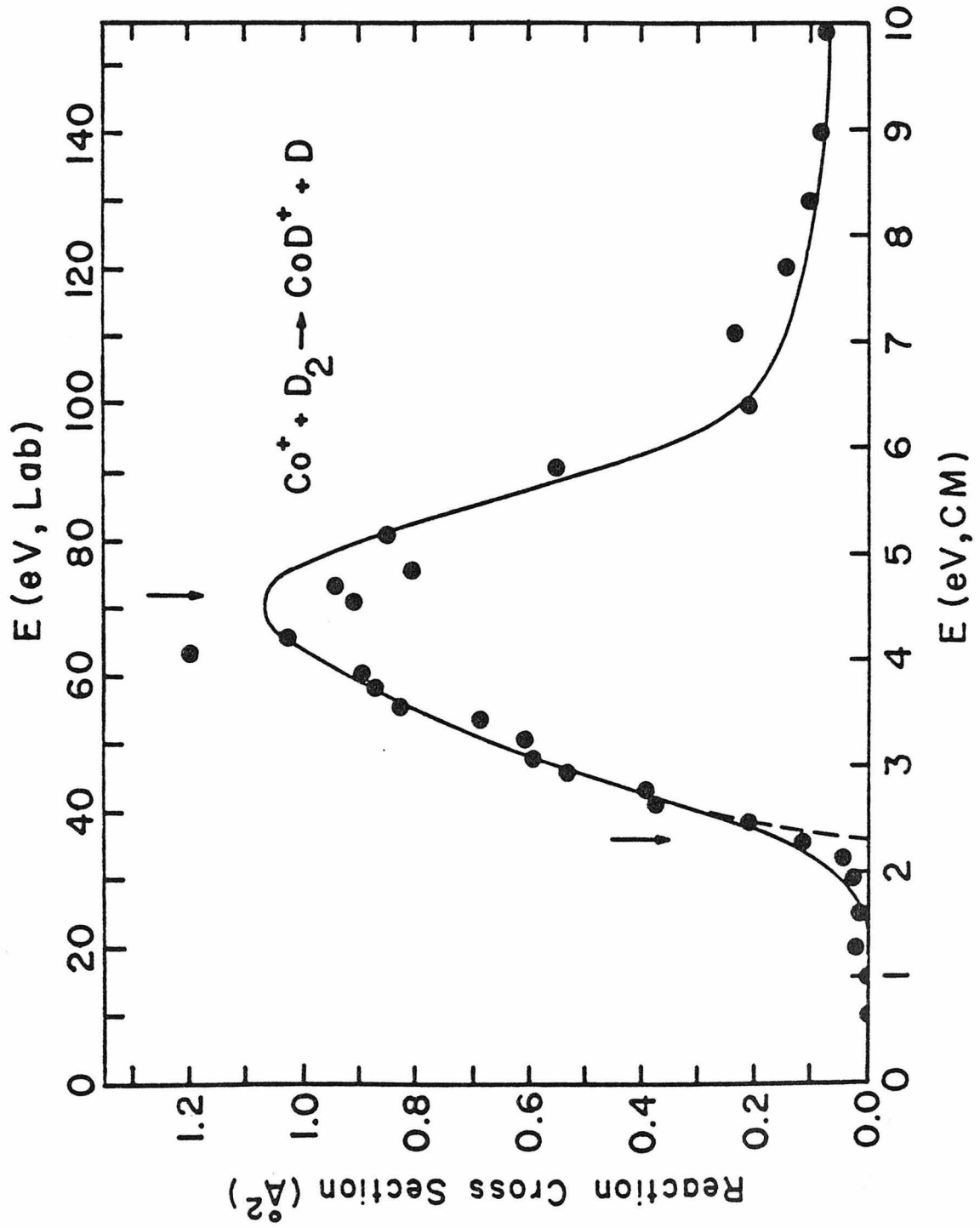
250 ± 3 kcal/mol,[19a] and U, 238 ± 4 kcal/mol.[11]

Reaction of Co^+ with Methane

The primary reaction of Co^+ with CH_4 is endothermic hydrogen abstraction, process 6. The quality of the data is insufficient to

$$Co^+ + CH_4 \rightarrow CoH^+ + CH_3 \qquad (6)$$

accurately analyze for an energy threshold. Two other products, $CoCH_2^+$ and $CoCH_3^+$, are also observed in this system. The cross sections for both ions peak at about 4 eV, but even at this energy, they account for less than 10% of the reaction products. The energetic requirements are such that the $CoCH_2^+$ product must be formed in reaction 7, calculated to be 1.1 eV endothermic[26] (Table I).

$$Co^+ + CH_4 \rightarrow CoCH_2^+ + H_2 \qquad (7)$$

Formation of two H atoms as the neutral products would require an additional 4.5 eV.

We postulate that both $CoCH_2^+$ and $CoCH_3^+$ are formed via inter-mediate $\underset{\sim}{1}$, produced by oxidative addition of a C-H bond to Co^+.

$$H-Co^+-CH_3$$
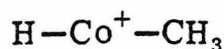
$$\underset{\sim}{1}$$

The lowest energy reaction of $\underset{\sim}{1}$ other than proceeding back to reactants, is rearrangement by α-hydrogen migration from carbon to cobalt,[27] yielding $\underset{\sim}{2}$, which can then reductively eliminate H_2.

$$\begin{array}{c} H \\ \diagdown \\ \diagup \\ H \end{array} Co^+ = CH_2$$

$$\underset{\sim}{2}$$
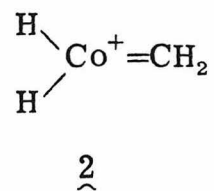
Alternatively, $\underset{\sim}{1}$ can decompose directly by breaking the cobalt hydrogen bond to give $CoCH_3^+$ or by breaking the cobalt carbon bond to yield CoH^+. Since the Co^+-CH_3 bond is stronger than the Co^+-H bond (see below), the former product is thermodynamically preferred. Yet, CoH^+ is the predominant product at all energies examined, suggesting CoH^+ is formed by direct hydrogen abstraction rather than through $\underset{\sim}{1}$.

Reaction of Co^+ with Ethane

Processes 8 and 9, both endothermic, are the two major

$$Co^+ + C_2H_6 \longrightarrow \begin{array}{l} CoH^+ + C_2H_5 \qquad (8) \\ CoCH_3^+ + CH_3 \qquad (9) \end{array}$$
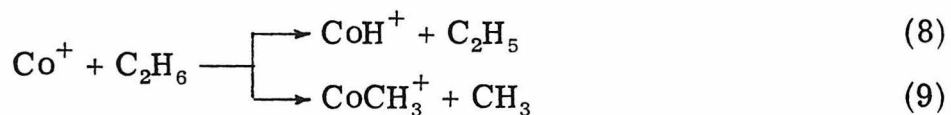
reactions observed in the interaction of cobalt ions with ethane. The CoH^+ product has a threshold which agrees qualitatively with the thermodynamics discussed above and a cross section of comparable magnitude to that of the $CoCH_3^+$ product. The data for reaction 9, shown in Figure 3, have been analyzed using equation (1). The fit obtained, Figure 3, uses $\sigma_0 = 14.0$ $Å^2$, $n = 5$, and $E_0 = 1.25 \pm 0.1$ eV. Above the carbon-carbon bond dissociation energy of ethane, 3.90 eV,[26] where dissociation of the $CoCH_3^+$ product may occur, the fit uses an analysis discussed in detail elsewhere.[14]

FIG. 3. Variation in experimental cross section for reaction 9 as
a function of kinetic energy in the center of mass frame
(lower scale) and the laboratory frame (upper scale).
Arrows mark the threshold energy at 1.25 eV and the
carbon-carbon bond energy of ethane 3.9 eV. The solid
line is the fit to the data described in the text.
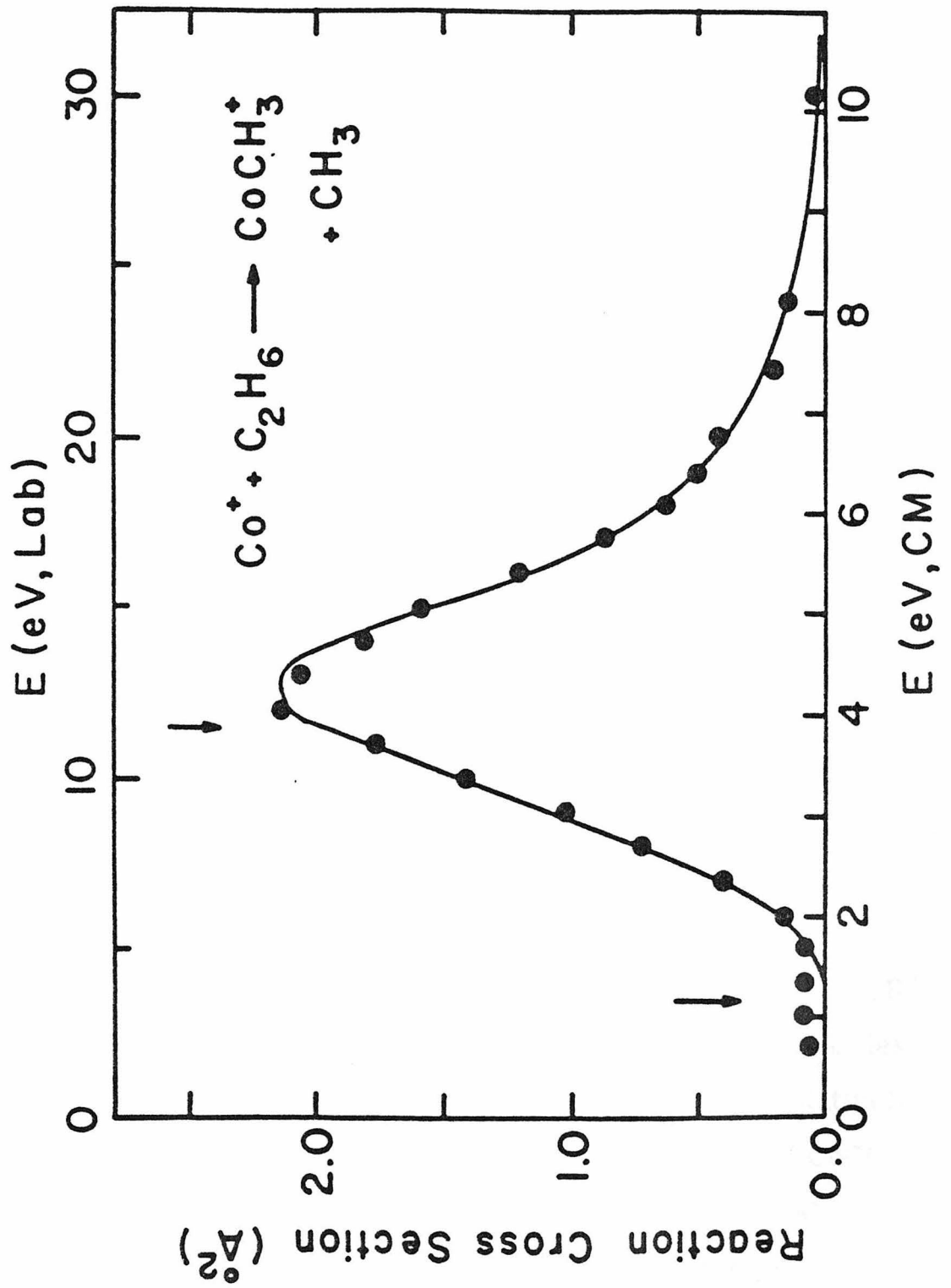
The Co^+-CH_3 bond energy, found to be 2.65 ± 0.17 eV (61 ± 4 kcal/mol), agrees well with the range of values determined by Allison and Ridge, 56-69 kcal/mol.[5c] The observation that $D^0(Co^+-CH_3) > D^0(Co^+-H)$ is unexpected since most metal hydrogen bonds are stronger than metal carbon σ bonds. The 9 kcal/mol difference here is attributed to the fact that a methyl group is substantially more polarizable than a hydrogen atom.[28]

We have implicitly assumed above that the structure of the species having the formula $(CoCH_3)^+$ corresponds to a cobalt methyl ion. It is possible, however, that one (or more) of the hydrogens is actually bonded to the metal. Using the heats of formation, $\Delta H_f^0(CoCH_3^+) = 256 \pm 4$ kcal/mol[29] and $\Delta H_f^0(CoCH_2^+) = 289 \pm 7$ kcal/mol,[14] we can calculate that process 12 must have a heat of reaction of 85 ± 11 kcal/mol. Since $D^0(Co^+-H) = 52$ kcal/mol, it seems unlikely

$$(CoCH_3)^+ \rightarrow (CoCH_2)^+ + H \tag{12}$$

that a bond energy of 85 kcal/mol represents a cobalt-hydrogen bond, but rather a C-H bond weakened by resonance stabilization of the $CoCH_2^+$ product.[30]

Minor products observed in the Co^+-ethane system are $CoCH_2^+$ and $CoC_2H_4^+$. The cross sections are of insufficient magnitude (less than 0.2 $\mathring{A}^2$) to allow accurate analysis of thresholds. Qualitatively, the energy dependence of the cross section for formation of $CoCH_2^+$ is similar to that of $CoCH_3^+$, peaking at about 4 eV. The $CoC_2H_4^+$ product exhibits the lowest apparent threshold of all the products, < 1 eV, and peaks at lower energies, about 3 eV. Energetic

requirements establish that these minor products are formed in reactions 13 and 14.

$$Co^+ + C_2H_6 \longrightarrow \begin{cases} CoCH_2^+ + CH_4 & (13) \\ CoC_2H_4^+ + H_2 & (14) \end{cases}$$
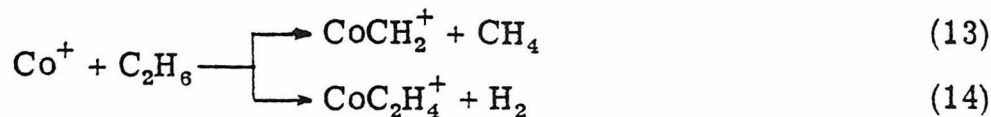
The various processes which occur when Co^+ interacts with ethane can now be understood and are outlined in Scheme I. The first step, oxidative addition of a C-H or C-C bond to Co^+ seems energetically feasible, considering the values for $D^o(Co^+-CH_3)$ and $D^o(Co^+-H)$. The lowest energy decomposition process for $\underset{\sim}{3}$ and $\underset{\sim}{4}$ is a rearrangement followed by reductive elimination of H_2 or CH_4. While $\underset{\sim}{4}$ can only rearrange by migration of an α-hydrogen, $\underset{\sim}{3}$ can rearrange by α-H transfer to eventually form the cobalt ethylidene ion, by α-Me transfer to yield the cobalt carbene ion, or by β-H transfer to form a cobalt ion ethene complex. Assuming $D^o(CH_2Co^+-H)$ $= D^o(Co^+-H)$, the energy necessary to transfer an α-hydrogen from the carbon of $CoCH_3^+$ to the metal is calculated to be 33 kcal/mol, which is above the approximate threshold for production of $CoC_2H_4^+$. The α-alkyl shift is considered an equally unfavorable process. Evidence presented below indicates that the β-H transfer, however, is quite facile.[4,5] Thus, in analogy with related studies in solution,[31] we conclude that β-H migration dominates rearrangement of intermediates such as $\underset{\sim}{3}$. This implies that the structure of $CoC_2H_4^+$ is a cobalt ion-ethene complex. At higher energies, $\underset{\sim}{3}$ and $\underset{\sim}{4}$ decompose by more direct routes involving fission of a metal-carbon bond. Such processes have higher frequency factors than rearrangement,[32]

and thus are the only important reactions once energetically allowed.

Scheme I
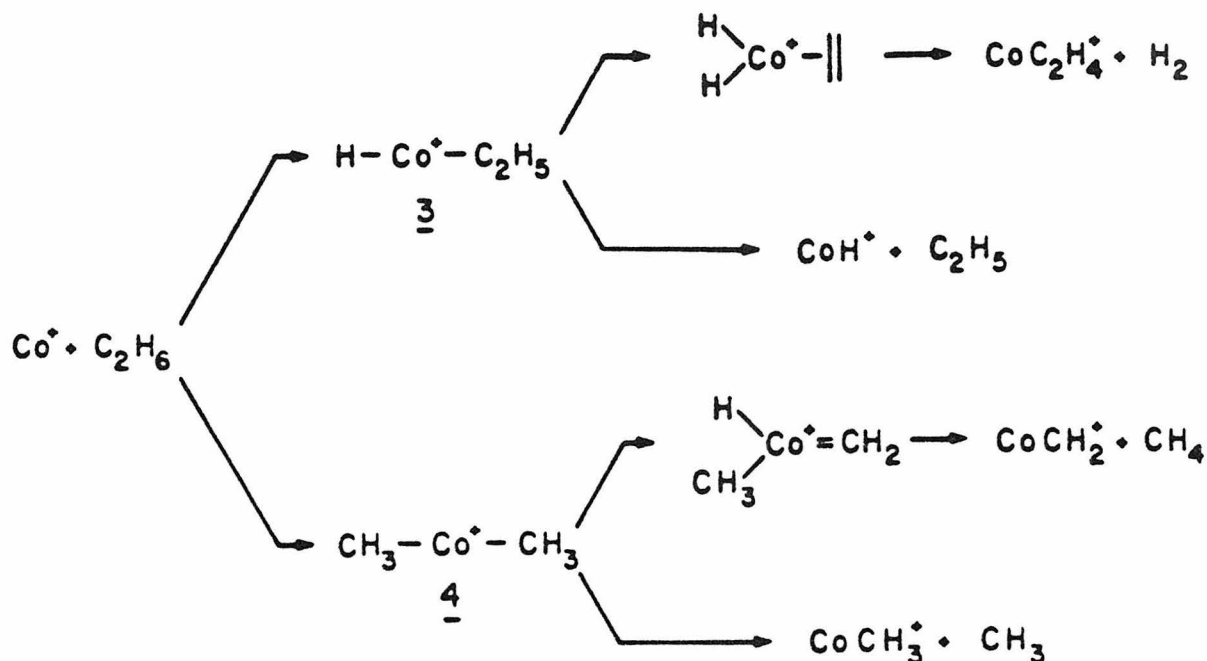
Reaction of Co$^+$ with Deuterated Ethanes

The magnitude and behavior as a function of energy of the cross section for reaction of cobalt ions with C_2D_6 and CH_3CD_3 are the same as with C_2H_6, within experimental error. In the reaction with CH_3CD_3, the only cobalt methyl ion species formed are $CoCH_3^+$ and $CoCD_3^+$. These two products have similar cross sections (within $\pm\,20\%$) at all energies. This is also true for the cobalt carbene ion products, $CoCH_2^+$ and $CoCD_2^+$, and the cobalt hydride ion products, CoH^+ and CoD^+. The isotopic composition of the cobalt ion ethene complex could not be determined due to low signal intensity.

Reaction of Co$^+$ with Propane

Results for the interaction of cobalt ions with propane are shown in Figure 4. Unlike previous data, the reaction cross sections are large and decrease monotonically with increasing energy. This indicates that reactions 15 and 16 are exothermic. Energetic require-

$$Co^+ + C_3H_8 \longrightarrow \begin{array}{l} CoC_3H_6^+ + H_2 \quad\quad\quad (15) \\ CoC_2H_4^+ + CH_4 \quad\quad\quad (16) \end{array}$$
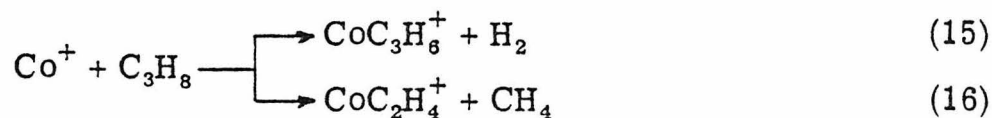
ments stipulate the neutral products indicated. This typifies the behavior observed for reaction of Co$^+$ with all larger alkanes. Also typical is the high energy region shown in Figure 4, where endothermic channels yield a variety of products.

We can understand the reactions of Co$^+$ with propane by again postulating initial oxidative addition of a C-H or C-C bond to cobalt ions, Scheme II. The intermediates formed, 7, 8 and 9, undergo further reaction to yield 10 and 11 which reductively eliminate H$_2$ and CH$_4$, respectively, giving the observed products. That 7, 8, or 9 rearrange by α-H or α-alkyl transfer is not considered likely, for reasons already discussed. Intermediate 8 could also rearrange by a γ-H transfer to the metal forming a metallocyclobutane. This process, discussed in greater detail below, is also considered improbable.

While Scheme II is definitely consistent with the products observed at low energies, it must also be capable of explaining products observed at higher energies. As discussed above, once endothermic bond fission processes become energetically accessible,
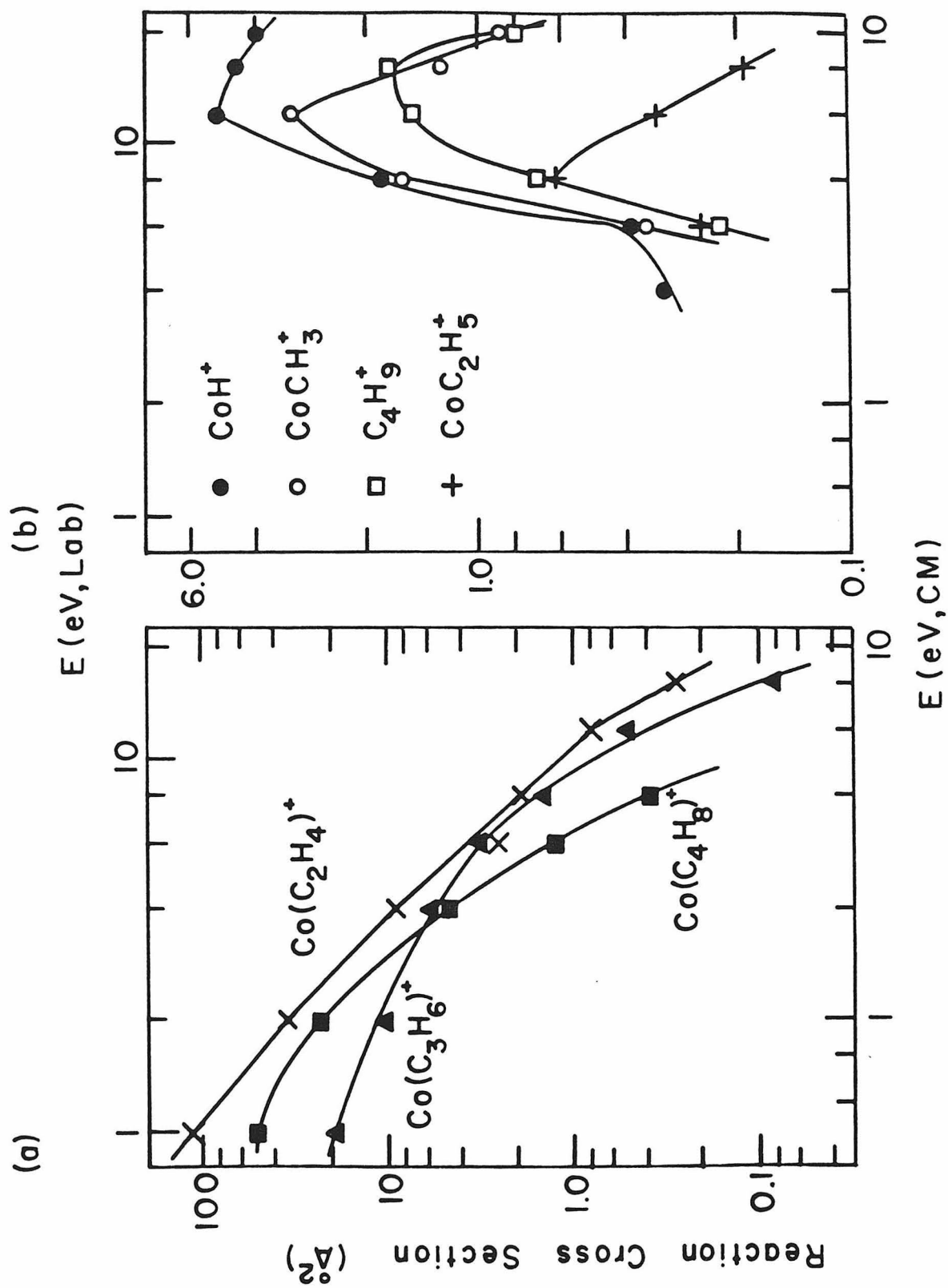
FIG. 4.   Variation in experimental cross section for the inter-
action of Co^+ with propane as a function of kinetic energy
in the center of mass frame (lower scale) and laboratory
frame (upper scale).

$E(eV, Lab)$

$Co^+ + CH_2(CH_3)_2$

$Co(C_3H_6)^+$

$Co(C_2H_4)^+$

- ● CoH^+
- ○ $CoCH_3^+$
- △ $C_3H_7^+$
- + $CoC_2H_5^+$

$E(eV, CM)$
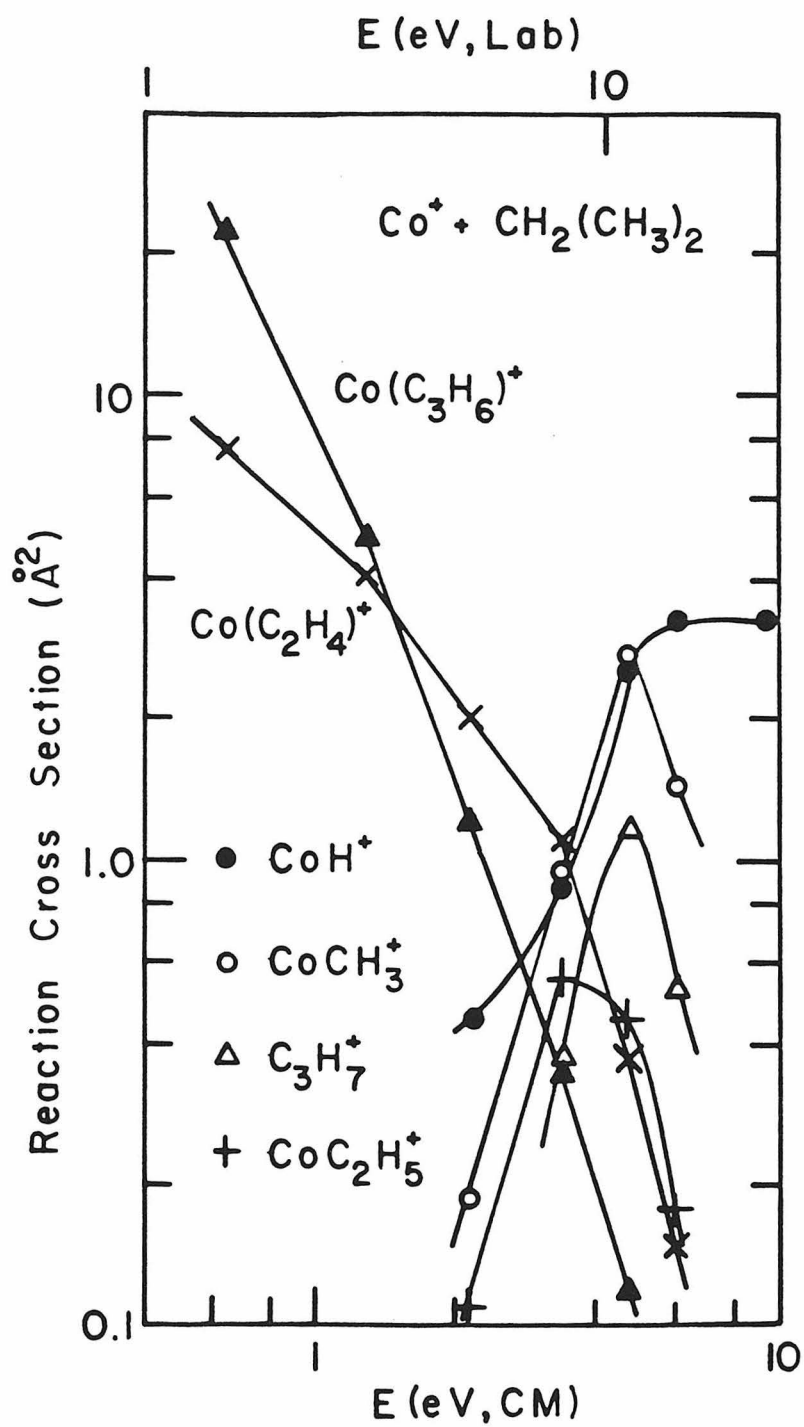
they become the dominant decomposition routes of intermediates such as $\underset{\sim}{7}$, $\underset{\sim}{8}$ and $\underset{\sim}{9}$. A qualitative potential energy surface for intermediate $\underset{\sim}{9}$, Figure 5, exemplifies these considerations. Below about 1 eV, only the exothermic reaction involving rearrangement can occur. At higher energies, $\underset{\sim}{9}$ can dissociate by cleavage of one of the cobalt-carbon bonds, the weakest in the complex. Formation of $CoCH_3^+$ and $CoC_2H_5^+$ at higher energies is taken as further evidence that oxidative addition of carbon-carbon bonds to Co^+ occurs. Formation of these products would not be expected if formation of $CoC_2H_4^+$ proceeded exclusively through intermediate $\underset{\sim}{8}$, Scheme II. While β-alkyl abstraction cannot be ruled out experimentally, this process is not required to explain the observed products.

Scheme II
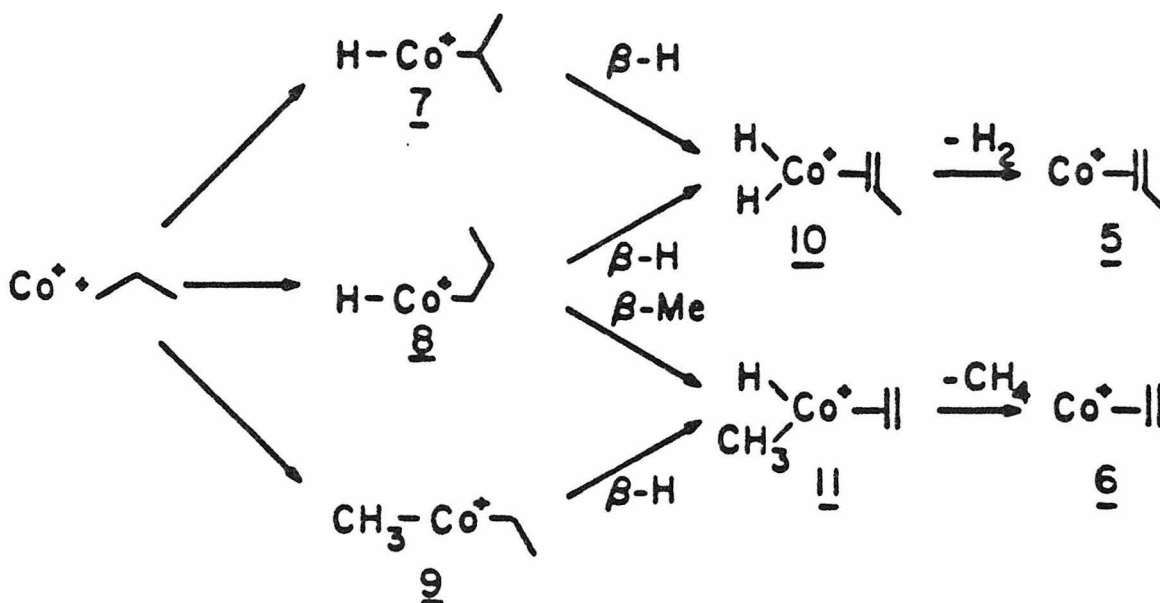
FIG. 5.   Postulated reaction coordinate energy diagram for
oxidative addition of the carbon-carbon bond of
propane to cobalt ions.

213
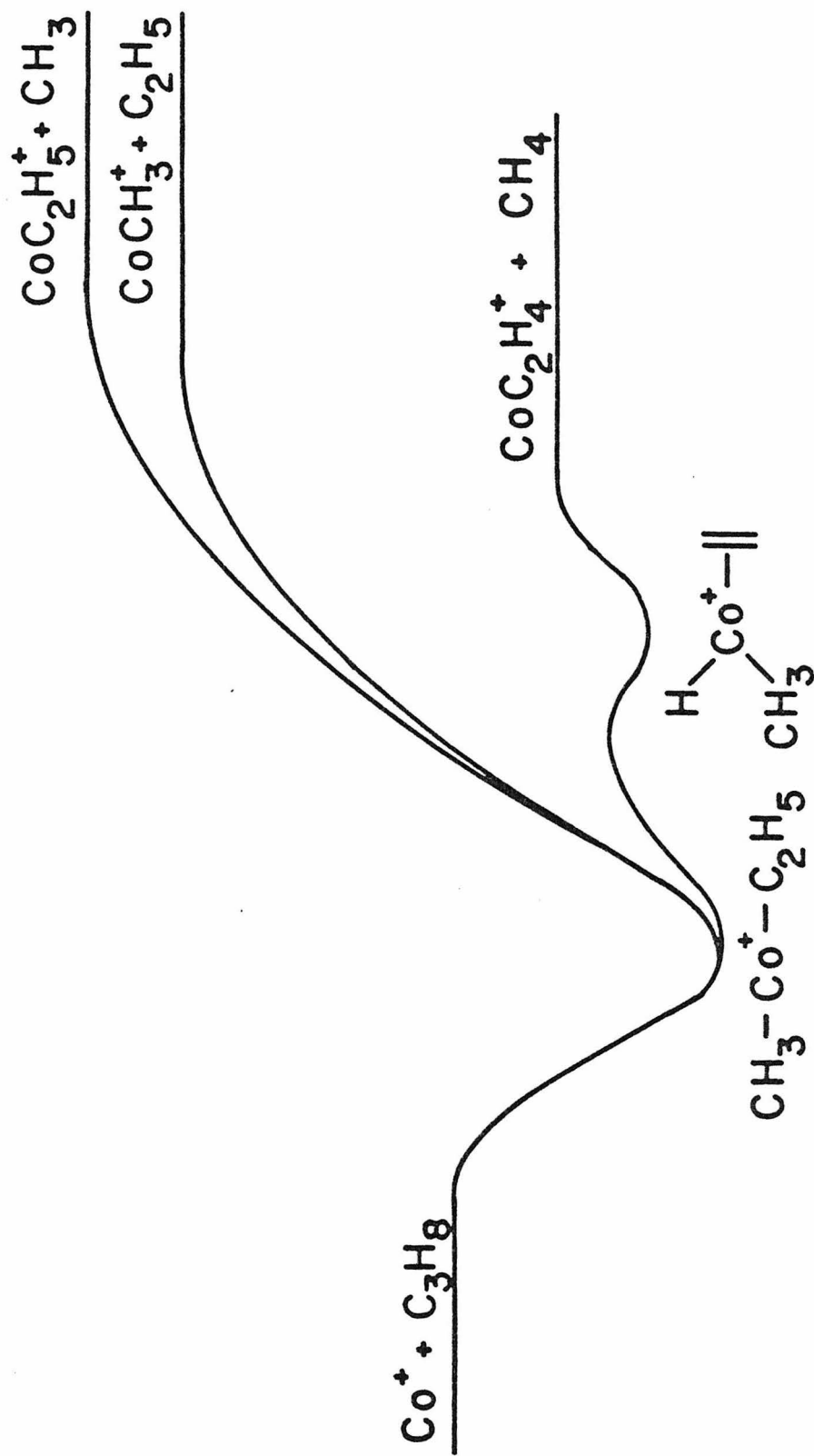
Reaction of Co$^+$ with n-Butane and 2-Methylpropane

The butanes represent the smallest isomeric alkanes. In addition, n-butane is the first alkane to have two types of carbon-carbon bonds. Results for the interaction of Co$^+$ with n-butane and 2-methylpropane are shown in Figures 6 and 7, respectively. While the total cross sections are comparable, the product distributions are substantially different. Two products, CoC$_2$H$_4^+$ and CoC$_3$H$_6^+$, corresponding to C-C bond cleavage are observed in the n-butane system, while only the latter product is seen in the 2-methylpropane case.

The high energy products of the n-butane and 2-methylpropane systems are also distinct. Cobalt hydride ions and cobalt methyl ions dominate both systems, but cobalt ethyl ions are observed only in reaction with n-butane. The only alkyl ion observed in the n-butane system is C$_3$H$_7^+$ in rather low abundance while with 2-methylpropane, C$_3$H$_7^+$ is more abundant and C$_4$H$_9^+$ is also observed. A mechanism analogous to Scheme II easily explains both the low and high energy results.

The relative yield for reaction 17 is one-fifth that of reaction 18. Yet, since the binding energy of propene to Co$^+$ should be greater than that of ethene,[33] process 17 should be more exothermic than 18.

$$Co^+ + n\text{-}C_4H_{10} \longrightarrow \begin{cases} CoC_3H_6^+ + CH_4 & (17) \\ CoC_2H_4^+ + C_2H_6 \ . & (18) \end{cases}$$
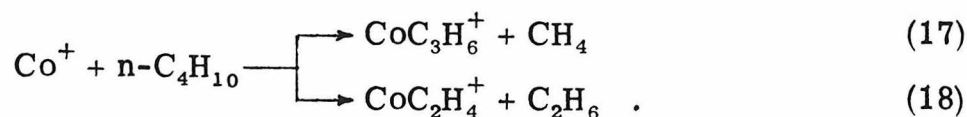
This result suggests that the product distribution is determined by the

FIG. 6. Variation in experimental cross section for the inter-
action of Co^+ with butane as a function of kinetic energy
in the center of mass frame (lower scale) and laboratory
frame (upper scale). Part a shows exothermic channels;
part b shows endothermic channels. Note change of scale.

FIG. 7.   Variation in experimental cross section for the interaction
of Co^+ with 2-methylpropane as a function of kinetic energy
in the center of mass frame (lower scale) and laboratory
frame (upper scale).   Part a shows exothermic channels;
part b shows endothermic channels.   Note change of scale.
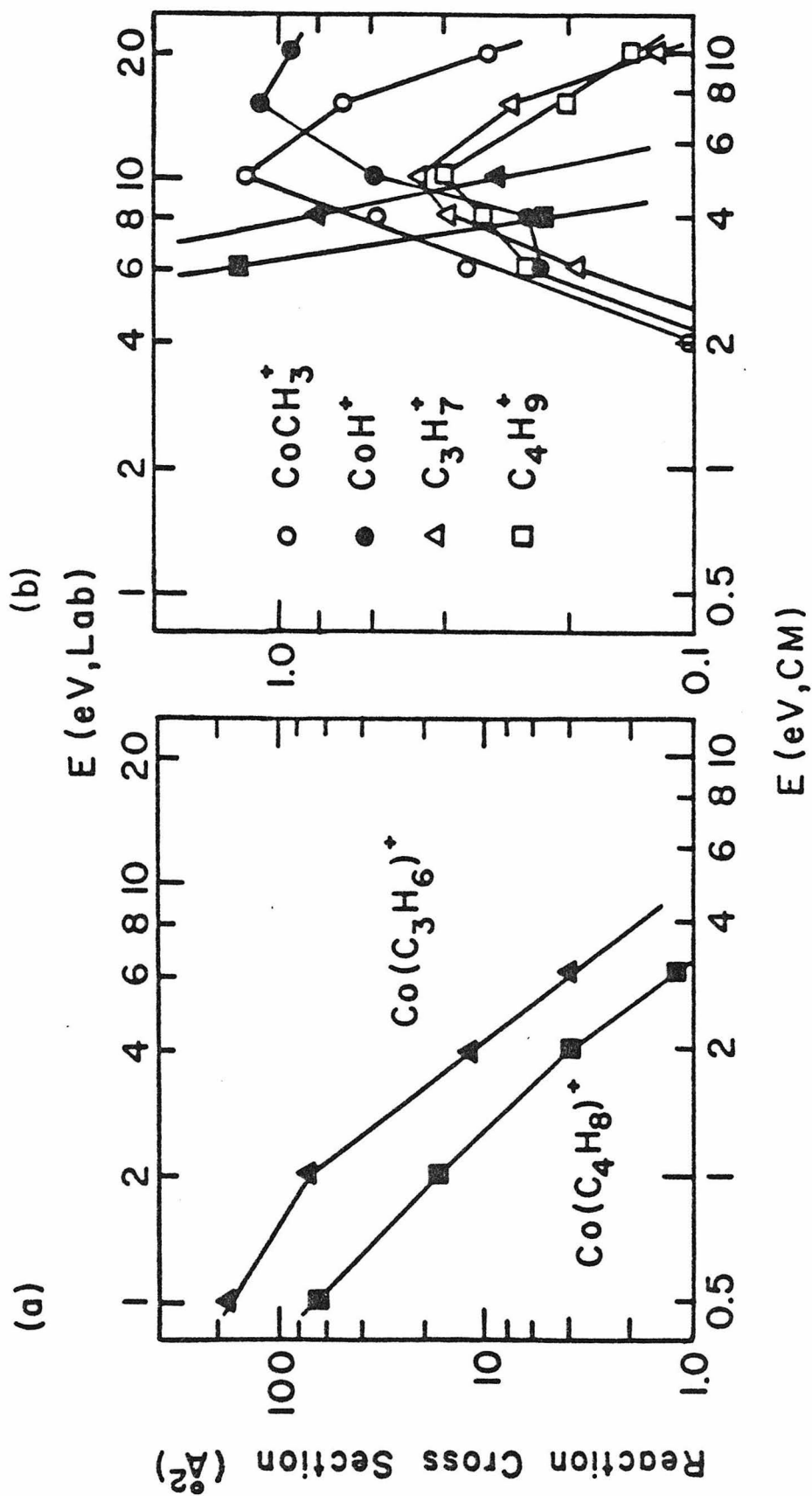
initial oxidative addition since the internal C-C bond in n-butane is weaker than the terminal bond by about 6 kcal/mol.[26]

Reaction of Co⁺ with Deuterated Butanes

The reaction of Co^+ with $1,1,1,4,4,4$-butane-d_6, $CD_3CH_2CH_2CD_3$, was examined to further elucidate the mechanism of the alkane reactions. The cobalt ion ethene complex product exemplifies the results. Only the $Co(C_2H_2D_2)^+$, 12, and $Co(C_2HD_3)^+$, 13, species are detected and in a 3:1 ratio at the lowest energies. As the collision energy is raised, the latter product decreases until only the former is observed. At the highest energies, the only cobalt ethyl ion seen is $CoC_2H_2D_3^+$. Scheme III proposes a mechanism to explain these results. A statistical distribution of products 12 and 13 is predicted by this mechanism to be 3:2. This is an obvious limit on the actual behavior since hydrogen scrambling must proceed via intermediate 14. As the interaction energy increases, decomposition of 14 to 12 precludes further rearrangement. Eventually, decomposition of 15 to $CoC_2H_2D_3^+$ dominates the reaction. We conclude that β-H transfer to and from the metal is facile. It is noted that scrambling of all ten hydrogens in the butane does not occur; no $CoC_2H_4^+$, $CoC_2H_3D^+$ or $CoC_2D_4^+$ products are detected. This observation also provides evidence that β-alkyl transfer is unlikely, since if this were a viable process, formation of $CoC_2H_4^+$ should occur (Scheme IV).

The cobalt propene ion and cobalt butene ion products also exhibit hydrogen scrambling. However, low signal intensity precluded obtaining data as accurate as that for the cobalt ethene ion product.

The predominant propene complex product is $Co(C_3H_3D_3)^+$, $>75\%$ at 0.5 eV and $\sim 100\%$ above 1 eV, consistent with a mechanism like Scheme III. At higher energies, the only cobalt methyl ion observed is the perdeuterated species. The dehydrogenation reaction to form cobalt butene ion consists of loss of H_2, HD, and D_2 with no discernible energy effect. Both CoH^+ and CoD^+ are observed at higher energies.

Scheme III

Scheme IV

Reaction of Co^+ with 2, 2-dimethylpropane

The results for the reaction of Co^+ with 2, 2-dimethylpropane are shown in Fig. 8. Observation of a single low energy product, $CoC_4H_8^+$, is entirely consistent with oxidative addition of a C-C bond to Co^+, β-H abstraction, and reductive elimination of CH_4. Formation of 16, 17, and 18, which require α-H transfer, γ-H transfer, and
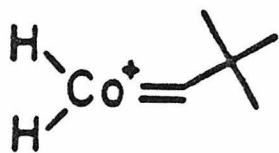
16   17   18
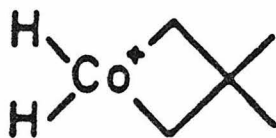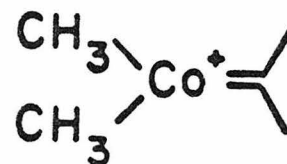
α-Me transfer, respectively, do not appear to occur as no $CoC_5H_{10}^+$, formed by reductive elimination of H_2 from 16 or 17, or $CoC_3H_6^+$, formed by reductive elimination of C_2H_6 from 18, is observed. This presumes, as seems likely, that reductive elimination is competitive with other decomposition reactions of 16, 17 and 18, including reverting to reactants.

Bond Energies of CoH and $CoCH_3$

As discussed above, the intermediates formed by the initial oxidative addition decompose at high energies by simple bond fission forming both cobalt alkyl ions or cobalt hydride ions and alkyl ions. In the dissociation of such a charged intermediate, the preferred ionic product is the fragment having the lower ionization potential (IP).[34] Thus, $C_3H_7^+$ is formed in lower abundance in the n-butane system than in the 2-methylpropane system because $IP(n-C_3H_7) = $

FIG. 8.   Variation in experimental cross section for the inter-

action of Co^+ with 2, 2-dimethylpropane as a function

of kinetic energy in the center of mass frame (lower

scale) and laboratory frame (upper scale). Part a

shows exothermic channels; part b shows endothermic

channels. Note change of scale.

(a)

(b)

$C_4H_9^+$

$CoCH_3^+$

CoH^+

$Co(C_4H_8)^+$

E (eV, Lab)

E (eV, CM)

Reaction Cross Section (Å^2)
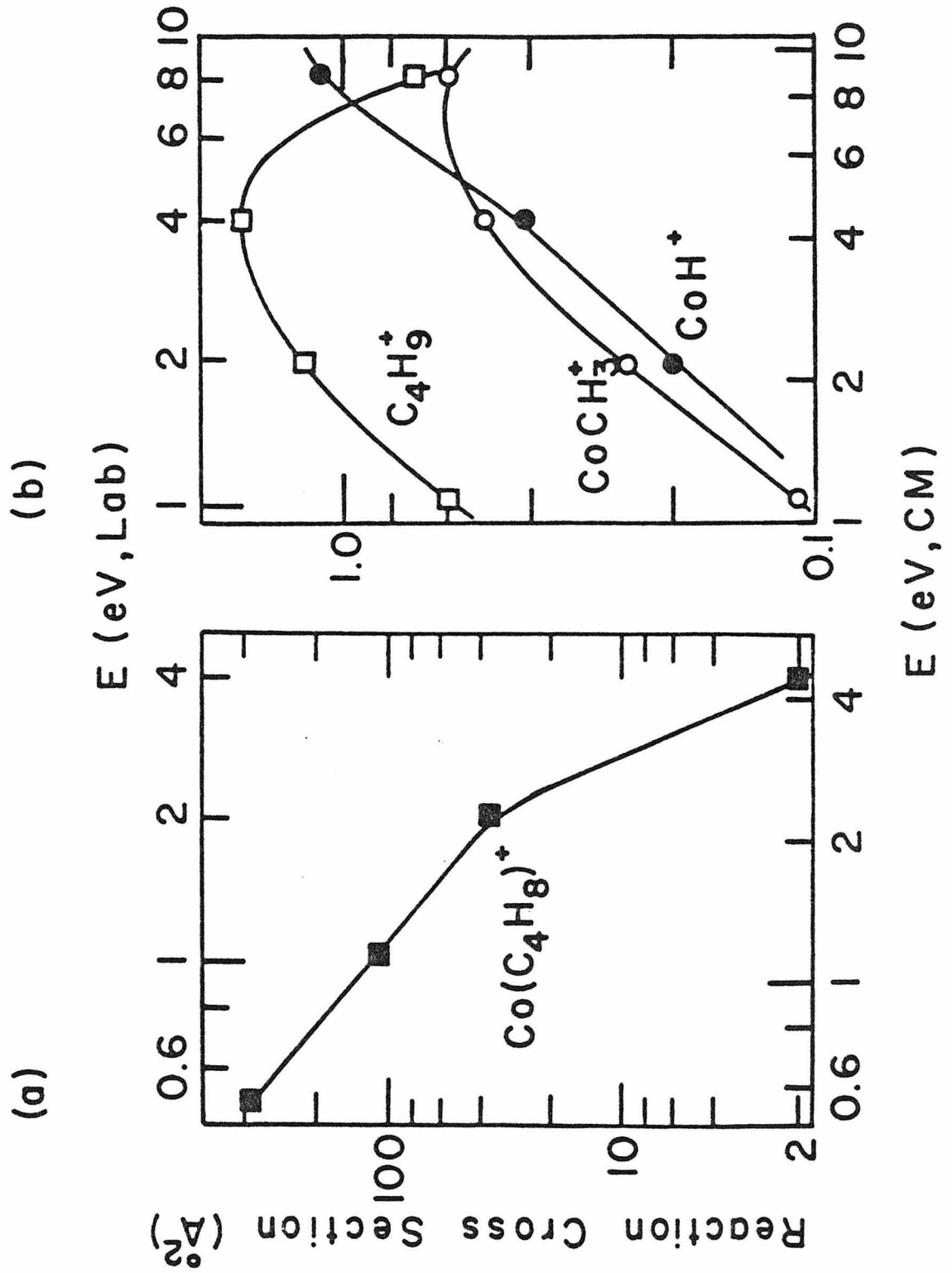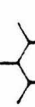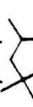
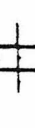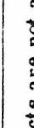8.16 eV[36] > IP (iso-C_3H_7) = 7.36 eV.[37] In addition, in both systems, the complementary product $CoCH_3^+$ is formed in greater yield than $C_3H_7^+$ implying IP ($CoCH_3$) < 7.36 eV. Similarly, in reaction with 2,2-dimethylpropane, $C_4H_9^+$ is the dominant product suggesting IP ($CoCH_3$) > IP (t-C_4H_9) = 6.70 eV.[37] By applying such considerations to all systems investigated, the ionization potentials obtained are $CoCH_3$, 7.0 ± 0.3 eV,[38] and CoH, 7.3 ± 0.1 eV,[41,44] Table I.

Using these ionization potentials and the bond energies for CoH^+ and $CoCH_3^+$ given in Table I, the bond energies of the neutral CoH and $CoCH_3$ species may be calculated to be 39 ± 6 kcal/mol and 41 ± 10 kcal/mol, respectively. The fact that these values are comparable lends credence to the idea that polarizability effects are responsible for the larger cobalt methyl ion bond energy. The values are also comparable to other known bond energies such as $D^0(CH_3-Mn(CO)_5) \sim$ 29 kcal/mol,[45] $D^0(CH_3-Re(CO)_5) = 53.2 \pm 2.5$ kcal/mol,[38] $D^0((CH_3)_2(\pi-C_2H_5)Pt-CH_3) = 39 \pm 5$ kcal/mol.[46]

Reaction of Co^+ with Larger Alkanes, $C_nH_{2n+2}(n = 5-8)$

The product distributions of the reactions of cobalt ions with several large alkanes at low energy are given in Table II. With few exceptions, these results may be explained by initial oxidative addition of a C-C or C-H bond, followed by β-H abstraction and reductive elimination of a neutral yielding a cobalt alkene ion. If sufficient internal energy is retained by this complex, further reaction may occur to yield a cobalt ion alkadiene complex. The mechanism for this process begins by insertion of the Co^+ into an allylic C-C of C-H

Table II. Product Distributions of Exothermic Reactions of Co$^+$ with Alkanes Measured at ~1 eV Relative Kinetic Energy

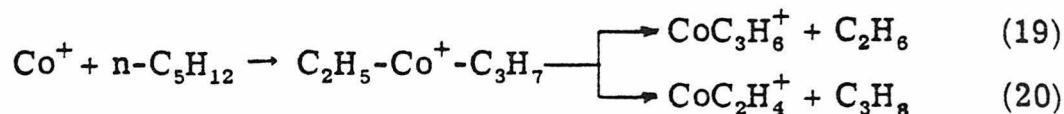| Alkane C_nH_{2n+2}	Structure	Neutral Products (C_mH_{2m+2}) Corresponding to Ionic Products, Co($C_{n-m}H_{2(n-m)}$)$^+$							Neutral Products Corresponding to Co(Alkadiene)$^+$ Products.				
		H_2	CH_4	C_2H_6	C_3H_8	C_4H_{10}	C_5H_{12}	C_6H_{14}	$2H_2$	H_2+CH_4	$H_2+C_2H_6$ / $2CH_4$	$H_2+C_3H_8$ / $CH_4+C_2H_6$	$H_2+C_4H_{10}$ / $CH_4+C_3H_8$ / $2C_2H_8$
C_3H_8		0.59	0.41										
C_4H_{10}		0.29	0.12	0.59									
		0.23	0.77										
C_5H_{12}		0.30	0.02	0.59	0.08								
		0.20	0.37	0.27	0.05				0.02	0.05			
			1.0										
C_6H_{14}		0.39	0.02	0.35	0.16	0.04					0.05		
		0.13	0.14	0.54	0.03*	0.05				0.04	0.06		
		0.12	0.30	0.40	0.03*	0.02				0.05	0.07		
		0.22	0.35		0.23					0.09	0.11		
C_7H_{16}		0.28	0.01	0.15	0.22	0.28	0.04					0.02	
		0.26	0.19		0.36	0.15					0.04		
C_8H_{18}		0.24	<0.01	0.10	0.18	0.20	0.15	0.02		0.02	0.10	0.01	0.07
		0.16	0.14		0.29	0.14*	0.07				0.09	0.02	0.04
		0.19	0.09			0.28	0.30				0.09		0.05
		0.07*	0.16		0.05*	0.13				0.03*	0.55		

Starred products are not accounted for by the general mechanism proposed in the text.

followed again by β-H abstraction and reductive elimination.[47] An example, the further reaction of Co(3-methyl-1-butene)$^+$, is illustrated in Scheme V.

Scheme V
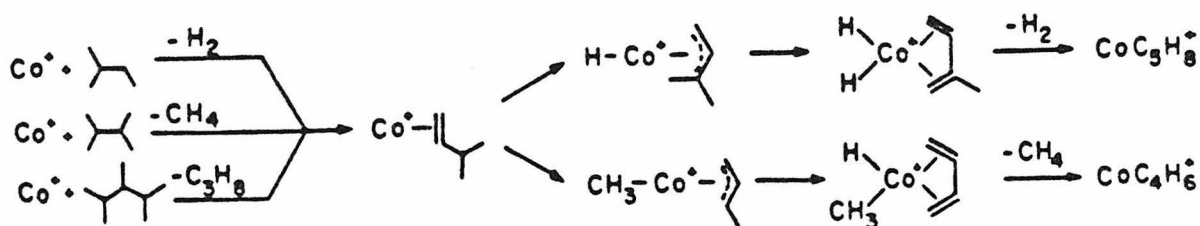
Qualitative trends in the product distributions are well accounted for by the proposed mechanism and simple thermochemical arguments. As discussed above, the initial oxidative addition occurs preferentially with the weakest bonds of the alkane. Thus, production of methane, resulting from insertion of Co$^+$ into terminal C-C bonds, occurs less frequently than the reactions from insertion into internal C-C bonds. Highly substituted alkenes are bound to Co$^+$ more tightly than smaller alkenes.[33] Thus, cleavage of the internal bond of 2-methylbutane or 2,2-dimethylbutane results preferentially in formation of CoC$_3$H$_6^+$ and CoC$_4$H$_8^+$, respectively, rather than CoC$_2$H$_4^+$, even when normalized for the different number of β-hydrogens. Transfer of secondary and tertiary β-hydrogens is found to be more likely than primary β-H transfer. Thus, for n-pentane (and all larger n-alkanes), products due to reaction 19 (secondary β-H transfer) are more prevalent than those from reaction 20 (primary β-H transfer),

$$Co^+ + n\text{-}C_5H_{12} \rightarrow C_2H_5\text{-}Co^+\text{-}C_3H_7 \begin{cases} \rightarrow CoC_3H_6^+ + C_2H_6 & (19) \\ \rightarrow CoC_2H_4^+ + C_3H_8 & (20) \end{cases}$$

even when accounting for the different numbers of the two types of β-hydrogens and the binding energy effect discussed above. An analysis of the 2,4-dimethylpentane system indicate a similar preference for tertiary versus primary β-H transfer.

Products, starred in Table II, which cannot be explained by the proposed mechanism are generally minor and involve highly branched alkanes. Alkyl migration can explain some of these results. Skeletal rearrangement of the hydrocarbons may also be occurring. Another intriguing possibility suggested by the dehydrogenation of 2,2,3,3-tetramethylbutane is the formation of the metallocyclopentane, 19.

19
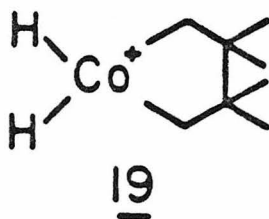
As the collision energy is raised, product distributions of Co^+ reacting with larger alkanes vary as would be expected. The example of 2,3-dimethylbutane, shown in Fig. 9, is typical. Cross sections for the ionic products, $CoC_6H_{12}^+$ and $CoC_5H_{10}^+$, are observed to decrease rapidly with increasing energies. This is presumably because the neutral products, H_2 and CH_4, respectively, have few internal degrees of freedom and thus leave the cobalt alkene ion with more internal energy than ionic products formed in conjunction with larger neutral products. The cobalt alkadiene ion products, $CoC_5H_8^+$ and $CoC_4H_6^+$, which are the result of secondary reactions, dominate the products at

FIG. 9.   Variation in product distribution for the interaction of
Co$^+$ with 2, 3-dimethylbutane as a function of kinetic
energy in the center of mass frame (lower scale) and
laboratory frame (upper scale). Several minor products
are omitted for clarity.
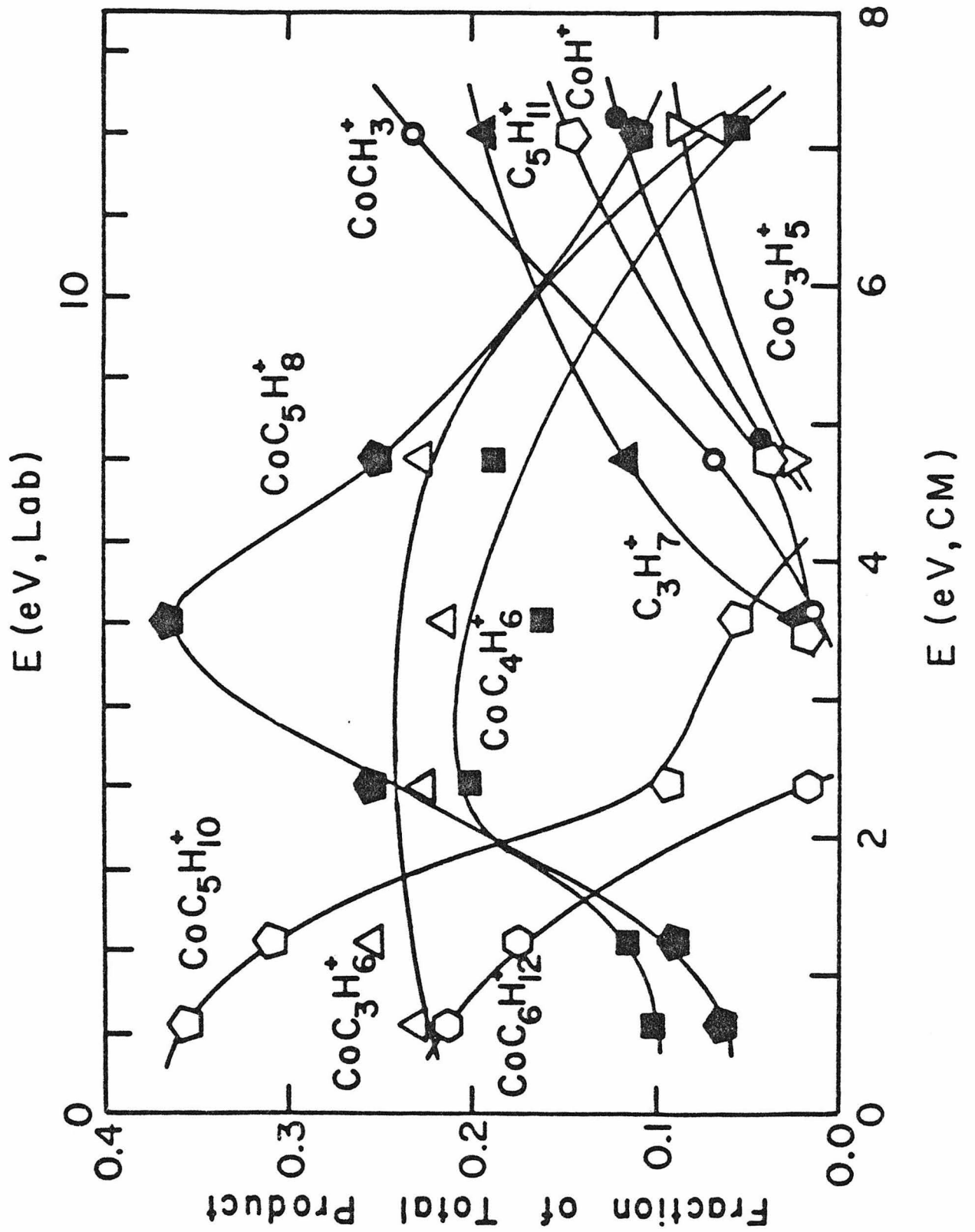
intermediate energies. At the highest energies, endothermic bond fission processes yield the observed results. As with the butanes, product distributions at these energies are sensitive to the structure of the reactant alkane.

A final elaboration of the general mechanism explains the observation of the $CoC_3H_5^+$ product ion, Fig. 9. In no system was any cobalt alkyl ion containing three or more carbons observed. We postulate that secondary dehydrogenation of such cobalt alkyl ions to yield cobalt allyl ions is a facile decomposition reaction.

Conclusion

The reactions of Co^+ with hydrogen and alkanes comprise a cohesive set of experiments. The strength of cobalt hydrogen and cobalt carbon bonds is determined to be sufficient that oxidative addition of C-H and C-C bonds to Co^+ is energetically feasible. Thus, dehydrogenation and carbon-carbon bond cleavage reactions are observed to occur at thermal energies with large cross sections. However, Co^+ is not so reactive as to preclude selectivity. Product distributions are sensitive to alkane structure and trends can be explained using thermodynamic arguments.

The present experiments indicate that a significant amount of chemistry may occur on a single metal center. These reactions may be viewed as a catalytic process for cracking and dehydrogenation of alkanes. The activation energy of these reactions is equivalent to the binding energy of an alkene to Co^+. Thus, conversion of alkanes to alkenes and smaller alkanes requires about 25-40 kcal/mol. This

energy is comparable to activation energies observed for hydrogen-olysis of alkanes on platinum surfaces.[48]

Extensions of the present study are many. Reaction of Co^+ with unsaturated hydrocarbons, alkenes and cyclic compounds, will be presented in a forthcoming paper. Studies involving organic compounds containing heteroatoms are under way, as are investigations of the reactivity of other transition metal ions.

References

(1) H. F. Schaefer, Accts. Chem. Res. 10, 287 (1977).

(2) J. A Connor, Topics Current Chem. 71, 71 (1977).

(3) A. K. Rappé and W. A. Goddard III, J. Am. Chem. Soc. 99, 3966 (1977); T. H. Upton and W. A. Goddard III, J. Am. Chem. Soc. 100, 321 (1978); T. H. Upton and W. A Goddard III, J. Am. Chem. Soc. 100, 5659 (1978).

(4) R. R. Corderman and J. L. Beauchamp, J. Am. Chem. Soc. 98, 3999 (1976); R. R. Corderman, Ph.D. Thesis, California Institute of Technology, 1977.

(5) (a) J. Allison and D. P. Ridge, J. Am. Chem. Soc. 98, 7445 (1976); (b) J. Allison, R. B. Freas and D. P. Ridge, J. Am. Chem. Soc. 101, 1332 (1979); (c) J. Allison and D. P. Ridge, J. Am. Chem. Soc. 101, 4998 (1979).

(6) A. E. Stevens and J. L. Beauchamp, J. Am. Chem. Soc. 100, 2584 (1978); 101, 245 (1979); A. E. Stevens and J. L. Beauchamp, J. Am. Chem. Soc., submitted.

(7) P. B. Armentrout and J. L. Beauchamp, J. Am. Chem. Soc., submitted.

(8) R. J. Remick, T. A. Asunta and P. S. Skell, J. Am. Chem. Soc. 101, 1320 (1979).

(9) P. H. Barrett, M. Pasternak and R. G. Pearson, J. Am. Chem. Soc. 101, 222 (1979).

(10) S. C. Davis and K. J. Klabunde, J. Am. Chem. Soc. 100, 5973 (1978).

References (continued)

(11) P. B. Armentrout, R. V. Hodges and J. L. Beauchamp,
      J. Chem. Phys. 66, 4683 (1977).

(12) R. V. Hodges, P. B. Armentrout and J. L. Beauchamp,
      Int J. Mass Spec. Ion Phys. 29, 375 (1979).

(13) The chamber is designed to allow efficient extraction of low
      energy ions. H. W. Werner, Int. J. Mass Spec. Ion Phys.
      14, 189 (1974).

(14) P. B. Armentrout and J. L. Beauchamp, J. Chem. Phys.,
      submitted.

(15) B. R. Turner, J. A. Rutherford and D. M. J. Compton,
      J. Chem. Phys. 48, 1602 (1968).

(16) R. J. Cotter and W. S. Koski, J. Chem. Phys. 59, 784 (1973).

(17) C. Lifshitz, R. L. C. Wu, T. O. Tiernan and D. T. Terwilliger,
      J. Chem. Phys. 68, 247 (1978).

(18) P. J. Chantry, J. Chem. Phys. 55, 2746 (1971).

(19) (a) P. B. Armentrout and J. L. Beauchamp, Chem. Phys.,
      submitted; (b) P. B. Armentrout and J. L. Beauchamp,
      Chem. Phys., submitted.

(20) G. Gioumousis and D. P. Stevenson, J. Chem. Phys. 29, 294
      (1958).

(21) B. de B. Darwent, Natl. Stand. Ref. Data Ser., Natl. Bur.
      Stand., 1970, 31.

(22) This estimate is based on an estimated frequency for CoH^+ of
      2000 cm^{-1}.

References (continued)

(23)   For comparison, electron impact ionization studies of the
       molecules, $HCo(CO)_x(PF_3)_{4-x}$, where x = 0-4, yield values for
       $D^0(Co^+-H)$ ranging from 1.8 to 3.3 eV with a mean of 2.6 eV.
       F. E. Saalfeld, M. V. McDowell, S. K. Gondal and A. G.
       Mac Diarmid, J. Am. Chem. Soc. 90, 3684 (1968).

(24)   Supplementary thermochemical data for ions and ionization
       potentials are taken from H. M. Rosenstock, K. Draxl, B. W.
       Steiner and J. T. Herron, J. Phys. Chem. Ref. Data, 6, (1977).

(25)   Calculated using $D^0(Zn^+-H)$ = 2.5 eV. G. Herzberg, "Spectra
       of Diatomic Molecules", Van Nostrand, New York, 1950.

(26)   Supplementary thermochemical data for hydrocarbons are taken
       from J. D. Cox and G. Pilcher: "Thermochemistry of Organic
       and Organometallic Compounds", Academic Press, New York,
       1970.

(27)   Such a process involving cobalt has been observed by L. S. Pu
       and A. Yamamoto, J.C.S. Chem. Comm. 9, (1974).

(28)   Differences between the methyl and hydrogen bond energies,
       $D^0(X^+-CH_3) - D^0(X^+-H)$, for the halide ions, X = I, Br, and Cl,
       are 5, 7 and 13 kcal/mol, respectively.

(29)   This heat of formation may be calculated without prior
       assumption about the structure of the ion directly from the
       endothermicity of reaction 9.

(30) $D^0(H-C_3H_5)$ = 86.6 kcal/mol. $D^0(H-CH_2\phi)$ = 87.9 kcal/mol.
       D. M. Golden, J. Am. Chem. Soc. 101, 1230 (1979).

References (continued)

(31) R. R. Schrock and G. W. Parshall, Chem. Rev. 76, 243 (1976).

(32) P. J. Robinson and K. A. Holbrook, "Unimolecular Reactions" Wiley, London, 1972.

(33) This conclusion is based on the exothermicity of reaction 15 which suggests $D^0(Co^+-C_3H_6) > 30$ kcal/mol, the endothermicity of reaction 14 which suggests $D^0(Co^+-C_2H_4) < 33$ kcal/mol, and the exothermicity of reactions with larger alkanes (2-methyl-butane and 2,2-dimethylbutane) which yield $CoC_2H_4^+$ suggesting that $D^0(Co^+-C_2H_4) > 24$ kcal/mol. Thermochemical data are from Ref. 26.

(34) Sometimes referred to as Stevenson's Rule,[35] this observation is a straightforward conclusion of RRKM theory.[32]

(35) D. P. Stevenson, Disc. Faraday Soc. 10, 35 (1951).

(36) F. A. Houle and J. L. Beauchamp, J. Am. Chem. Soc., submitted.

(37) F. A. Houle and J. L. Beauchamp, J. Am. Chem. Soc. 101, 4067 (1979).

(38) IP(sec-C_4H_9) ~ 7.25 eV[39] > IP(CoCH$_3$) > IP(tert-C_4H_9) = 6.70 eV.[37]

(39) This value is lowered from Lossing's value of 7.41 eV[40] by the discrepancy between Lossing's value for IP(iso-C_3H_7) = 7.55 eV[40] and that of Houle and Beauchamp, 7.36 eV.[37] Lossing's values correspond more nearly to the vertical rather than the adiabatic ionization potential.

(40) F. P. Lossing and G. P. Semeluk, Can. J. Chem. 48, 955 (1970).

References (continued)

(41)   IP$(iso-C_3H_7)$ = 7.36 eV[37] > IP(CoH) > IP$(cyclo-C_5H_9)$[42] = 7.21 eV.[43]

(42)   P. B. Armentrout and J. L. Beauchamp, to be published.

(43)   F. A. Houle and J. L. Beauchamp, J. Am. Chem. Soc., submitted.

(44)   Comparison of CoH^+ to the complementary alkyls must be made at the lowest possible energies to minimize the amount of CoH^+ formed by direct hydrogen abstraction.

(45)   D. Lalage, S. Brown, J. Connor and H. A. Skinner, J. Organometal. Chem. 81, 403 (1974).

(46)   K. W. Egger, J. Organometal. Chem. 24, 501 (1970).

(47)   This process has been observed previously. See for example, Ref. 4 and 5.

(48)   G. Leclercq, L. Leclercq and R. Maurel, J. Catalysis, 44, 68 (1976).